GABRIELE MELLIES

TWO CASE STUDIES OF EXCAVATIONS IN FRACTURED ROCK

Mémoire présenté
à la Faculté des études supérieures de l'Université Laval
dans le cadre du programme de maîtrise en génie des mines
pour l'obtention du grade de maître ès sciences (M.Sc.)

DÉPARTEMENT DE GÉNIE DES MINES, DE LA MÉTALLURGIE
ET DES MATÉRIAUX
FACULTÉ DES SCIENCES ET DE GÉNIE
UNIVERSITÉ LAVAL
QUÉBEC

2009

Résumé

La stabilité des excavations dans les roches fracturées est influencée, entre autres, par le régime structural, qui est inhérent à la roche. Divers outils sont disponibles pour les analyses de stabilité, mais la qualité des résultats dépend considérablement des données d'entrée disponibles et des outils utilisés. Dans ce mémoire, deux études de cas sont présentées, qui étudient l'influence de la représentation de données structurales sur l'analyse de stabilité.

La première étude de cas traite de la stabilité d'une pente de roche le long d'une route près de Fleurimont, qui a subi des effondrements de dièdre. L'objectif était de découvrir si les effondrements pourraient avoir été prédits et d'évaluer la probabilité de la rupture de dièdre le long de la pente. Plusieurs analyses d'équilibre limite ont été effectuées, y compris une analyse déterministe rétrospective de deux ruptures de dièdres, et une analyse probabiliste des dièdres individuels. De plus, une analyse probabiliste de système de joints a été effectuée en utilisant les modèles 3D de système de joints, qui ont été générés avec des données de terrain. Les données nécessaires pour les analyses ont été recueillies sur place.

Les résultats d'analyse rétrospective ont indiqué l'instabilité potentielle des dièdres observés, et les approches probabilistes ont confirmé l'occurrence des effondrements de dièdre le long de la pente, mais ils ont également démontré que la probabilité d'effondrements semblables est faible. Les résultats ont démontré qu'une analyse de données exhaustive en utilisant plusieurs outils d'analyse est requise pour obtenir une évaluation fiable du comportement de la roche.

La deuxième étude de cas discute de la stabilité des galeries à la mine souterraine LaRonde de l'Agnico Eagle, qui sont concernées par de grandes déformations à cause de la convergence des parois. L'analyse de la convergence observée s'est concentrée sur la génération d'une série de modèles numériques 2D selon la méthode des éléments finis, visant à reproduire le mécanisme d'effondrement et les déformations résultantes. La foliation in situ a été reproduite par des joints, qui ont été introduits explicitement dans le modèle. Les données structurales requises ont été rassemblées sur place. Les modèles ont été calibrés avec les données de convergence disponibles.

Les résultats de modélisation numérique ont atteint une bonne concordance avec les observations sur place. Les deux profils caractéristiques observés et l'ordre de grandeur des déformations mesurées ont pu être reproduits. Il a été démontré que le modèle numérique appliqué est un outil utile pour modéliser les conditions complexes observées à la mine. Plus d'expériences de validation devraient être effectuées, mais la méthode peut potentiellement être employée pour élaborer de meilleures stratégies pour les travaux de développement minier dans des conditions semblables.

Les deux études de cas ont démontré l'influence de la représentation des données structurales sur l'analyse de données. En outre il a été montré que le choix des outils d'analyse influence les résultats obtenus.

Abstract

The stability of excavations in fractured rock is influenced among others by the structural order inherent in the rock mass. Various analysis tools are available for stability analysis, but the quality of results depends considerably on the available analysis data and the tools used. In this thesis two case studies of excavations in fractured rock are presented that investigate the influence of structural data representation on the stability analysis.

The first case study focused on the stability of a rock slope along a road cut near Fleurimont that has experienced wedge failures. The aim was to find out, if the failures could have been predicted, and to evaluate the probability of wedge failures along the slope. Different limit equilibrium wedge analyses were carried out, including a deterministic back-analysis of two wedge failures and a probabilistic analysis of individual wedges. Furthermore a probabilistic joint system analysis was carried out using 3D joint system models generated out of field data. As part of this work the required analysis data was collected on site.

The back-analysis results suggested potential instability of the observed wedges, and the probabilistic approaches confirmed the occurrence of wedge failures along the slope, but also indicated the only low probability for these failures. The results demonstrated that a comprehensive data analysis using various analysis tools is required to reach a reliable assessment of the rock behaviour.

The second case study discusses the stability of drifts at Agnico Eagle's LaRonde underground mine that are affected by large deformations due to rock squeezing. The analysis of the observed drift convergence focused on the generation of a series of numerical 2D finite element models, aiming to reproduce failure mechanism and resulting deformations. The in situ foliation was reproduced by explicitly introducing joints into the model. The required structural data was collected on site. As reference data for the model calibration available convergence data was used.

The modelling results reached a good agreement with the observations on site. Both observed characteristic deformation profiles as well as measured deformation magnitudes

could be adequately reproduced. It could be demonstrated that the applied numerical model is a useful tool to model the complex squeezing ground conditions observed at the mine. More validation experiments should be carried out, but the method can potentially be used to develop better mine development strategies in similar conditions.

Both case studies demonstrated the influence of structural data representation on the data analysis. Furthermore it could be shown that the choice of analysis tools influences the obtained results.

Avant-Propos

Table of contents

Annex

List of figures

Case study 1: Rock slope in fractured rock

Case study 2: Underground drifts in fractured rock

List of tables

Case study 1: Rock slope in fractured rock

Case study 2: Underground drifts in fractured rock

1 Introduction

The stability of excavations in rock masses is influenced by discontinuities inherent in the rock mass. These discontinuities can control the behaviour of the rock mass, and have to be taken into account when designing excavations. The consideration of discontinuities is not only a question of safety, i.e. to avoid damages and casualties due to rock failures, but it is also important for economic reasons. A good understanding of the rock mass behaviour is a crucial precondition for an adequate design, and helps to avoid excessive costs and rehabilitation work, e.g. for rock support or due to time consuming repair measures after rock failures.

Rock masses are three-dimensional structures, while observations are usually carried out only in one or two dimensions. As a result, assumptions have to be made to describe rock or discontinuities properties. Hence, a systematic data collection, careful assumptions, and a comprehensive data analysis are essential for a reliable assessment of a rock mass and its behaviour.

In the present work stability problems in fractured rock masses were analyzed by means of two case studies. These case studies were carried out in fractured rock under different rock conditions, aiming to study and understand the behaviour of the investigated rock, and to reproduce the observed failure mechanisms with the aid of numerical models.

The first case study was the investigation of an eight meters high fractured rock slope along a highway, which experienced two large wedge failures during construction of the road in 1995. Although no further failures were reported since then, the site was selected as it provided an opportunity for a back-analysis of wedge failures.

The second case study was carried out in an underground mine in heavily layered rock with excavations at great depths. Several drifts in certain mine areas experienced large rock deformations and potential closure of the openings caused by squeezing of the rock.

The common objective was to investigate the influence of structure on the stability of surface and underground excavations. The specific objectives and the applied methodology for each case study are discussed in the next sections.

1.1 Case study 1: Rock slope in fractured rock

The prediction of the potential behaviour of rock slopes in fractured rock is an important part of rock engineering. Rock slopes can be found at many places in our environment, e.g. along roads or in surface mines, and their stability has an impact on safety as well as economic consequences.

Objective

The objective of the first case study was the assessment of the slope stability for wedge failures. Of interest was the stability analysis of the rock exposure as well as the back-analysis of two wedge failures observed during the construction of the road using deterministic and probabilistic analysis tools. Since the slope was stable during the past years and no further instabilities were observed, the investigation of this site was not triggered by an acute danger due to imminent rock falls. The aim was to determine if the wedge failures could have been predicted if more geological and geotechnical data would have been available, and to evaluate the probability of wedge failure.

Methodology

The following procedure was applied:

- Visual investigation of the rock exposure
- Data collection by scanline mapping
- Visualisation of the field data including site description
- Field data interpretation including
  ⇒ Structural analysis
  ⇒ Statistical analysis
  ⇒ Kinematical wedge analysis
- Limit equilibrium analysis of single wedges using collected field data including
  ⇒ Deterministic back-analysis of two large wedge failures
  ⇒ Probabilistic analysis of single wedges to determine probability of failure
- Limit equilibrium analysis of 3D joint system models of the rock mass including
  ⇒ Model building and calibration of a 3D joint system model using collected field data
  ⇒ Generation of possible joint system models

⇒ Probabilistic analysis of generated joint system models in view of wedge failures along the crest of the rock slope to determine frequency and failure probability of wedges

1.2 Case study 2: Underground drifts in fractured rock

The stability of underground excavations is of essential importance for underground mining processes. Not only the safety of people working underground has to be ensured, but also for economic reasons the behaviour of the rock mass around the underground openings is of interest. A good understanding of rock mass behaviour enables the design of cost effective support measures, and can help avoiding expenses for excessive support as well as for rehabilitation work after failures.

Objective

The objective of the second case study was the analysis of the observed drift convergence by reproducing the rock mass failure mechanism with the aid of numerical modelling. The focus was on the generation of several drift models that represent the squeezing rock conditions on site. The aim was to reproduce the complex interplay of rock mass, stress, and underground excavation using the finite element method.

Methodology

The following procedure was applied:

- Visual investigation of underground drifts identified by the mine as subject to large deformations
- Data collection on site
- Visualisation of the field data including site description
- Analysis of drift deformations
  ⇒ Field data interpretation by numerical modelling including model generation and calibration using collected field data

1.3 Structure of the thesis

In the following chapters both case studies are presented independently. Chapters 2 to 4 present the first case study, while chapters 5 to 7 discuss the second case study.

Chapter 2 introduces the investigated rock slope. A site description is given, followed by a structural analysis of the collected field data. Chapter 3 presents the results of the wedge stability analysis, including a kinematic analysis, a deterministic back-analysis of wedge failures, and two probabilistic wedge analysis approaches. Chapter 4 summarizes the results and the limitations of the first case study, draws conclusions based on the objectives, and provides an outlook on future work.

Chapter 5 introduces the investigated underground drifts. A description of the rock mass and of the investigated drifts is given, as well as the available analysis data. Chapter 6 presents the results of the numerical convergence analysis using the finite element method. In addition, a review of numerical modelling applications in squeezing rock is provided. Chapter 7 discusses the results of the second case study, the objectives met and the limitations, and draws conclusions. An outlook is given on future work.

In chapter 8 general conclusions of both case studies are presented.

2 Characterization of the Fleurimont rock slope

The first case study addresses a rock slope in a fractured rock mass. It was carried out at a rock slope along a highway cut near Fleurimont, where wedge failures were reported during the construction of the road.

Rock slope instabilities can be caused by different reasons. According to Hudson and Harrison, 1997 four basic failure mechanisms are associated with rock slope instability: plane failure, circular failure, wedge failure, and toppling failure. These four mechanisms are illustrated in Figure 1.
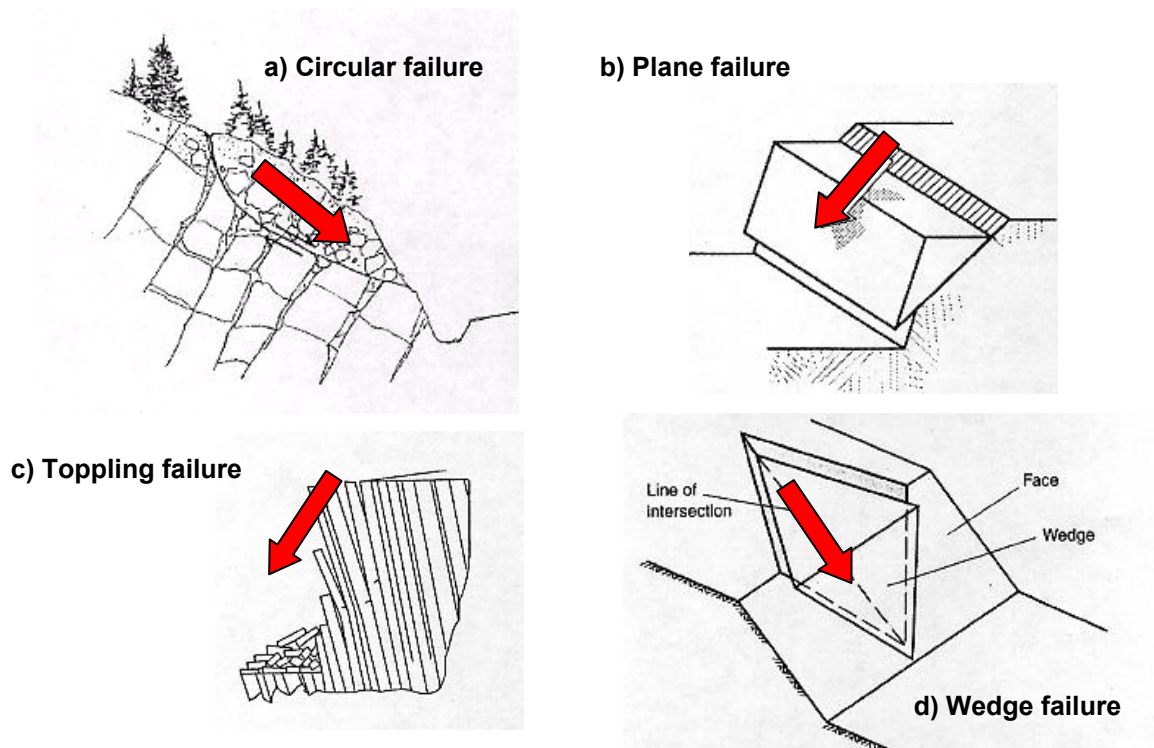
Figure 1: Basic failure mechanisms associated with rock slopes (after a) Wyllie and Norrish, 1996, b) Norrish and Wyllie, 1996, c) Hoek and Bray, 1981 and d) Wyllie and Mah, 2004)

All four failure modes depend on the discontinuities inherent in the rock mass. However, while plane failure, wedge failure, and toppling are controlled by individual, clearly defined discontinuities, circular failure does not. It occurs usually in highly weathered or heavily fractured rock, consisting of very small blocks with irregular oriented discontinuities, that behaves similar to soil (Wyllie and Mah, 2004). In contrast, plane failure usually occurs if a major structural feature of planar form is present in the rock, which is weaker than the rock.

Generally, sliding will occur along this structure. The wedge failure mechanism is similar, but sliding is associated with two intersecting planes. Toppling failure usually occurs in layered or foliated rock masses and describes the instability of single blocks or slabs of rock, depending on block or slab geometry and inclination of the slope. (Goodman and Bray, 1976).

The failures observed on the investigated site are associated with two intersecting planes, i.e. the probable failure mode at least for the observed instabilities is wedge failure (see Figure 2). Hence, the focus for the following analysis is on wedge failure. All other failure mechanisms are beyond the scope of this thesis, and are not discussed further.

Figure 2: Investigated rock slope near Fleurimont with area of wedge failure (May24, 2007)

In the following sections first the data collection methodology is given. A description of the investigated site is provided, followed by a structural data analysis.

2.1 Material and methods

The field data required for the wedge analysis was collected by the author during several visits to the investigated rock slope near Fleurimont. In the summers of 2007 (May 24 and June 07) and 2008 (June 30) structural data measurements were carried out as well as measurements to determine the compressive strength of the joints.

This section describes the collected data, the measuring instruments used for the data collection, and the applied data collection method.

2.1.1 Scanline mapping

The structural data was collected using the scanline mapping technique. Scanline mapping is a geological sampling method along a defined line stretched along the investigated slope face, e.g. with the aid of a measuring tape. Along this line, the orientation of all joints intersecting the line is taken, and the place of intersection between joints and scanline is noted.

In this work scanline mapping was carried out in four steps (scanline 1 to 4) along a horizontal line of a total length of about 100 meters. The scanlines had a trend of approximately 256º and a plunge of 0º. Mapping was performed from east to west. In all, the orientation and location of 98 joints were measured. During the first visit on site, the dip and dip direction of 56 joints along two scanlines of respectively 24.40 m (scanline 1, see Figure 3) and 26.00 m (scanline 2) length were taken.

Figure 3: Scanline 1 (Fleurimont rock slope, May 24, 2007)

During the second visit, the dip and dip direction of 42 joints were measured along two scanlines with a length of respectively 24.20 m (scanline 3) and 30.30 m (scanline 4). Length and location of all four scanlines are given in Figure 4. In June 2008 a third visit took place to collect data on the variability of the slope face orientation, and to take additional measurements for the reported wedge failures. The collected data is given in detail in Annex A and B.

West   East

Scanline 4	Scanline 3	Scanline 2	Scanline 1
30.30 m	24.20 m	26.00 m	24.40 m
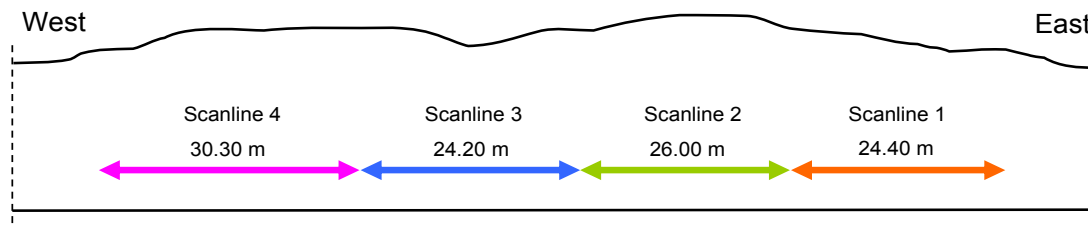
Figure 4: Length and location of scanlines 1 to 4 along the investigated Fleurimont rock exposure

For the joint orientation measurements a stratum compass COCLA ("Clar" compass) of the company Breithaupt, Germany, was used that was developed especially for geological measurements (see Figure 5). The advantage of this type of compass is the possibility to measure dip and dip direction of a plane in one step. Although a declination (i.e. the angle between magnetic north and true north) of ± 30º can be directly taken into account, no declination was considered during the field measurements. For the structural data analysis (see section 2.3) a west declination of 16º was subtracted from the measured dip direction values. This declination was determined with the aid of the magnetic declination calculator of "Natural Resources Canada" (www.geolab.nrcan.gc.ca).
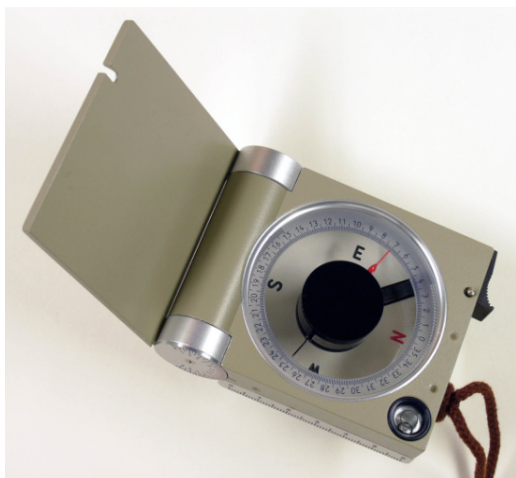
Figure 5: Stratum compass COCLA, Firma Breithaupt, Germany (www.breithaupt.de)

Figure 6: Schmidt hammer, model L, Proceq SA, Switzerland

2.1.2 Schmidt hammer measurements

The measurements for the determination of the uniaxial compressive strength of the joints were carried out with a "Schmidt hammer", model L, of the company Proceq SA, Switzerland (see Figure 6). This measuring method is an indirect test of compressive

strength. The hammer measures the rebound of a spring loaded mass impacting against the examined surface. While performing the measurements the hammer should be held right angled to the surface. The rebound values are given in an arbitrary scale ranging from 10 to 100. For the determination of the uniaxial compressive strength the rebound values have to be used with a correlation chart taking into account rebound number, rock density, and inclination of the examined surface (see Figure 7). Variations in the latter are considered by applying the corrections given in Table 1. Besides the uniaxial compressive strength (σ_c) the correlation chart also specifies the dispersion of the strength values.

At the investigated site, "spot" measurements with the Schmidt hammer were carried out. Altogether four series of ten measurements were taken on the surfaces of four joint planes. The collected data is given in Annex C.
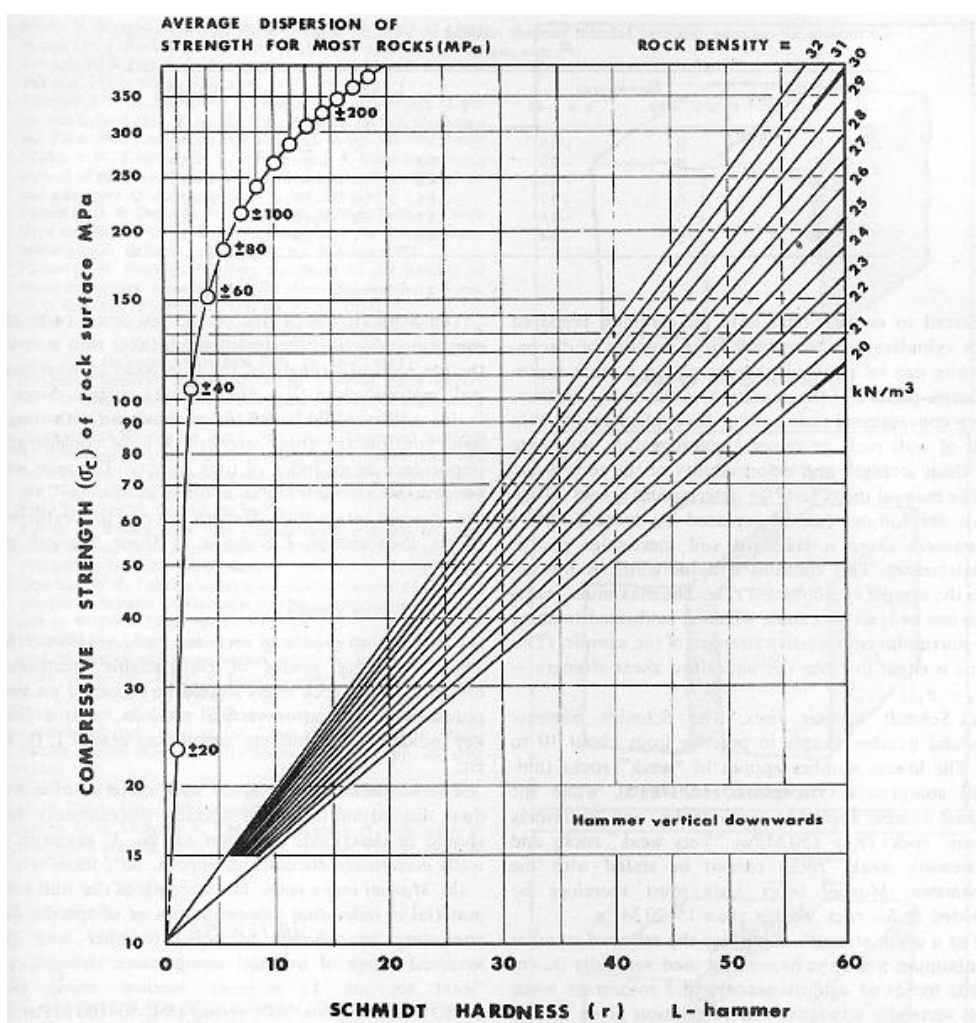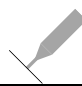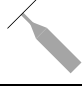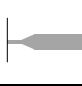
Figure 7: Correlation chart for Schmidt hammer, model L (ISRM, 1978)

Table 1: Corrections for measured Schmidt hammer rebounds for applications other than vertically downwards (after Brown, 1981)

Rebound r	downwards		upwards		horizontal
	α = -90°	α = -45°	α = +90°	α = +45°	α = 0°
10	0	-0.8	--	--	-3.2
20	0	-0.9	-8.8	-6.9	-3.4
30	0	-0.8	-7.8	-6.2	-3.1
40	0	-0.7	-6.6	-5.3	-2.7
50	0	-0.6	-5.3	-4.3	-2.2
60	0	-0.4	-4.0	-3.3	-1.7

2.2 Site description

During the construction of Highway 610 (former part of Highway 10) in 1995 at several places rock cuts were necessary for the route alignment. One of these cuts is a rock slope near Fleurimont that was investigated for this work. This section provides a description of the investigated site, including location and geology.

2.2.1 Location

The Fleurimont site is located near Sherbrooke in the south of the province of Québec. The investigated site is situated along the northern side of Highway 610 between km 1 and 2 (see Figure 8). The site coordinates, measured with GPS, are N 45° 26.412′ and W 71° 56.107′ with an error of ± 12 m. The height above sea level was measured as 144 m.
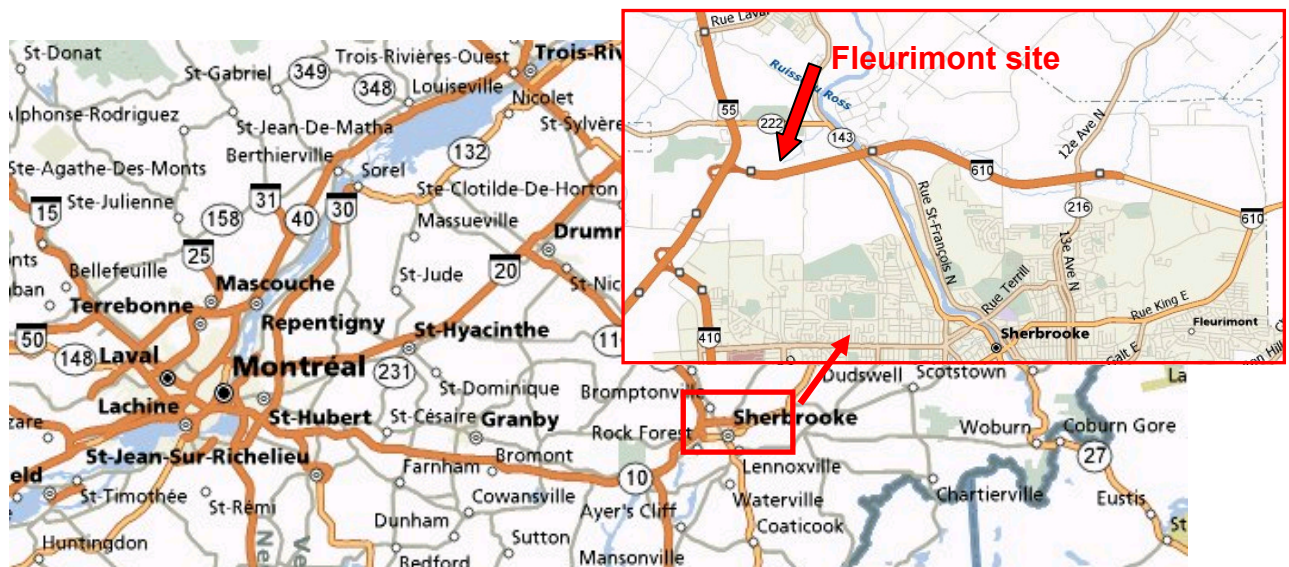
Figure 8: Location of the Fleurimont site near Sherbrooke, province of Québec

2.2.2 Geology

The Sherbrooke region belongs to the Appalachian orogenic belt, an about 400 million years old mountain range south of the St. Lawrence River that extends for more than 3000 km along the eastern margin of North America. The area has undergone orogenic (i.e. mountain building) movements, accompanied by volcanic eruptions and metamorphism, and the rocks in these regions have experienced folding, faulting, and uplift (www.atlas.nrcan.gc.ca).

The immediate region of the investigated Fleurimont site is related to the Magog group. Within this geological group six known stratigraphic units are allocated to two different geological formations, the Beauceville formation and the Saint-Victor formation. The Beauceville formation with its volcanic rocks forms the base of the Magog group, and is overlaid by the Saint-Victor formation, which consists of metamorphic and sedimentary rock, especially schist, sandstone, and siltstone (Tremblay, 1992).

The stratigraphic unit of the investigated Fleurimont site belongs to the Saint-Victor formation. The rock in this stratigraphic unit consists of blackish schist with interbeddings of sandstone or siltstone (Tremblay, 1992).

2.2.3 Description of the rock exposure

In this section a detailed description of the investigated rock slope is presented. The description procedure including the specific terms used is in accordance with Ulusay and Hudson, 2007.

The rock exposure at the Fleurimont site faces south. The area in front of the face is covered mainly with grass and smaller shrubs, whereas the top of the exposure is overgrown with trees and shrubs (see Figure 9). In front of the slope runs a small stream of water. The rock exposure has a total length of approximately 350 meters, and a maximum height of about 8 meters. The distance between rock slope and highway is approximately 12 m.

Figure 9: View along the Fleurimont rock slope in west direction (left) and east direction (right), May 24, 2007

Rock type

At the Fleurimont site, the schist is dark grey and locally penetrated by white to grey colored quartzite (see Figure 10), often arranged in thin layers. Signs of folding are visible at several places of the slope (see Figure 11). Over the total length of the exposure the rock has small cubic (up to about 0.1 cm^3) golden-colored inclusions of the sulfide mineral pyrite (see Figure 12). At places the rock surface shows russet discolorations caused by oxidation, in this case most likely as a reaction between the iron sulfide pyrite, water, and oxygen (see Figure 12). In contrast, the visible black discolorations are most probably a result of air pollution caused by car traffic.

Figure 10: Local deposits of quartzite (Fleurimont rock slope, May 24, 2007)

Figure 11: Folding of rock (Fleurimont rock slope, June 07, 2007)

Cubic, golden colored, metallic lustrous pyrite (scale in cm)
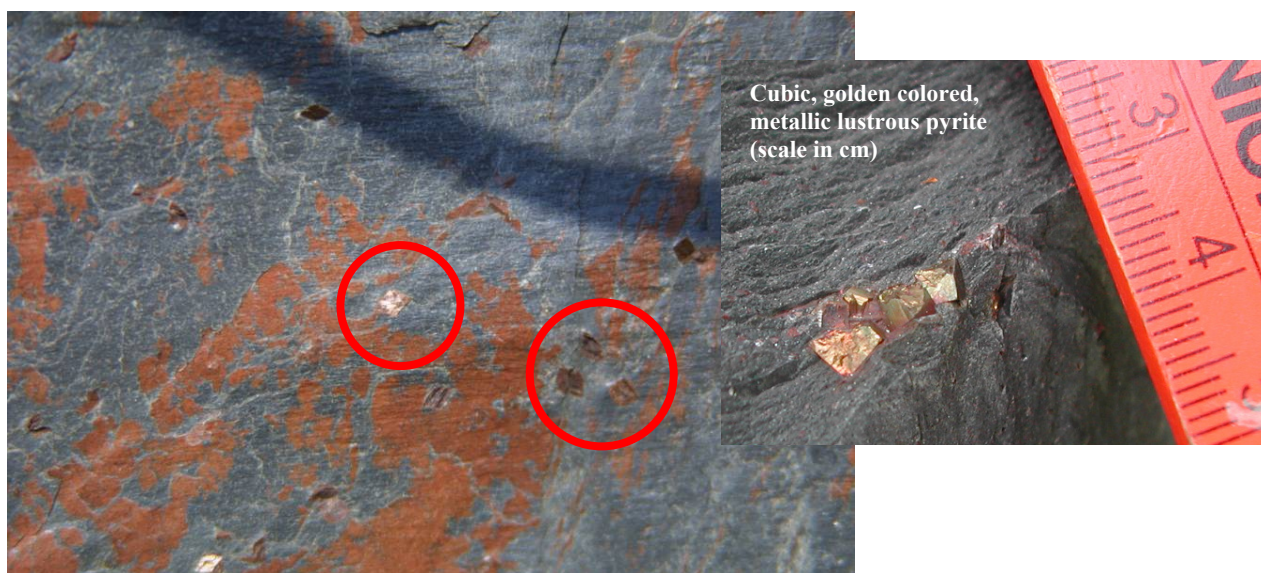
Figure 12: Discolorations on the rock surface and inclusions of pyrite (Fleurimont rock slope, May 24/ June 07, 2007)

Weathering

The rock surface is only slightly weathered, as shown by the discolorations on the surface and the small pieces of crumbled rock lying at the foot of the slope. This can be confirmed by comparing photos of the sliding plane surfaces of a failed wedge, taken in March 1995 and in May 2007 respectively (wedge B, see Figure 13). The pictures look nearly identical; the changes concern only the grown vegetation on top of the rock slope and in the area in front of the slope. Furthermore, in 2007 more black discolorations can be found especially on the surface of the right sliding plane of the wedge. However, all discontinuity traces as well as outer breaking edges and corners, which already existed in 1995, are still present in 2007. Therefore, it is a reasonable assumption that during the past twelve years the state of the exposed rock surface has changed only slightly.

Figure 13: Sliding planes of a wedge failure (wedge B) observed at the Fleurimont rock slope: March 31, 1995 (left) and May 24, 2007 (right)

Number of joint sets

Three joint sets can be distinguished on the rock surface (see Figure 14). Joint set 1 is defined by the foliation of the schist with a south-east orientation. Joint set 2 is oriented towards south-west, and approximately perpendicular to joint set 1. Joint set 3 in contrast runs subhorizontal with an orientation approximately to the north.
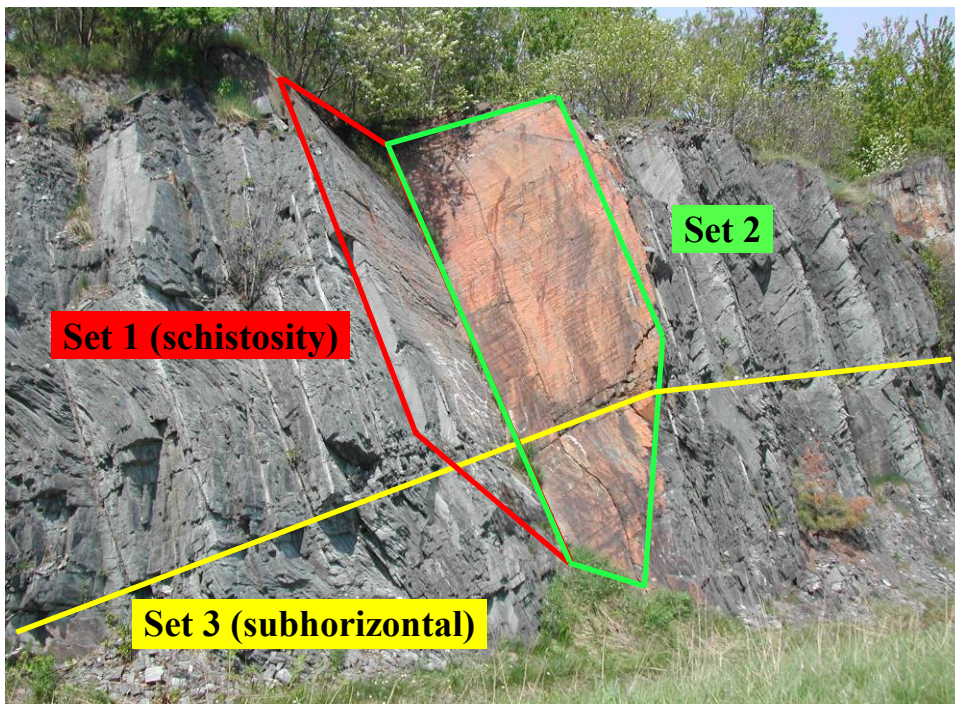
Figure 14: Joint sets identified at the Fleurimont rock slope (May 24, 2007)

Spacing

The spacing of joint set 1 varies over the length of the slope. Especially in the eastern part of the exposure locally the rock is very schistose (see Figure 15) with schist layers having a very close to close spacing (5 to 10 cm). In the other areas the spacing is moderate to wide (20 to 200 cm). The spacing of joint set 2 is moderate to very wide (about 20 cm, up to 500 cm). The spacing of joint set 3 varies between approximately 70 cm and several meters (wide to extremely wide spacing), although in some areas a moderate spacing (about 20 cm) can be found (see Figure 16).

Roughness

The joint surfaces are smooth and planar. Locally slightly rough surfaces were found, and some surfaces are undulated or folded.

Figure 15: Schistose rock in eastern part of the exposure (Fleurimont rock slope, May 24, 2007)
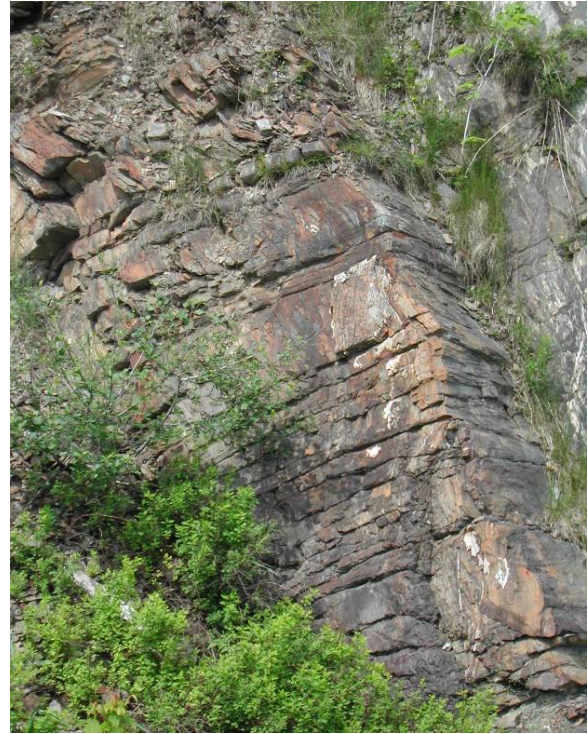
Figure 16: Subhorizontal joints (set 3) with locally moderate spacing (Fleurimont rock slope, June 07, 2007)

Aperture

The majority of the observed joints are closed. Their aperture is very tight (< 0.1 mm) to tight (0.1-0.25 mm). Only some joints have an aperture of 0.5-2.5 mm. The aperture of a minor number of gapped joints has a moderately wide opening up to 10 mm.

Filling

Most of the observed joints are not filled. Some of the gapped features have a filling consisting of crumbled rock material, and some joints are filled with thin layers of quartzite (see Figure 17).

Seepage

Apart from the small stream of water at the foot of the rock exposure nearly no water was found. Locally some discharges of water out of joints were detected (see Figure 18), but the amount of water trickling or dripping out of these joints is very small. This was the case during all site visits, including the spring of 2007 and the summer of 2008.
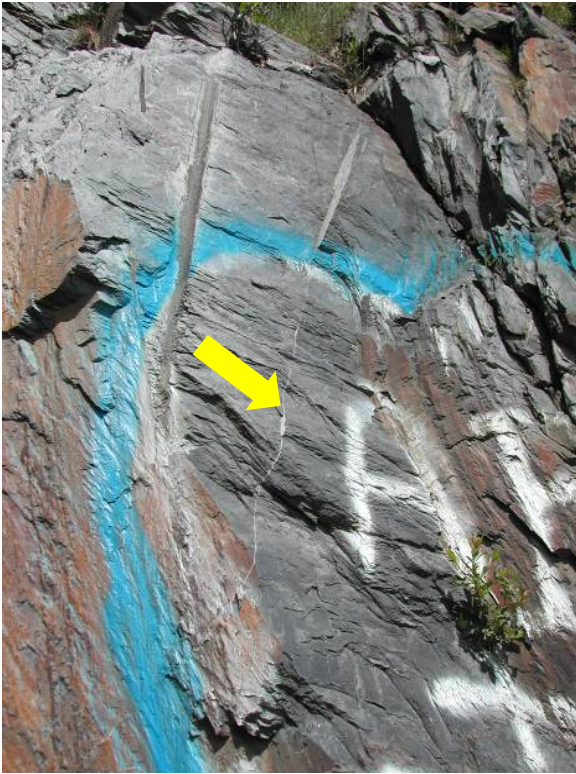
Figure 17: Thin layer of quartzite, filling a joint of set 2 (Fleurimont rock slope, June 07, 2007)

Figure 18: Water discharges out of joints (Fleurimont rock slope, June 07, 2007)

2.3 Structural analysis

In this section the structural analysis of the collected field data is described. In addition to the structural analysis the field data was analyzed statistically in view of various parameters, e.g. joint trace length and joint orientations.

The structural analysis was carried out using the software DIPS, version 5.1, a program for the analysis of orientation based geological data (Rocscience, 2008a). It allows the analysis and visualization of structural data with the aid of stereonets, e.g. the identification of joint sets within the structural data, including the calculation of mean orientations, and an assessment of the possible failure mode of a slope. Joints that do not belong to a particular joint set are defined as random joints. During the data collection no declination was considered. For the data analysis with DIPS a west declination of 16º was introduced, i.e. the measured dip direction values were reduced by 16º.

With the structural analysis the three joint sets observed on site could be identified. In Table 2 mean values and distribution of dip and dip direction are given for the major planes of all joint sets and for the slope face. Some of these values differ from the values used in Grenon et al., 2008; based on the additional data collected in June 2008 the values for the slope face orientation and the wedge planes were updated. In addition the number of joints associated with the sets is shown in Table 2. The detailed structural analysis information is given in Annex D.

Table 2: Dip and dip direction* of joint sets and slope face, and number of associated joints

	Dip (mean)	Dip direction (mean)*	Fisher's K (unweighted)	Variability (68.3%) (unweighted)	Number of joints	Percentage of joints
Set 1	72	130	33	15	59	60.2 %
Set 2	87	225	15	23	31	31.6 %
Set 3	35	318	36	15	6	6.1 %
Random	n/a	n/a	n/a	n/a	2	2.0 %
Slope face	69	166	n/a	n/a	n/a	n/a

*corrected for 16° west declination

In Figure 19 the pole plot of the sampled joints is shown. While Figure 19 a) shows the poles of all measured joints and the identified three joint sets, Figure 19 b) illustrates poles and major planes of the three sets.
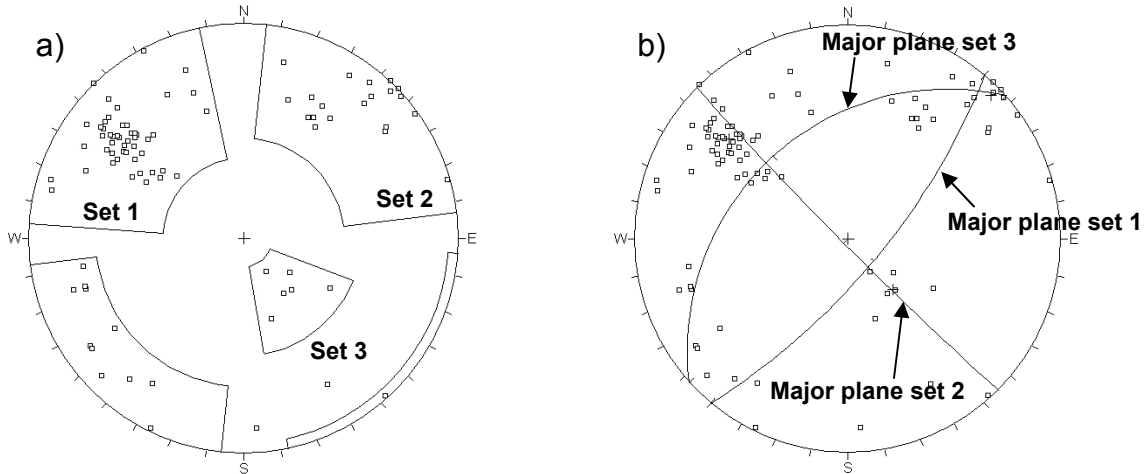
Figure 19: Stereonet a) with poles and joint sets, and b) with poles and major planes

In Figure 20 the number of joints belonging to each joint set as well as the number of joints per scanline is shown. The joints of set 1 can be found in large number over the whole length of the exposure. However, Figure 20 does not represent the total number of these joints. For several areas of pronounced schistosity, particularly in scanline 1 and 2, only one representative joint was measured. Consequently the total number of joints of set 1 is greater than presented in Figure 20. In contrast to set 1 the number of joints belonging to set 2 is clearly smaller, but also distributed over the whole length of the exposure, with a small tendency to the western part. Since the joints of set 3 run subhorizontal, i.e. roughly parallel to the scanline, and their spacing is very wide, they can be found only in a very small number along the total scanline.

The distribution of dip and dip direction is shown in Figure 21. The joints of set 1 have dip directions between 90º and 180º, whereby the great majority range between 120º and 150º. The dip directions of the joints of set 2 are distributed between 30º and 90º and between 180º and 240º. The joints of set 3 mostly have a dip direction of 300º to 330º.

The dip of all joint sets has a wider distribution. The joints of set 1 have a dip between 50º and 90º with an emphasis between 60º and 80º. The dip of the joints of set 2 varies between

60º and 90º with a focus on 70º to 90º, whereas the dip of set 3 lies between 20º and 50º. With 70º to 90º the dip distribution of the random joints correspond to that of set 2.
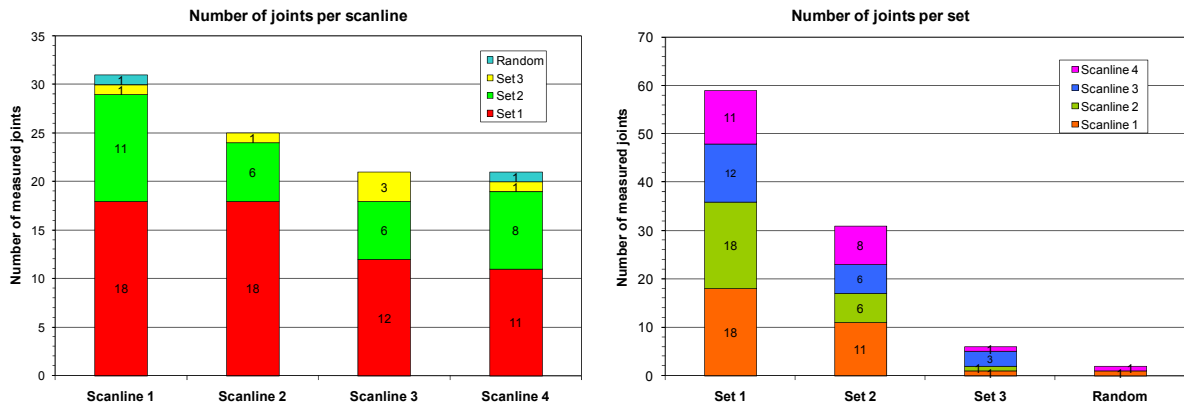
Figure 20: Number of joints per scanline (left), and per joint set (right)
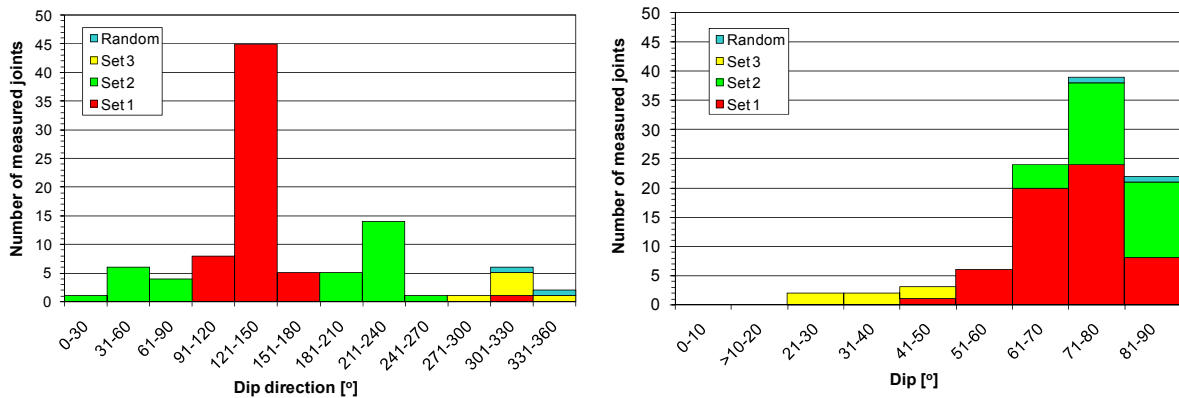
Figure 21: Distribution of joint orientation: dip direction (left) and dip (right)

In Figure 22 the trace lengths distribution is shown separately for each joint set and for the random joints. Most joints of set 1 have small trace lengths up to 1 meter. The longer the trace length (up to 8 meters), the smaller the number of measured joints of set 1. In view of the relatively small sample numbers, it is difficult to assign with confidence the measured trace lengths to a certain probability distribution. The regular distributed trace lengths of set 1 with their decreasing number of joints for increasing joint lengths can be classified as negative exponential distributed. In contrast, the joints of set 2 have a uniform distribution with approximately the same number of joints for trace lengths between 1 and 4 meters. Fewer joints were mapped with smaller (0 to 1 meters) and longer (4 to 5 meters) lengths.

In addition, with 7 to 8 meters several mapped joints extend over the total height of the rock exposure. The data about the trace lengths of set 3 is not very meaningful, since only a few of these subhorizontal joints were mapped and, caused by their orientation, the correct determination of the trace lengths was difficult.
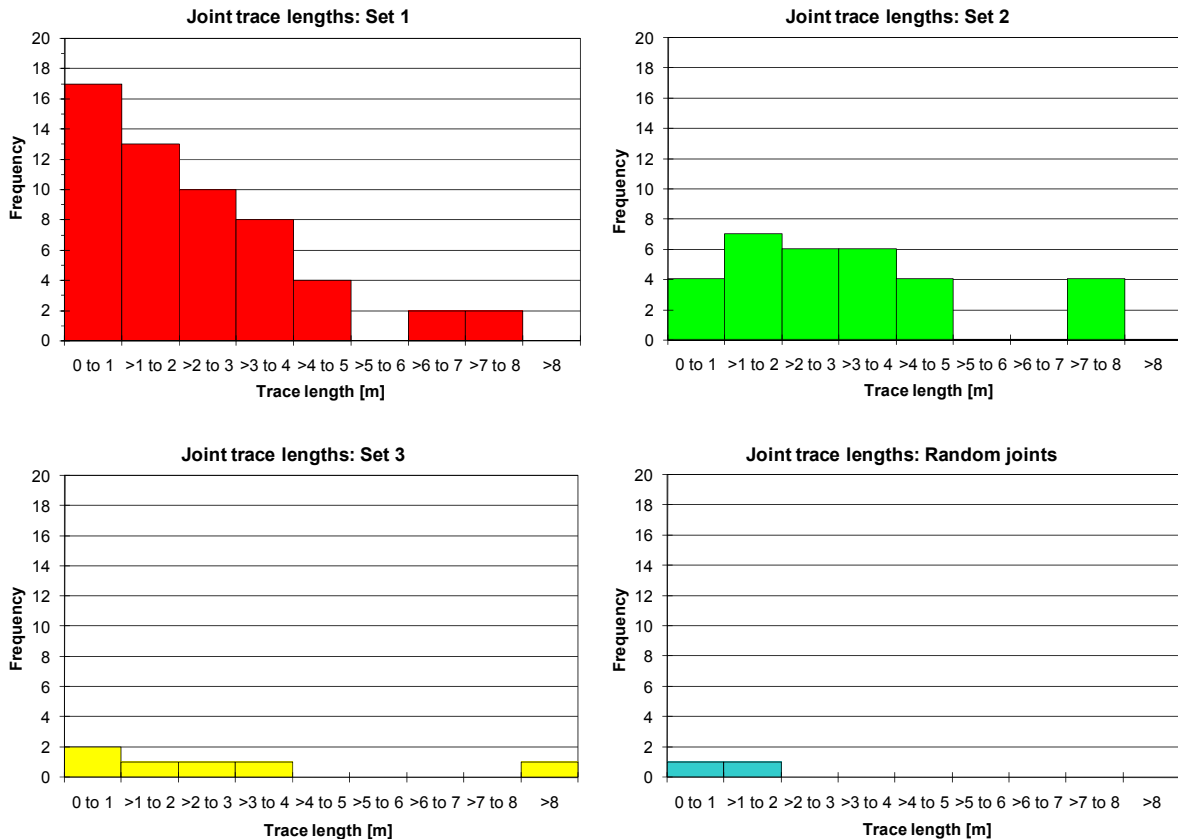
Figure 22: Joint trace lengths distribution per joint set

Mean trace length as well as joint frequency and spacing for all three joint sets are given in Table 3. In accordance with Priest, 1993 the joint frequency along the sampling line was calculated for each joint set by dividing the number of mapped joints (see Table 2) by the total length of the scanline (l_{total} = 104.9 m). The reciprocal of the joint frequency of each set provides the mean joint set spacing.

Table 3: Mean values of joint trace length, spacing, and joint frequency

	Mean value of joint trace length [m]	Joint frequency λ [joints/m]	Joint spacing 1/λ [m]
Joint set 1	2.6 (stdev 1.8)	0.6	1.8
Joint set 2	3.5 (stdev 2.1)	0.3	3.4
Joint set 3	3.4 (stdev 3.5)	0.1	17.5
Random joints	1.5 (stdev 0.6)	-	-

Most of the observed joints have one defined termination and one undefined or obscured one. Generally the lower ending is undefined, since it is obscured by the ground. If also the upper ending is undefined, the joint usually ends outside the exposure. A defined termination means that the joint ends in another joint or in intact rock. In Figure 23 the number of joints per set regarding their termination is shown. For several joints (23 % of all joints) no information about the ends was recorded on site. This is a recognized shortcoming of this work.
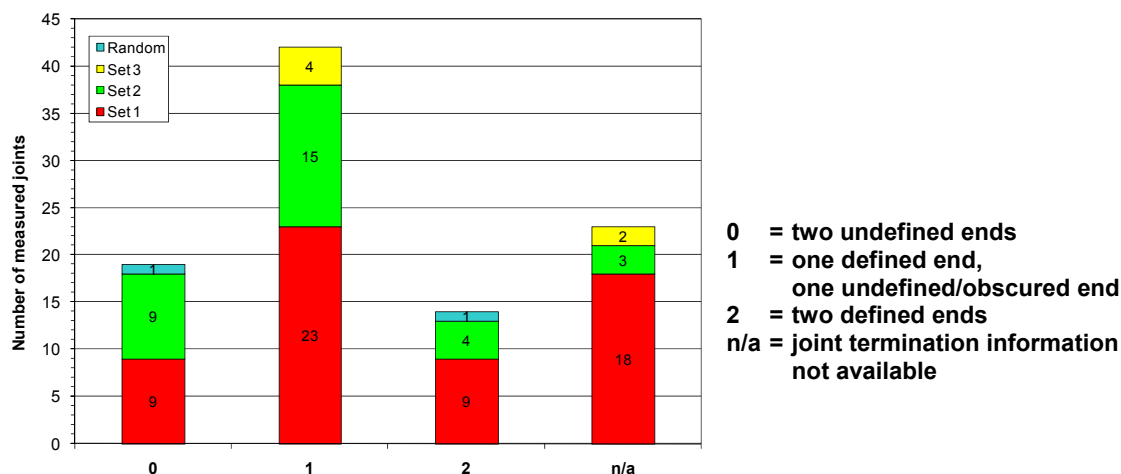
Figure 23: Joint termination

Only 14 % of all measured joints have two defined ends, i.e. only for these joints the "true" joint trace lengths were determined. For most of the joints (62 %) only the visible lengths or, according to Villaescusa and Brown, 1992, the "censored" lengths were recorded. To account for this censoring bias, the mean trace lengths were corrected by using an approach provided by Villaescusa and Brown, 1992 (referring to Laslett, 1982) that results in the following equation for the estimation of unbiased mean trace lengths.

$$\mu_L = \frac{\sum_{i=1}^{n} X_i + \sum_{j=1}^{m} Y_j + \sum_{l=1}^{p} Z_l}{2n+m}$$

With:

μ_L	Mean trace length [m]
$X_1, ..., X_n$	Observed trace lengths with both ends observable [m]
$Y_1, ..., Y_m$	Observed trace lengths with one end observable [m]
$Z_1, ..., Z_p$	Observed trace lengths with no ends observable [m]

As input data for this approach trace lengths measured along a scanline are required. Since this is in accordance with the data and the data collection procedure used in this case study, the approach of Villaescusa and Brown, 1992 was considered as best fit. There are several other approaches available; however, these were not applicable to this case study due to differences regarding the sampling method (e.g. Kulatilake and Wu, 1984, who used window mapping, or Zhang and Einstein, 1998, who used circular windows) or the sampled data (e.g. Priest and Hudson, 1981, who sampled semi trace lengths of joints).

The unbiased mean trace lengths calculated after Villaescusa and Brown, 1992 are given in Table 4. The detailed calculation is provided in Annex E.

Table 4: Biased and unbiased mean joint trace lengths (calculated according to Villaescusa and Brown, 1992)

	Biased mean trace length [m]	Unbiased mean trace length [m]
Joint set 1	2.6 (stdev 1.8)	2.2
Joint set 2	3.5 (stdev 2.1)	4.0
Joint set 3	3.4 (stdev 3.5)	1.8

The mean trace length of the subhorizontal joint set 3 is based on only a few joints measured along the horizontal scanline. This leads to the orientation bias within the collected data. Villaescusa and Brown, 1992 state that "joints striking parallel to the surveying line are sampled to a lesser degree than joints striking normal to the sampling direction." This can be avoided by sampling not only in horizontal, but also in vertical direction. As a shortcoming of this work, this bias was not corrected due to unavailable data.

According to Villaescusa and Brown, 1992 there are two further biases related to scanline mapping that have to be taken into account in the data analysis.

1. Truncation bias: observations below or above a certain value are disregarded during field mapping (e.g. traces shorter than 100 mm)

2. Size bias: large joints have a greater probability i) to intersect the rock surface and ii) of being sampled than small joints

The truncation bias can be considered either by the sampling method or, according to Villaescusa and Brown, 1992, by applying an analytical method (e.g. Warburton, 1980). In this work the truncation bias was avoided by mapping all joints intersecting the scanline, independent of their length.

As stated in Villaescusa and Brown, 1992 the above-named censoring bias correction adjust also the second aspect of the size bias (probability of joints of being sampled). According to Villaescusa and Brown, 1992 the first aspect of the size bias (probability of joints of intersecting the rock surface) has an influence on the simulated average joint size in 3D joint system models. Since in the following analysis the measured and simulated unbiased trace lengths were compared, but not the joint sizes (see section 3.3, 3D joint system analysis), the correction of this size bias aspect was considered as of minor interest for this work and, therefore, disregarded.

2.4 Determination of analysis input data out of field data

Most of the necessary input data for the wedge analysis was determined by field measurements (like joint orientation, joint geometry, etc.), visual investigation (like alteration, etc.), and with the structural analysis (like mean trace length, joint frequency, etc.). Out of the collected field data further input parameters were determined: the uniaxial compressive strength (σ_c) and the shear strength parameters (friction angle and cohesion).

2.4.1 Joint compressive strength

The uniaxial compressive strength σ_c of the joints was determined using the "Schmidt hammer" rebound numbers taken on joint surfaces on site (see section 2.1.2). Two series of measurements were taken for both joint sets 1 and 2. According to Ulusay and Hudson,

2007 the mean values of the determined rebound numbers were calculated with the five highest values of each measurement of ten values (see results in Annex C). With the correlation chart and the corrections for non-vertical hammer orientation (see section 2.1.2, Figure 7 and Table 1) a mean value for the uniaxial compressive strength was determined as well as the dispersion of this value. The results for an assumed average rock unit weight of $\gamma = 2.6$ t/m^3 are shown in Table 5.

Table 5: Uniaxial compressive strength of the joints (for $\gamma = 2.6$ t/m^3)

	Set 1	Set 2	Set 1 + 2
Mean value of rebound numbers [-] (determined with the upper 50% rebound numbers)	49.9 (stdev 2.7)	49.5 (stdev 1.6)	49.7 (stdev 0.3)
Corrected mean value of rebound numbers [-] (corrected with -2.2 for a horizontal hammer orientation)	47.7	47.3	47.5
Uniaxial compressive strength σ_c [MPa] (determined with correlation chart)	124	122	123
Dispersion [MPa] (determined with correlation chart)	$\pm$ 50	$\pm$ 50	$\pm$ 50

2.4.2 Shear strength parameter

The shear strength parameters friction angle and cohesion were determined with the aid of the Barton-Bandis strength criterion for joints (Barton and Choubey, 1977). The determination was carried out as sensitivity analysis for a range of input parameter values using the software RocData, version 4.0 (Rocscience, 2008c). The empirical Barton-Bandis criterion calculates the maximum shear strength of joints with the following equation:

$$\tau = \sigma_n \tan\left[\text{JRC} \log_{10}\left(\frac{\text{JCS}}{\sigma_n}\right) + \varphi_r \right]$$

With:

τ	Maximum shear strength [MPa]
σ_n	Applied normal stress [MPa]
JRC	Joint roughness coefficient [-]
JCS	Joint wall compressive strength [MPa]
φ_r	Residual friction angle [°]

The joint roughness coefficient (JRC) was determined using the chart provided in Figure 24. Regarding the mostly smooth and planar joint surfaces the joint roughness coefficient was determined to JRC = 0 to 2. The joint wall compressive strength (JCS) corresponds to the strength values determined with the aid of Schmidt hammer measurements (see section 2.4.1). Hence JCS = 123 MPa with a variation of ± 50 MPa was applied.

The residual friction angle was determined for dry slate, and, referring to Barton, 1973, the range was set to φ_r = 25 to 30°. The input values are summarized in Table 6.

TYPICAL ROUGHNESS PROFILES for JRC range:

1	0 - 2
2	2 - 4
3	4 - 6
4	6 - 8
5	8 - 10
6	10 - 12
7	12 - 14
8	14 - 16
9	16 - 18
10	18 - 20

0   5   10 cm   SCALE
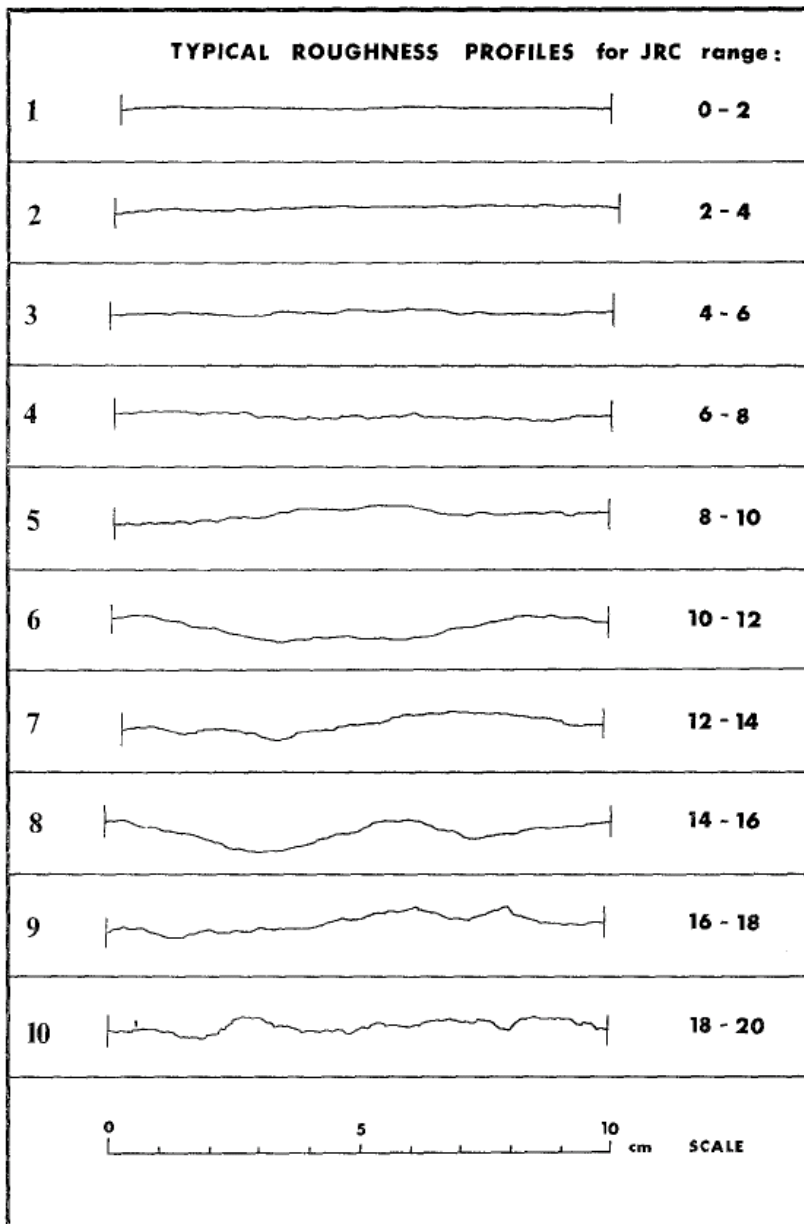
Figure 24: Roughness profiles and corresponding range of JRC values (Barton and Choubey, 1977)

Table 6: Input data for determination of joint shear parameters friction angle and cohesion

Parameter	Source	Range	Average
Joint roughness coefficient JRC [-]	Determined with roughness profile chart	0 - 2	1
Joint wall compressive strength JCS [MPa]	Determined with Schmidt hammer measurements	73 - 173	123
Residual friction angle φ_r [°]	Provided by Barton, 1973 for dry slate	25 - 30	27.5

Out of this input data RocData (Rocscience, 2008c) calculates the shear parameters friction angle and cohesion. The resulting values are given in Table 7. An average friction angle of $\varphi = 30°$ was calculated for the average input parameter values (JRC = 1, JCS = 123 MPa, φ_r = 27.5°). The range was between 25° and 35.3°. The resulting average cohesion tends to zero, and the differences for different parameter combinations are marginal. The analysis results in detail are provided in Annex F. As mean values for the following wedge analysis a friction angle of $\varphi = 30°$ and a cohesion of $c = 0$ MPa was defined.

Table 7: Joint friction angle and cohesion

Parameter	Range	Average	Mean values chosen for analysis
Friction angle φ [°]	25.0 - 35.3	30.0	30
Cohesion c [MPa]	0 - 0.002	0.001	0

2.5 Summary

In this first case study a rock slope of about 8 m height and 350 m length along a road cut was investigated. The slope is situated in layered schist and has experienced wedge failures during the construction of the road in 1995. Although no further failures were observed since then, the slope was investigated during the summers of 2007 and 2008. The objective was to determine if the wedge failures could have been predicted, and to assess the probability of wedge failures. Rock mass data was collected on site to enable a slope stability analysis for wedge failure and a back-analysis of the observed wedge failures using deterministic and probabilistic analysis tools.

The field data was collected by horizontal scanline mapping, carried out along a 100 meters long section of the exposure. Thereby information about all joints intersecting the scanline, like orientation, spacing, and trace length, were recorded. In addition measurements with the "Schmidt hammer" were carried out to determine the compressive strength of the joints. The complete field data is provided in Annex A, B, and C. With the field data several input parameters for rock classification and wedge analysis were determined.

In this chapter the rock mass was described in detail, and a structural analysis of the collected field data was carried out. Three joint sets were determined in the rock mass. For these joint sets several parameters like spacing, joint frequency, and mean trace lengths were evaluated. The latter was corrected regarding the censoring bias inherent in the field data due to the data collection method.

3 Wedge stability analysis for the Fleurimont rock slope

In this chapter the results of the wedge stability analysis are presented. First a kinematic analysis was performed to evaluate the kinematic feasibility for the two large wedges observed during the construction of the highway. Kinematic feasibility of wedge instability was also evaluated for the three identified joint sets. This was followed by a deterministic limit equilibrium back-analysis for the two observed wedges.

The second part of this chapter describes how the structural data, collected during site visits in 2007 and 2008, was used to investigate the frequency and the stability of wedges along the length of the exposure. It provides the results of limit equilibrium wedge analyses. This involved a probabilistic analysis of individual wedges, and a 3D joint system analysis as described in Grenon and Hadjigeorgiou, 2008a. The latter was used to further investigate the potential of wedge instability along the crest of the rock slope.

3.1 Kinematic analysis

The observed failure mode in the investigated area is wedge failure. Approximately in the middle of the rock exposure the sliding planes of two large wedges are visible (wedges A and B, see Figure 25 and Figure 26). The wedge heights were about 4.5 m and 8.0 m respectively. Both wedges were exposed during the highway construction in 1995; wedge A failed during construction, while wedge B was blasted as a precautionary measure.

According to Hudson and Harrison, 1997 the kinematic feasibility of wedge instability involves the following criteria (see Figure 27):

1. The dip of the slope (ψ_s) must exceed the plunge of the intersection line (ψ_i) of the two discontinuity planes associated with the potentially unstable wedge ($\psi_s > \psi_i$).

2. The intersection line of the two discontinuity planes associated with the potentially unstable wedge must daylight on the slope plane.

3. The plunge of the intersection line (ψ_i) of the two discontinuity planes associated with the potentially unstable wedge must be such that the strengths of the two planes are

reached; for friction-only case: the plunge of the intersection line must exceed the angle of friction ($\psi_i > \varphi$).

Figure 25: Wedge A (Fleurimont rock slope, May 24, 2007)
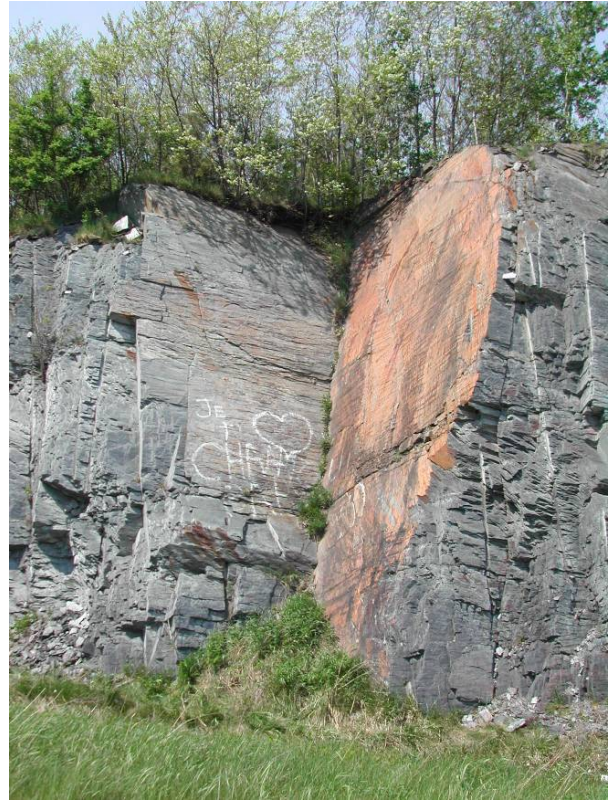
Figure 26: Wedge B (Fleurimont rock slope, May 24, 2007)
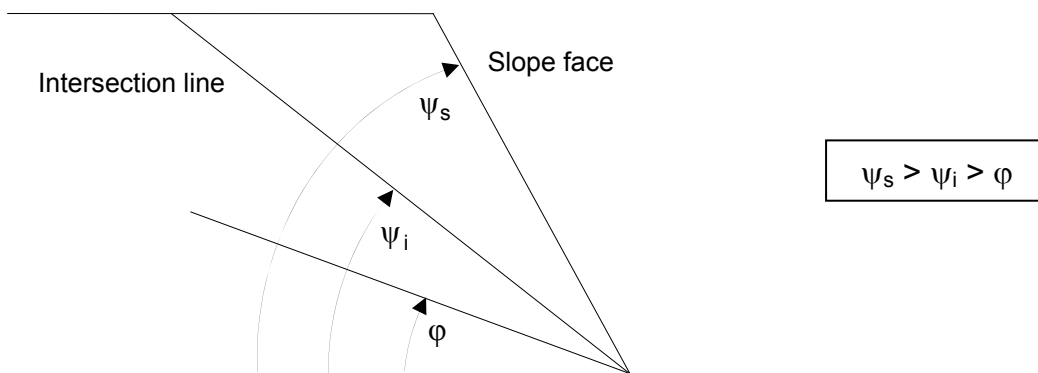
Figure 27: Criteria for kinematic feasibility of wedge failure

In Table 8 the dip of the slope, the friction angle, and the plunge of the intersection line are given for wedges A and B as well as for the major planes of all three possible joint set

combinations. The major planes are defined by the mean orientation values of the joint sets. It can be noted that criterion 1 ($\psi_s > \psi_i$) is not fulfilled for the combination of joint sets 1 and 2 since the plunge of the intersection line ($\psi_i = 71°$) is greater than the mean slope inclination ($\psi_s = 69°$). Criterion 3 ($\psi_i > \varphi$) is not satisfied for the combination of joint sets 1 and 3 since the plunge of the intersection line is smaller than the friction angle. For all joint set combinations criterion 2 is not satisfied as demonstrated in the stereonet in Figure 28. The intersection line of the major planes of all three joint set combinations do not daylight on the slope plane, caused either by the dip direction of the intersection line or by the nonconformity of criterion 1. Therefore, kinematic feasibility was not established for the major planes of all three joint set combinations using the mean orientation values. However, since wedges were observed on site there must have been kinematic feasibility due to "variations" of the defined major planes.

Considering a measured mean slope angle of $\psi_s = 69°$ in the vicinity of wedge A and of $\psi_s = 67°$ in the vicinity of wedge B, and intersection lines inclined by 64° and 58° respectively, the criteria 1 and 3 for kinematic feasibility are fulfilled for both wedges. Since criterion 2 is also satisfied (as shown in Figure 29), both wedges are kinematically feasible.

Taking into account slope and joint set orientations as well as the two observed wedges formed form joints belonging to set 1 and 2, wedges along the slope are most probably formed by a combination of joint sets 1 and 2.

Table 8: Assessment of kinematic feasibility (criterion 1 and 3)

	Dip of slope ψ_s [°]	Plunge of intersection line ψ_i [°]	Friction angle φ [°]
Major planes of joint sets 1 and 2	69	71	30
Major planes of joint sets 1 and 3	69	5	30
Major planes of joint sets 2 and 3	69	35	30
Wedge A	67	64	30
Wedge B	69	58	30
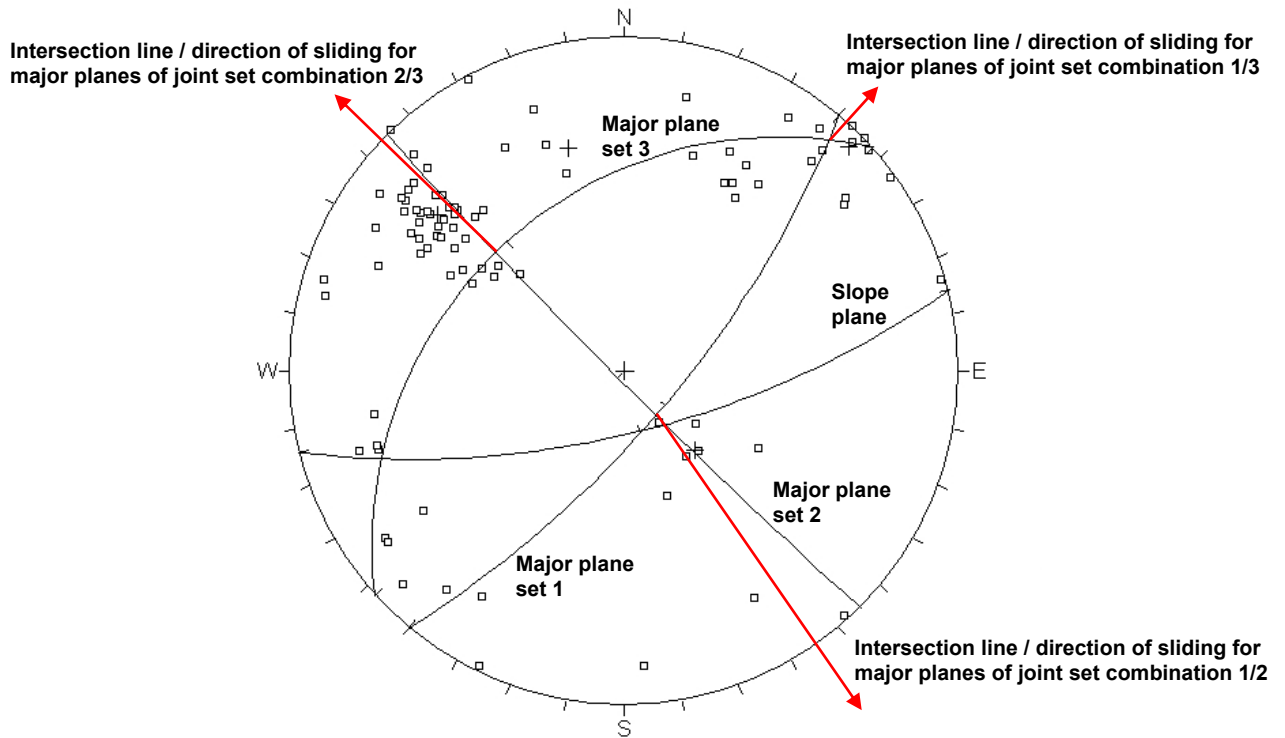
Figure 28: Stereonet with major planes of joint sets and slope plane (Fleurimont rock slope)
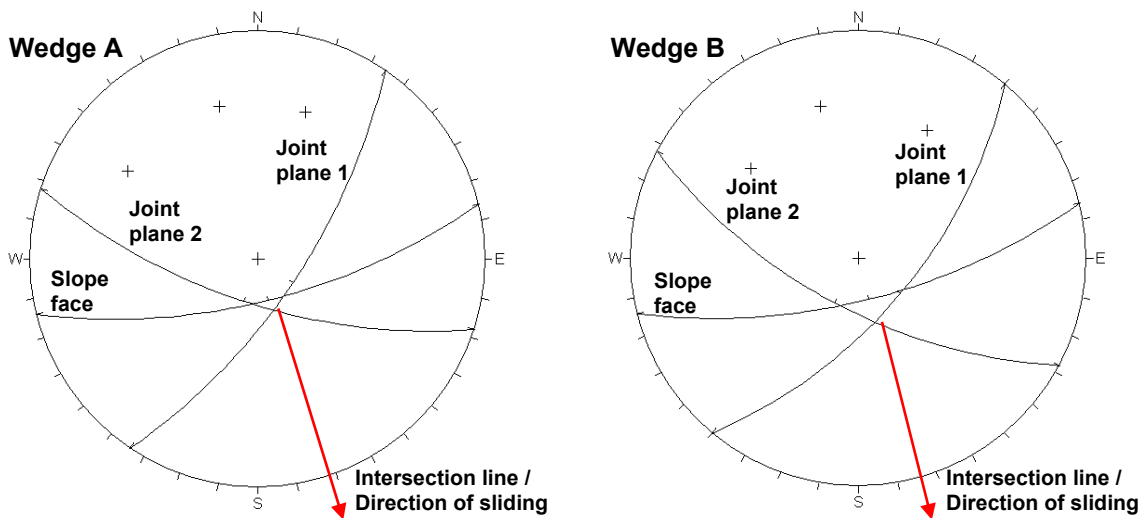
Figure 29: Stereonet wedge A (left) and wedge B (right) (Fleurimont rock slope)

3.2 Wedge analysis

The software SWEDGE, version 5.0 (Rocscience, 2008d) was used to evaluate the geometry and the stability of surface wedges. The program allows a deterministic limit equilibrium analysis with the calculation of a factor of safety (FS) for a specific wedge as well as a probabilistic limit equilibrium analysis to determine the failure probability of a wedge. The program enables only the stability analysis of a specific pair of discontinuities, i.e. of individual wedges; it is not possible to assess the stability of the whole length of a rock slope.

Using SWEDGE 5.0 the following main assumptions and limitations have to be considered:
- Wedges are defined by two intersecting discontinuities
- Discontinuities are persistent
- Wedges are moving as rigid bodies with no internal deformation
- Wedges are moving as one block without unravelling
- Sliding takes place along a plane or along the line of intersection
- Direction of sliding is parallel to line of intersection
- Discontinuity surfaces are perfectly planar
- Failure mode is a translational slip (no rotation or toppling)
- All acting forces pass through the centroid of the sliding block

By default SWEDGE always calculates the maximum sized wedges, which are formed by the persistent joints. The "scale down" option can be used to reduce the joint trace lengths according to measured lengths, and to calculate smaller wedge sizes.

The following sections provide the results of limit equilibrium wedge analyses. The stability of the two observed wedges was assessed with a deterministic back-analysis (stability described by factor of safety), followed by a probabilistic analysis of the three identified joint sets (stability described by probability of failure). The SWEDGE deterministic analysis information is given in Annex G (for wedge A) and H (for wedge B). The SWEDGE probabilistic analysis information (for joint set combination 1 and 2) is given in Annex J.

3.2.1 Back-analysis of two failed wedges

In this section the deterministic limit equilibrium back-analysis of two observed wedges (wedge A and wedge B, see Figure 25 and Figure 26) is described. These two large wedges were formed by joints of joint set 1 and 2. The input data for the back-analysis is provided in Table 9.

As mentioned above, the software SWEDGE assumes an infinite joint length. Since the values for the trace lengths are known, the back-analysis was carried out with the scale down function, which allows the input of defined trace lengths. The analysis was carried out as sensitivity analysis for the joint shear parameters cohesion and friction angle and for the unit weight of the rock, i.e. these parameters were varied to assess their influence on the stability of the two wedges. The variation range is given in Table 10. The range for friction angle and unit weight was chosen considering the average values defined in section 2.4.2. The influence of cohesion was examined by introducing successively cohesion in a range from 0 to 1 t/m^2.

Table 9: Input data, used for back-analysis of wedge A and B

		Wedge A	Wedge B
Joint 1: Dip / Dip direction*	[º]	69 / 124	63 / 130
Joint 2: Dip / Dip direction*	[º]	68 / 198	65 / 208
Joint 1: Trace length	[m]	4.20	8.00
Joint 2: Trace length	[m]	4.00	8.00
Slope height	[m]	4.50	8.00
Intersection line: Plunge / Trend	[º]	64 / 163	58 / 166
Slope face: Dip / Dip direction	[º]	69 / 166	67 / 166

*corrected for 16° west declination

Table 10: Variation range for parameters cohesion, friction angle, and unit weight, used for back-analysis of wedge A and B

Cohesion c	[t/m^2]	0 - 1
Friction angle φ	[º]	28 - 40
Unit weight γ	[t/m^3]	2.6 - 2.8

The results of the sensitivity analysis are presented in Figure 30 (wedge A) and in Figure 31 (wedge B), whereby only the upper and lower extremes are shown. The results for all other analyzed parameter combinations range between the given extremes. All resulting factors of safety (FS) calculated for the different parameter combinations are given in Annex I.

The results show that the influence of the variation in unit weight on the factor of safety is not significant for both wedges, especially for factors of safety FS $\leq$ 1.0. The influence of a varying friction angle on the wedge stability is also small. For wedge A the factor of safety increases by 0.18 by increasing the friction angle from 28° to 40°. The influence for wedge B is slightly stronger. For a friction angle increasing from 28° to 40° the FS increases by 0.24. The crucial factor of influence on the stability of both wedges is cohesion. The introduction of a small cohesion leads to an immediate increase of the factor of safety. For wedge A a minimum cohesion of 0.14 t/m^2 (for φ = 40°) and a maximum cohesion of 0.21 t/m^2 (for φ = 28°) is required to reach a factor of safety FS = 1.0. For equilibrium of wedge B a cohesion between 0.30 t/m^2 (for φ = 40°) and 0.53 t/m^2 (for φ = 28°) respectively is necessary.

Furthermore, in Figure 30 and Figure 31 the results for average joint properties, as defined in section 2.4.2, are shown. For the average case of friction angle φ = 30°, cohesion c = 0 t/m^2, and unit weight γ = 2.6 t/m^3 no stable conditions were reached for both wedges. For this case a factor of safety FS = 0.34 was calculated for wedge A, and FS = 0.44 for wedge B. To reach equilibrium with the average values φ = 30° and γ = 2.6 t/m^3 a cohesion of c = 0.18 t/m^2 (for wedge A) and of c = 0.46 t/m^2 (for wedge B) is required. A summary of these results is provided in Table 11.

In addition the calculated volume and weight for both wedges are given in Table 11. For wedge A a volume of 0.5 m^3 (corresponding to an approximate weight of 1.3 t) was calculated. The volume of wedge B was evaluated to 8.9 m^3, which corresponds to a weight of 23.0 t.

Wedge A: sensitivity analysis
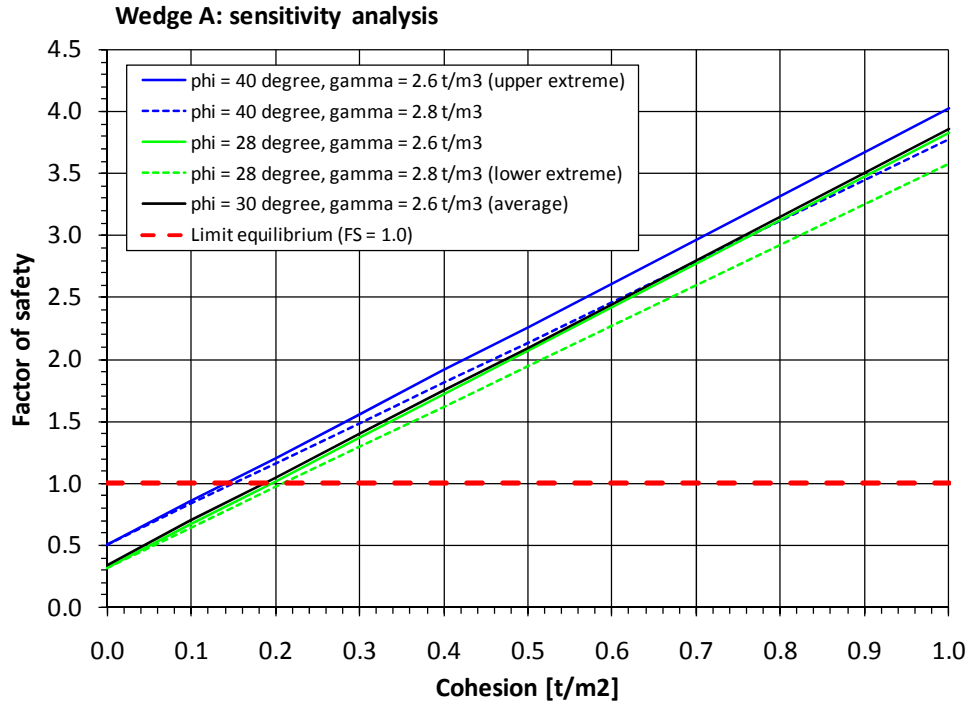
Figure 30: Sensitivity analysis for unit weight, cohesion, and friction angle for wedge A

Wedge B: sensitivity analysis
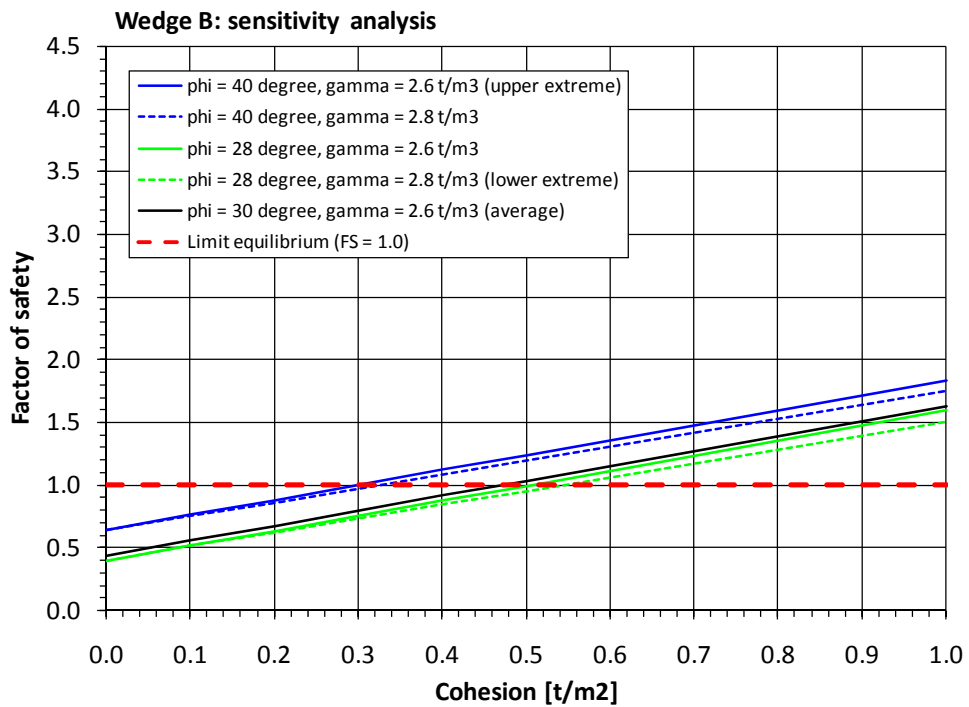
Figure 31: Sensitivity analysis for unit weight, cohesion, and friction angle for wedge B

Table 11: Back-analysis results for wedge A and B

		Wedge A	Wedge B
Average values for:			
Joint friction angle φ	[°]	30	30
Joint cohesion c	[t/m^2]	0	0
Unit weight of rock γ	[t/m^3]	2.6	2.6
FS for average values of φ, c, and γ	[t/m^3]	0.34	0.44
Required cohesion for equilibrium (FS = 1.0)	[t/m^2]	0.2	0.5
Wedge weight	[t]	1.3	23.0
Wedge volume	[m^3]	0.5	8.9

The back-analysis results correspond to the fact that wedge A failed. Considering that wedge B was blasted, this wedge was near equilibrium or stable. One reason for the stability could be that the foot of the wedge was supported, so that the wedge could not fail. It is also possible that the wedge did not fail as one single wedge, but as several pieces.

3.2.2 Probabilistic analysis of individual wedges

In this section the probabilistic limit equilibrium analysis of individual wedges is described. The analysis was carried out using the rock mass data for the whole slope, and included the investigation of the influence of dispersion in joint set data on the rock behaviour.

As mentioned above, the software SWEDGE analyses the probability of failure of individual wedges without regarding the spatial distribution of wedges along a rock slope.

As input data for the probabilistic analysis the mean orientation values of the joint sets were used (see section 2.3). The probability of wedge failure was determined for the major planes of the joint sets, taking into account the mean joint set orientations (i.e. mean dip and mean dip direction) and their dispersion around the mean. The dispersion was described by a Fisher distribution, as proposed by Priest, 1993 for discontinuity orientation data. The Fisher distribution describes the angular distribution of orientations about a mean orientation vector. The distribution is symmetric about the mean, and the dispersion is expressed by the Fisher constant (K). K describes the tightness of an orientation cluster; a large K-value implies a tight cluster, and a small K-value implies a more dispersed cluster. The K-values used in this analysis were determined in the structural analysis in section 2.3.

A preliminary analysis with SWEDGE for unscaled wedges led to unrealistically large wedges with joint trace lengths of more than the slope height of 8 m. Therefore, the stability analysis was carried out for wedges that were scaled in view of their trace lengths. As input data the unbiased mean trace lengths, determined in section 2.3, and the average values for friction angle, cohesion, and unit weight, as determined in section 2.4, were used. No dispersion of these parameters was considered. All input data is summarized in Table 12 and Table 13.

Table 12: Input data for probabilistic wedge analysis: joint orientation and geometry

		Joint set 1	Joint set 2	Joint set 3	Slope
Dip / Dip direction* (mean)	[º]	72 / 130	87 / 225	35 / 318	69 / 166
Fisher K (for dip and dip direction)	[º]	33	15	36	--
Unbiased mean trace length	[m]	2.20	4.00	1.80	--
Height	[m]	--	--	--	8

*corrected for 16° west declination

Table 13: Input data for probabilistic wedge analysis: average values for friction angle, cohesion, and unit weight

		Joint set 1, 2, and 3
Friction angle φ	[º]	30
Cohesion c	[t/m^2]	0
Unit weight γ	[t/m^3]	2.6

Since in SWEDGE wedges are defined by two intersecting joints, only wedges along the crest of the slope are taken into account. Wedges that form within the slope face by the intersection of three joints cannot be calculated.

All three possible joint set combinations (sets 1-2, 1-3, and 2-3) were analyzed using a Monte Carlo sampling method with a number of 10,000 samples. Within these samples SWEDGE defines all valid wedges, i.e. all kinematically feasible wedges that can be removed from the slope, irrespective of whether a wedge is stable or unstable. The total number of valid wedges is the sum of all unstable (FS < 1.0) and stable (FS ≥ 1.0) wedges that form at the slope crest.

In SWEDGE the probability of failure (PF) is defined as number of failed wedges / number of samples, and describes the "overall probability of wedge failure for a given set of probabilistic input data" (Rocscience, 2008d). As another approach of probabilistic failure SWEDGE calculates the probability of sliding (PS) defined as number of failed wedges / number of valid wedges. PS describes the probability that a valid wedge will fail. In Table 14 the analysis results for sliding and failure probability are shown.

The results suggest that it is mainly joint set combination 1-2 that forms unstable wedges along the crest of the slope, and that the joint combinations 1-3 and 2-3 are of minor importance for wedge failure. The combination of joints out of set 2 and 3 forms nearly no wedges. In contrast, joints belonging to combination 1-3 form many wedges, but nearly all of them are stable. A look at the distribution of the trend of the intersection lines (see Figure 32) shows that the potential sliding direction of these wedges does not agree with the dip direction of the slope of 166°, i.e. the intersection lines of joint combination 1-3 do not daylight in the slope. Hence, the second kinematic criterion for wedge failure (see section 3.1) is not fulfilled for joint combination 1-3. As a result, the probability of failure for the joint combinations 1-3 and 2-3 is nearly zero (PF = 0.0001). The subhorizontal joint set 3 does not contribute to wedges formed along the slope crest. Consequently, only joint set combination 1-2 is further analyzed in this chapter.

Table 14: Wedge sliding and failure probability (for scaled wedge trace lengths)

	Joint set combination 1-2	Joint set combination 1-3	Joint set combination 2-3
Samples	10,000	10,000	10,000
Valid wedges (kinematically feasible wedges)	3815	3439	3
Failed wedges (wedges with FS < 1.0)	3666	1	1
Stable wedges (wedges with FS ≥ 1.0)	149	3438	2
Probability of failure (ratio of failed wedges to number of samples)	0.3666	0.0001	0.0001
Probability of sliding (ratio of failed wedges to valid wedges)	0.9609	0.0003	0.3333
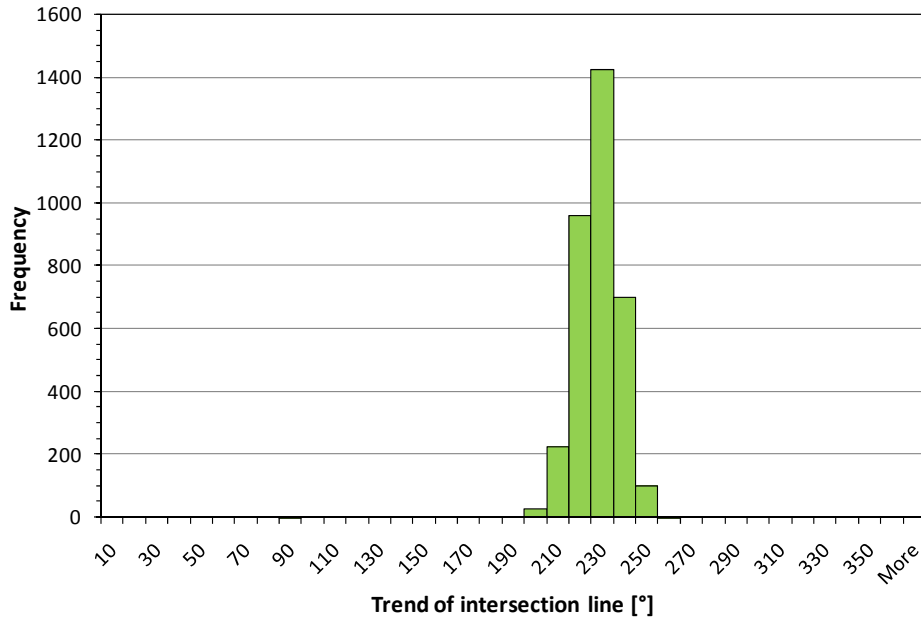
Figure 32: Trend distribution for intersection lines formed by joint set combination 1-3 (for scaled wedge trace lengths)

Within the 10,000 samples of joint set combination 1-2 a total number of 3815 kinematically feasible (valid) wedges were found. 3666 of these valid wedges failed, i.e. they have a factor of safety of FS < 1.0. Therefore, the probability of wedge failure for combination 1-2 is PF = 36.7 %. The probability of sliding was calculated to PS = 96.1 %. Only 149 wedges were stable (3.9 % of all valid wedges). The distribution of the calculated factors of safety is shown in Figure 33. The mean factor of safety is FS = 0.51 with a standard deviation of 0.23. The SWEDGE probabilistic analysis information (for the minimum FS) is given in Annex J.
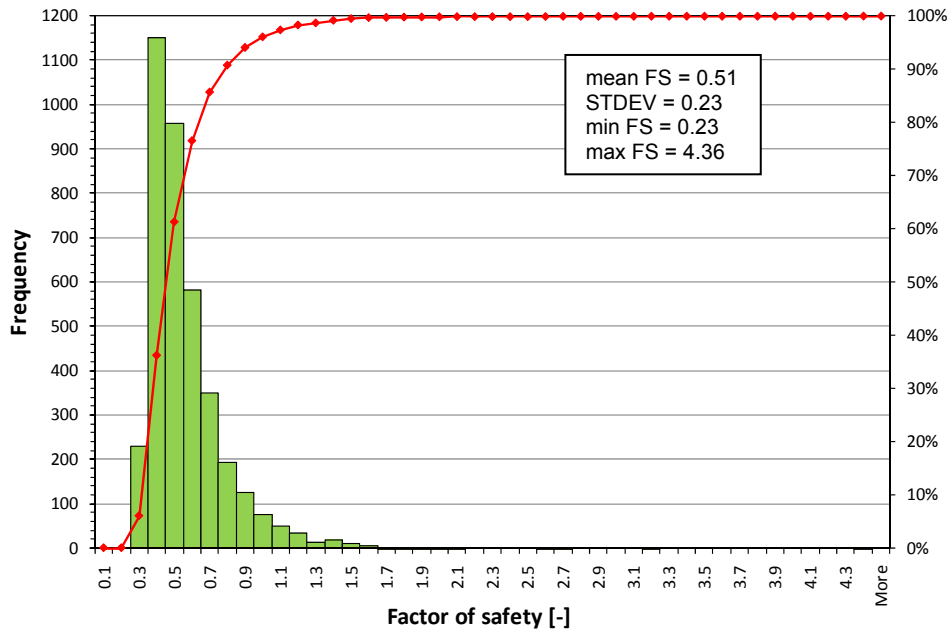
Figure 33: Factor of safety distribution for joint combination 1-2 (for scaled wedge trace lengths)

Due to the scaled joint trace lengths, i.e. due to the use of unbiased mean trace lengths to scale the resulting wedge size, the formed wedges are relatively small in size (maximum wedge volume of 1.3 m^3).

3.3 3D joint system analysis

As discussed in Hadjigeorgiou and Grenon, 2005 using the SWEDGE software package provides information only for individual wedges. The analysis allows no consideration of the location of joints in a rock mass, and no information can be obtained about the frequency and the stability of wedges along a certain slope length. This information can be gained using the 3D joint system analysis that accounts for spatial distribution of joints in the rock mass.

In this work the 3D joint system analysis was carried out with the aim to obtain information about frequency and failure probability of wedges formed along the crest of the investigated rock slope. The analysis was performed with two different computer programs, developed at Université Laval at the Département de génie des mines, de la métallurgie et des matériaux, which are based on the software package MATLAB. The first program (Fracture-SG, Version 2.17 (Grenon and Hadjigeorgiou, 2008b)) provides a tool for

generating 3D joint system models of rock masses out of field data. The second program (Fracture-Slope, Version 1.25 (Grenon and Hadjigeorgiou, 2008c)) enables an analysis of wedge stability along the crest of a rock slope of any length out of the generated 3D joint system models. The methodology used for this analysis follows the approach published by Grenon and Hadjigeorgiou, 2008a.

3.3.1 Generation of 3D joint system models

According to Grenon, 2007 the theory behind the software Fracture-SG is based on the Veneziano model, whereby joints are assumed as of polygonal shape. Essentially, the generation of the joint system models is based on three stochastic processes (Dershowitz and Einstein, 1988):

1. Generation of planes within a defined volume

2. Dividing the generated planes into polygonal regions

3. Randomly marking a portion of polygons as jointed; the remaining polygons are defined as intact rock

After analyzing the field data statistically, a 3D joint system model is generated and calibrated using the results of the statistical analysis (like mean values of dip and dip direction, joint trace lengths, and spacing). The 3D joint system model of the rock mass leads to simulated joint data, which can also be statistically analyzed. A comparison between field data and simulated data allows a statement about the validity of the generated joint system model.

In this work the 3D joint system models were generated using the collected and corrected (unbiased) field data of the three joint sets (see section 2.3). As input data for the joint set simulation especially the mean joint set orientations (dip and dip direction) and their distribution (68.3%-variability) were used (see Table 15). In Table 16 the input data to define scanline and scanplane within the joint system models are given. All input data, including the calibrated parameters joint intensity and joint area are given in Annex K.

Table 15: Input data for joint sets (used for Fracture-SG)

		Set 1	Set 2	Set 3
Dip / Dip direction	[°]	72 / 130	87 / 225	35 / 318
68.3 % variability for dip and dip direction (standard deviation)	[°]	11	15	11

Table 16: Input data for scanline and scanplane (used for Fracture-SG)

		Scanline	Scanplane
Dip / Dip direction	[°]	-	65 / 166
Plunge / Trend	[°]	0 / 76	-

The model volume was chosen as a function of the investigated rock mass in situ. Since the investigated total scanline has a length of 100 m, the length of the generated volume was also set to 100 m. The height of the investigated site is 8 m at its highest point, but the calculated mean spacing of the subhorizontal joint set 3 was 17.5 m. To avoid edge effects and to enable a reliable model calibration, height and depth of the joint network volume were both chosen to 40 m. The resulting total model volume is 160,000 m^3.

The calibration of the model was carried out by varying the program input parameters "joint intensity (P32)" and "joint area (E(aire)')". According to Meyer, 1999 the joint intensity is defined as cumulative joint area per unit volume. This parameter defines the resulting spacing of the simulated joints of a set. The joint area expresses the mean joint size and defines the trace lengths of the simulated joints. To check the exactness of the model the simulated joint data had to be compared with reference data. Therefore, the mean values for spacing and trace length obtained with the simulated joint system were compared with the mean values for spacing and trace length determined from the field data. The results, summarized in Table 17, show that a good agreement between simulated and field data was reached. Trace lengths and spacing of all three joint sets were reproduced successfully in the rock mass models. Annex L shows the calibration results in detail.

Table 17: Comparison of field data and simulated data

		Set 1	Set 2	Set 3
Unbiased mean trace length [m]	Field data	2.2	4.0	1.8
	Simulated data	2.3 (stdev 0.3)	4.1 (stdev 0.7)	1.8 (stdev 0.5)
Mean spacing [m]	Field data	1.8	3.4	17.5
	Simulated data	1.8 (stdev 0.3)	3.3 (stdev 0.6)	18.6 (stdev 13.6)
68.3 % variability for dip and dip direction [m]	Field data	15	23	15
	Simulated data	15	22	15

Altogether 1000 possible 3D joint system models were generated with a volume of 160,000 m^3 (X/Y/Z = 50m/20m/20m). In Figure 34 one of these models is shown exemplarily. As improvement over previous work at the Fleurimont site (as described in Grenon et al., 2008) the joint system models were generated with all three joint sets to account for the influence of joint set 3. Figure 35 shows the same model as in Figure 34, but independently for all three joint sets.
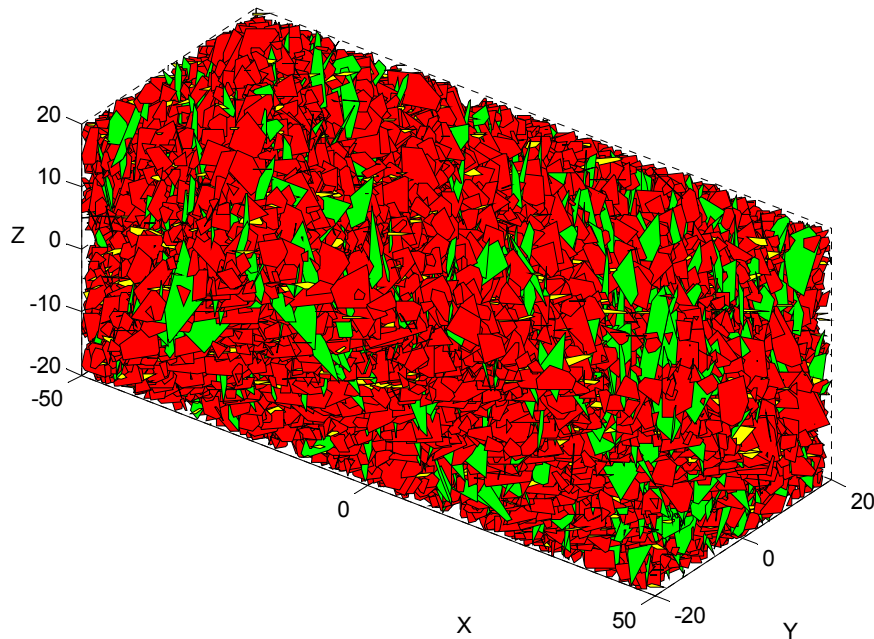
Figure 34: 3D joint system model of the Fleurimont rock slope, generated out of field data
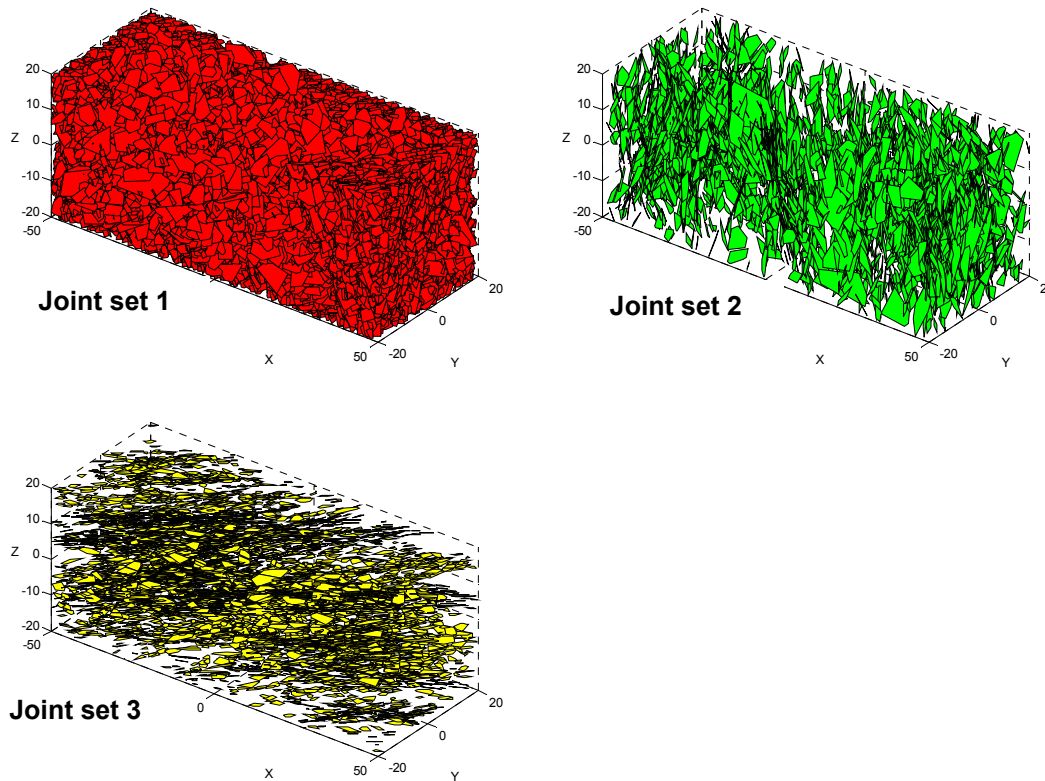
Figure 35: Generated 3D joint system model of the Fleurimont rock slope (the same model as in Figure 34), shown independently for the three identified joint sets

3.3.2 Probabilistic analysis of multiple wedges along the rock slope

The wedge analysis for the rock slope was carried out with the software Fracture-Slope (Grenon and Hadjigeorgiou, 2008c). This program enables the determination of number and size of potential wedges at the crest of a slope in a simulated rock mass, and allows a prediction of wedge frequency and wedge failure probability. The analysis was carried out as limit equilibrium analysis, i.e. the stability of potential wedges is assessed by their factor of safety (FS). Wedges with FS < 1.0 are considered as unstable, while wedges with FS $\geq$ 1.0 are considered as stable. The program determines only wedges along the crest of the slope, formed from two intersecting joints. Wedges within the slope face that are defined by three joints are not taken into account.

The generated 1000 joint system models were used as input data for the wedge analysis with Fracture-Slope. For the determination of potential wedges along the crest of a defined slope with a defined orientation, the slope data has to be introduced into the generated rock mass models. As input values for the slope the collected field data was used (dip = 69°, dip direction = 166°, see Annex B). This led to 1000 simulated slopes of 100 m length that were analyzed in view of frequency and failure probability of wedges.

A total number of 3526 wedges were generated along the crests of all 1000 slope models. In Figure 36 the number of wedges determined within each of the 1000 models is given, whereby no distinction of stable and unstable wedges was made. The determined wedges were formed from all possible joint combinations and not only from joint combination 1-2 as in the analysis of individual wedges by SWEDGE (see section 3.2.2). In 51 of the 1000 joint system models no wedges were formed, i.e. within 5.1 % of the analyzed models no wedge occurs along a simulated slope crest of 100 m length. In 94.9 % of the analyzed models at least one wedge was formed along the whole crest. On average three wedges were formed per 100 m slope length. More than three wedges were determined in 455 models. The most wedges per 100 m slope length (14 wedges) were found only in one model, so that the probability therefore tends to zero (0.1%).
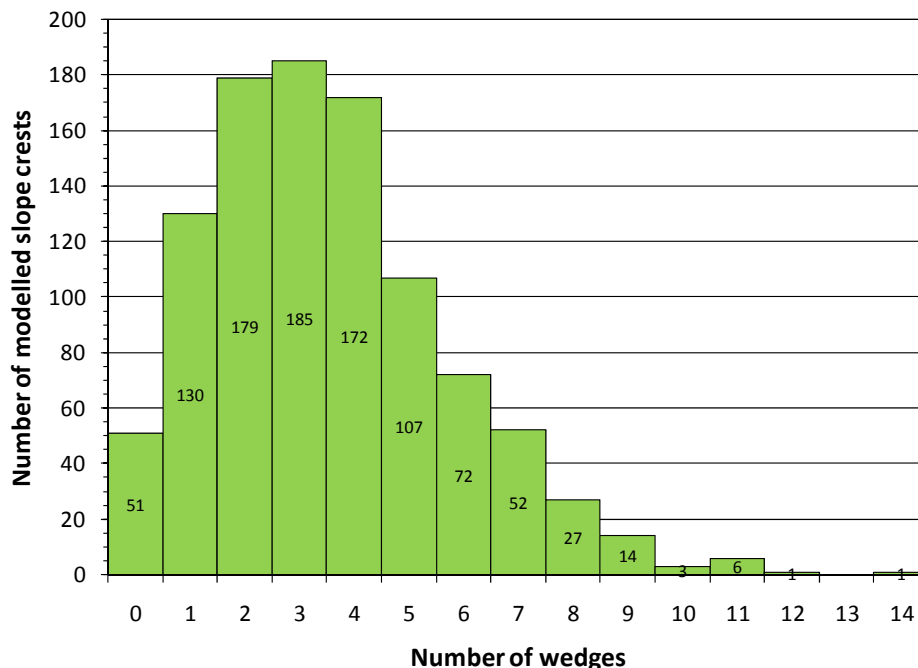
Figure 36: Number of formed wedges per slope crest model

Within 949 out of 1000 analyzed slope crest models wedges were formed (see Table 18). The unstable wedges were distributed over 820 models, whereby in 185 of them only unstable wedges were formed, and in 635 models a variation of stable and unstable wedges occurred.

Table 18: Wedges within the analyzed joint system models

1000 analyzed models			
51 without wedges	**949 with wedges**		
	635 with stable and unstable wedges	185 only with unstable wedges	129 only with stable wedges

In Figure 37 the distribution of the factor of safety for all formed wedges is shown. Out of the total of 3526 wedges approximately the half is unstable with FS < 1.0 (1997 out of 3526 or 56.6 %). 1529 wedges (43.4 %) are stable.
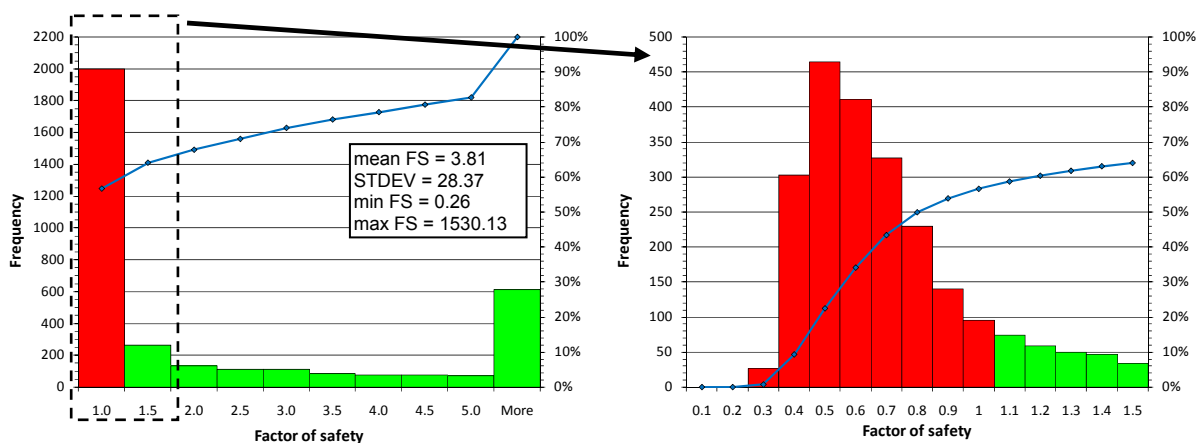
Figure 37: Distribution of factor of safety for all wedges (left), and in detail for wedges with FS ≤ 1.5 (right)

The distribution of the wedge volume is represented in Figure 38. Most of the wedges (3203 wedges out of 3526 or 90.8 %) are very small with a volume up to 0.10 m^3, whereby 1788 of these wedges are unstable and 1415 are stable. Within the group of wedges with a volume > 0.10 m^3 (323 wedges out of 3526 or 9.2 %) stable and unstable wedges can be found independently from their volume. 209 of them are unstable, 114 are stable. A total of 75 wedges (2.1 %) has a volume > 0.5 m^3, and 27 wedges (0.8 %) with a volume > 1.0 m^3 were formed, whereby 20 of them (0.6 %) are unstable. The largest wedge has a volume of

4.95 m^3 and a factor of safety of FS = 0.78. Using a unit weight of γ = 2.6 t/m^3, this wedge has a weight of 12.9 t.
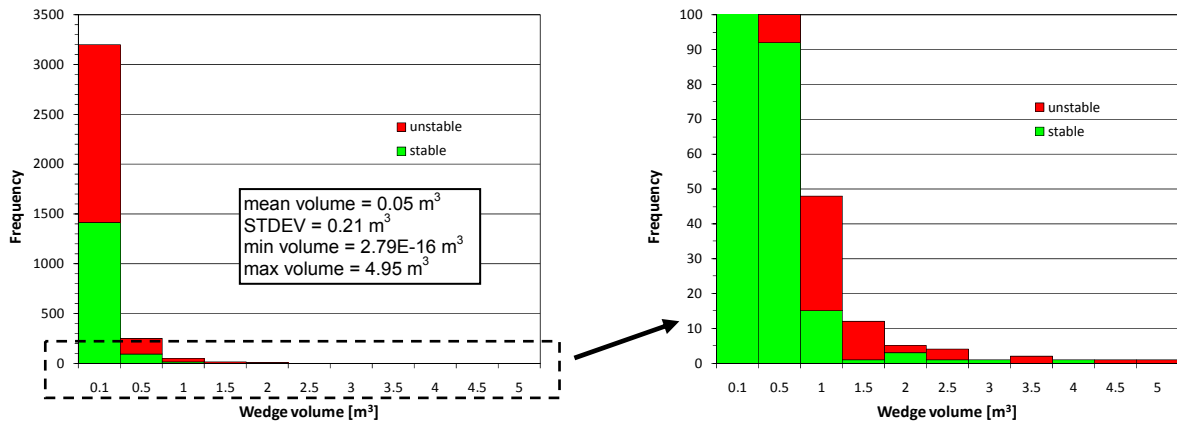
Figure 38: Distribution of wedge volume for all wedges (left) and in detail for lower frequencies (right)

The results consider all possible joint combinations. To assess the influence of each joint combination, all wedges were grouped based on the associated joint combination, as shown in Figure 39. Most of the unstable wedges are formed by a combination of joints of set 1 and 2. Only a few wedges of this joint combination are stable. Stable wedges are mainly formed from joint pairs out of the same joint set, especially out of joint set 1. Only a few wedges are related to joint pairs including joints of set 3; all of these wedges are stable. This is in agreement with the observation on site and also with the analysis of individual wedges, and confirms the assumption that joint set 3 is of minor relevance for wedge failures along the slope crest. Due to the large number of instable wedges, joint combination 1-2 is the most important combination regarding wedge stability. With 1916 unstable wedges out of 2094 the probability of failure in this group, i.e. the probability that a formed wedge fails, is 91.5 %.
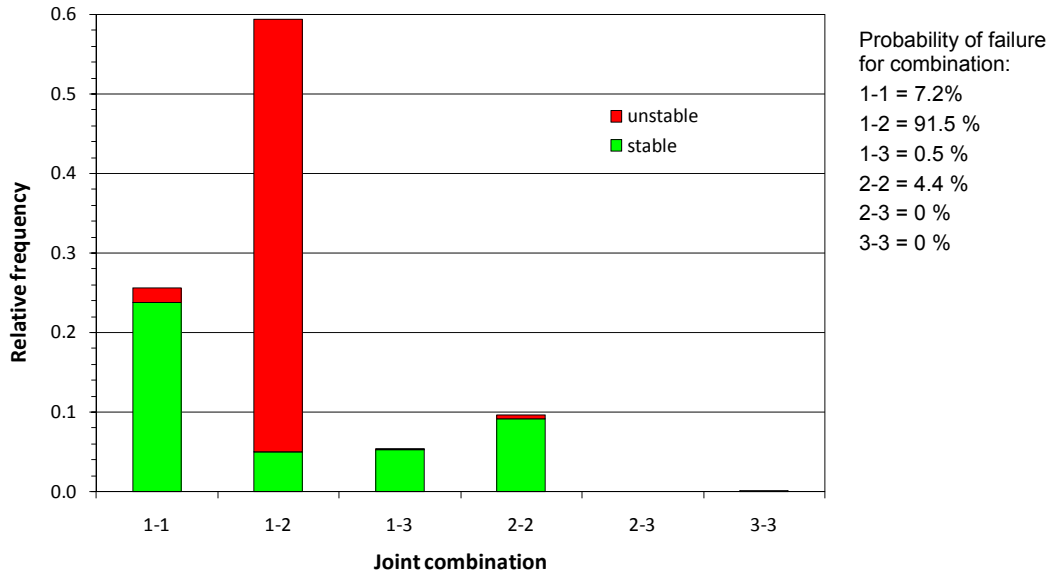
Figure 39: Relative frequency of wedges in view of joint combinations

In Figure 40, the resulting factors of safety and wedge volumes are assigned to the different joint combinations. Referring to Figure 40 a1, it is possible to miss information in the lower range of the factor of safety. Hence, a close up on this data is given in Figure 40 a2, and again in more detail in Figure 40 a3. The same applies to Figure 40 b1, providing the results for wedge volume. A close up on the results for smaller wedge volumes is shown in Figure 40 b2 and b3.

Most wedges (59% or 2094 out of 3526) were formed from joint combination 1-2, whereby the majority of these wedges are unstable (92 % or 1916 wedges). Most wedges have a volume ≤ 1.0 m^3. Only a few wedges with a volume > 1.0 m^3 were found within all joint combinations (0.8 % or 27 out of 3529 wedges); most of these larger wedges (81 % or 22 out of 27 wedges) were found in joint combination 1-2, whereby 20 of them (91 %) are unstable.
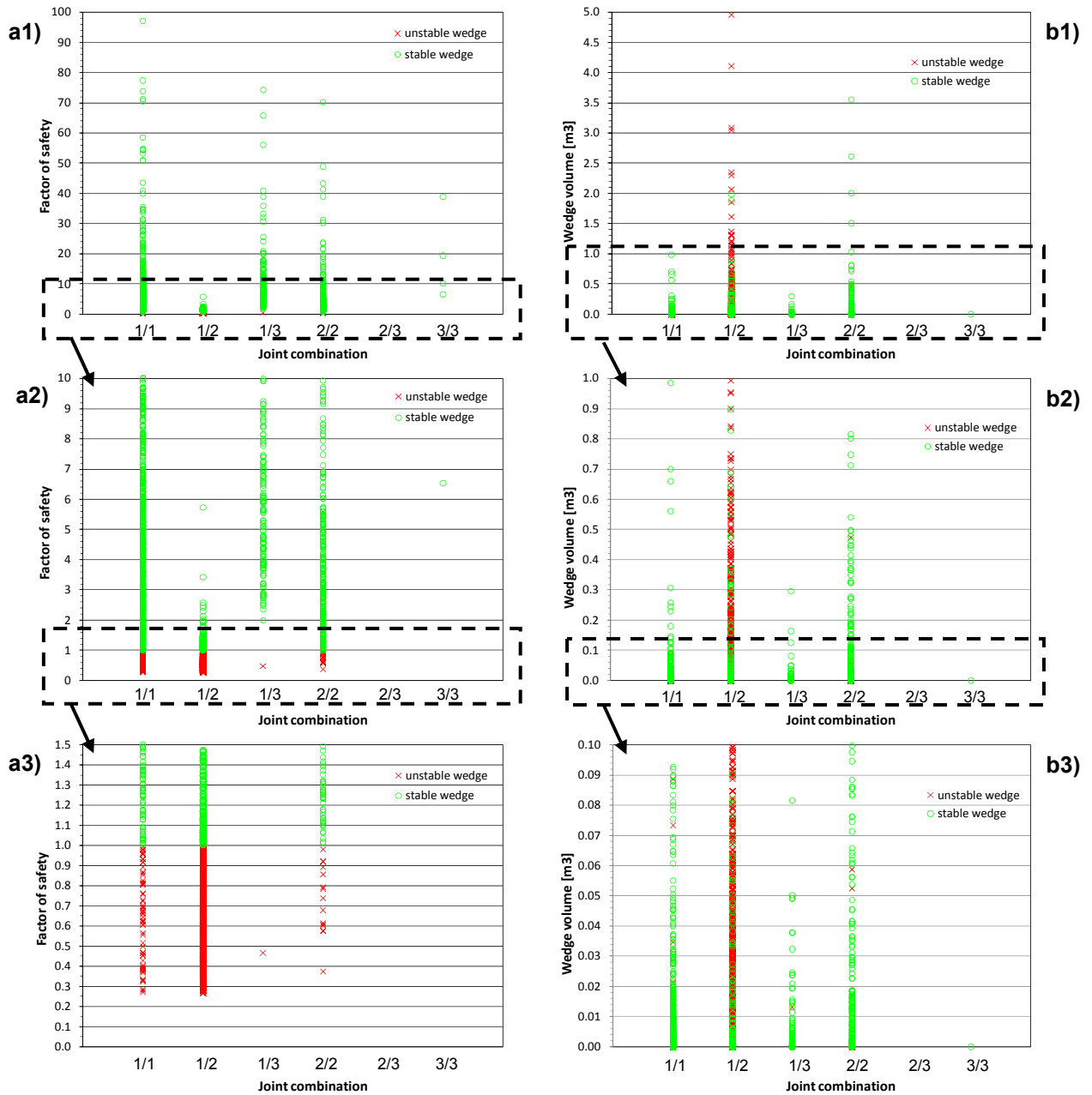
Figure 40: Factor of safety (left) and wedge volume (right) related to joint combinations

The wedge volume distribution for joint combination 1-2 is shown in Figure 41. It can be noted that only 1.1 % wedges larger than 1.0 m^3 were found. No wedge of a larger volume than 5.0 m^3 was formed in the joint system analysis. Comparing the resulting wedge sizes with the back-analysis results for the two large wedges A and B, wedge A with a volume of 0.5 m^3 occurs within the 8.5 % range of wedges with a volume between 0.1 and 0.5 m^3. A wedge with a large volume comparable to wedge B (volume of 8.9 m^3) could not be found along the simulated slope crests.
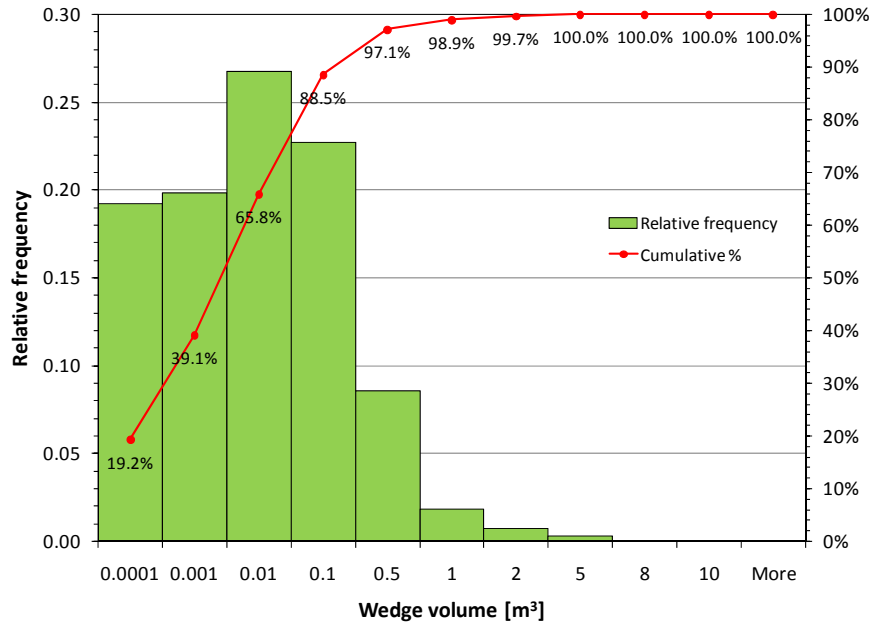
Figure 41: Distribution of wedge volume (for 3D joint system analysis)

All other joint combinations have a minor impact on the wedge stability. The 902 wedges formed by joint combination 1-1 are mainly small with a volume of less than 0.1 m^3, and only 12 wedges out of this group (1 %) are unstable. The joint combinations 1-3, 2-2, 2-3, and 3-3 form fewer wedges. Altogether 15 % of all wedges (530 out of 3526) belong to these combinations, whereby most of them are stable (97 %) and small (84 % ≤ 0.1 m^3).

In Figure 42 the average number of unstable wedges (FS < 1.0) along the crest of the simulated slope of 100 m length is shown, subdivided based on volume. All joint set combinations were considered in this diagram. The graphs show the development of the average number of wedges with an increasing number of simulations. The graph representing the results for all unstable wedges, regardless of size, shows that on average two unstable wedges will occur along the crest of the a simulated slope. Considering only unstable wedges with a volume of more than 0.001 m^3, the average number of wedges decreases to 1.2 per slope crest. Only 0.65 unstable wedges with a volume > 0.01 m^3 and 0.2 unstable wedges > 0.1 m^3 will potentially form. The average number of probable large wedges with a volume >1.0 m^3 tends towards zero (0.02 wedges per 100 m slope crest). Considering that at least one of the two large wedge failures (> 0.1 m^3) observed in 1995 was natural, the modelling results differ from the field observations and indicate that the probability for large wedge failures is low.
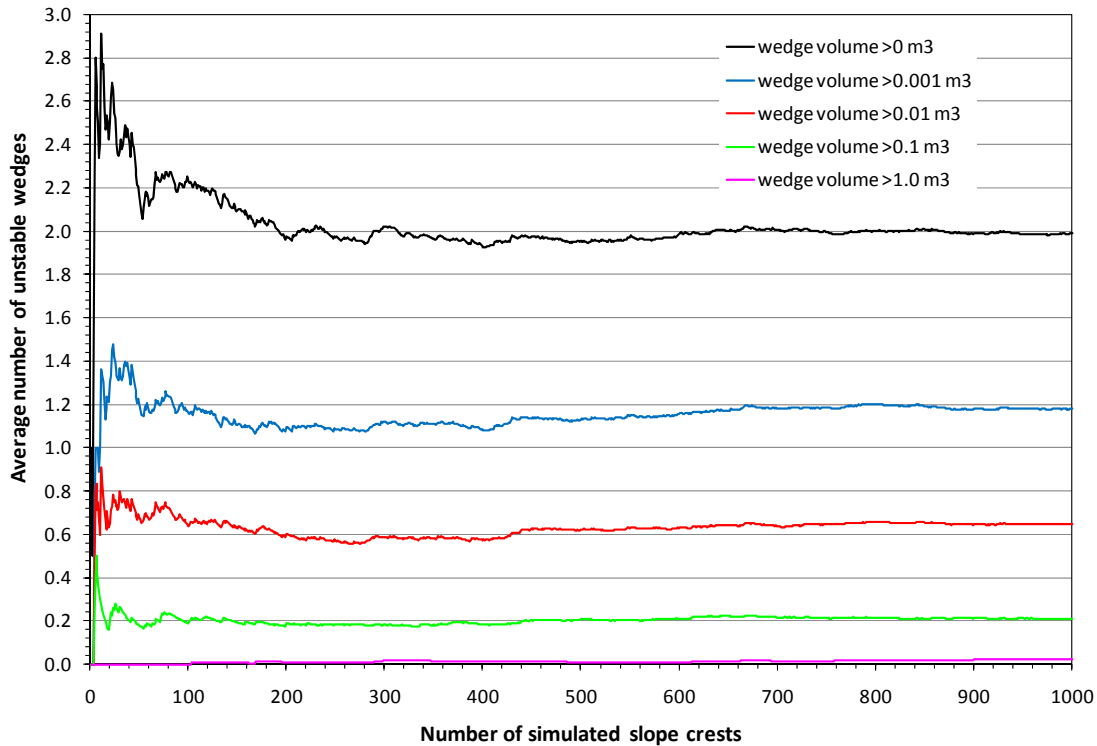
Figure 42: Number of unstable wedges (FS < 1.0) per 100 m slope length in relation to number of simulated slope crests

In Figure 43 the number of unstable wedges that have to be expected along a slope crest of 100 m length is given as a percentage of the total number of probable wedges. As before, the wedges are subdivided based on their size. The results are influenced by the number of simulations. It can be noted that on average 60 % of all probable unstable wedges have a volume > 0.001 m^3, while 33 % of all wedges are > 0.01 m^3. 11 % of all wedges have a volume > 0.1 m^3, and only 1 % of all wedges are larger than 1.0 m^3.
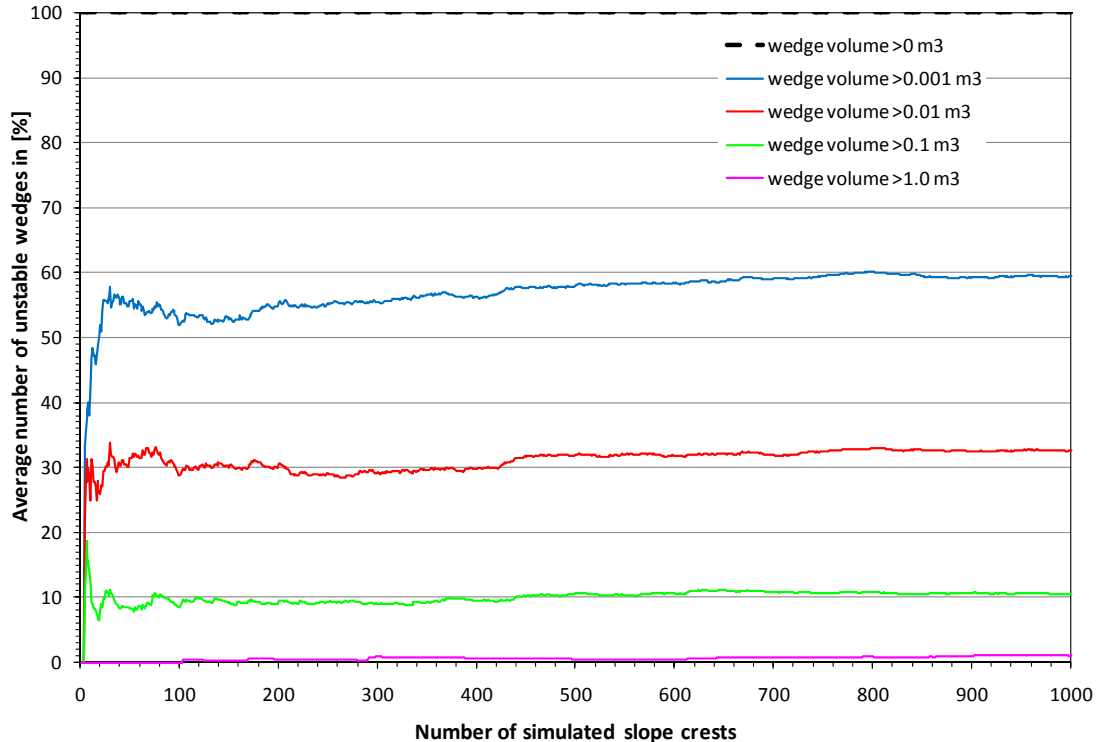
Figure 43: Average percentage of unstable wedges (FS < 1.0) per 100 m slope length in relation to number of simulated slope crests

The aim of this type of probabilistic analysis, i.e. of analyzing the development of results concerning the number of simulations, is to reach acceptable results by analyzing a sufficient great number of simulated rock slopes. Grenon and Hadjigeorgiou, 2008a suggest the following criterion and thresholds to determine the number of required simulations for reliable data analysis. According to Grenon and Hadjigeorgiou, 2008a this criterion should be fulfilled for five consecutive simulations. It follows that

$$0.995 \leq \nu/\nu_{mean} \leq 1.005$$

With:

ν Value resulting from a simulation n

ν_{mean} Mean value resulting from the 20 previous simulations (moving average)

In the data presented in Figure 42 and Figure 43 the value ν represented the mean number of wedges occurring along a 100 m long slope crest, classified by their weight. Using the same thresholds as in Grenon and Hadjigeorgiou, 2008a the results conform to the proposed criterion and fulfill the requested five repetitions. Hence, in accordance with

Grenon and Hadjigeorgiou, 2008a the chosen number of 1000 simulated rock slopes was considered as adequate for reliable results. In Table 19 the numbers of required simulations to fulfill the criterion are given.

Table 19: Number of required slope crest simulations (Fleurimont rock slope)

Wedge volume	> 0 m^3	> 0.001 m^3	> 0.01 m^3	> 0.1 m^3	> 1.0 m^3
Number of simulations	186	223	272	417	941

One difference between the case study presented in Grenon and Hadjigeorgiou, 2008a and the case study in this work is the total number of wedges occurring along the slope. While in the former on average approximately 20 wedges of a volume > 1.0 m^3 occurred along the slope crest, in the latter only an average of 0.02 wedges of this size (calculated as the mean) was formed. The relatively large number of simulations required to meet the proposed five repetitions in this work (especially for wedges > 1.0 m^3) result from this difference, i.e. they are caused by the extremely small mean numbers of wedges occurring along the slope. These small mean numbers, representing the value ν, respond very sensitive to small changes in the total number of wedges. This leads to relatively large variations in the values calculated with the above mentioned criterion, and the chosen range can hardly be kept, although the change in the mean number is marginal. For the case of wedges > 1.0 m^3 the mean number of wedges along a 100 m slope changed between 0.019 and 0.020 over the last 100 simulations.

3.4 Summary

In this chapter the collected field data of the investigated rock slope along a highway was analyzed for wedge failure. A kinematic analysis was carried out, aiming to evaluate the kinematic feasibility of wedge failure for the major planes of the different joint sets as well as for the wedges failed during the road construction. It turned out that kinematic feasibility was given for the two failed wedges, but not for the major planes of the joint sets.

The wedge stability analysis was carried out as limit equilibrium analysis. First the two wedge failures observed in 1995 were back analyzed deterministically. The analysis was carried out as sensitivity analysis for the joint shear parameters friction angle and cohesion,

and for the unit weight of the rock. Both wedges were evaluated as potentially instable for assumed average joint properties. A probabilistic analysis was carried out for single wedges using the mean values and the statistical distribution for joint set orientations and trace lengths. Due to the fact that mean trace lengths were used, the analysis resulted in mostly small wedges. The evaluated low probability of failure supports the fact that only a few wedges were observed along the investigated slope.

A probabilistic 3D joint system analysis was carried out to obtain information about wedge frequency and wedge failure probability along the investigated slope length. 3D joint system models were generated and calibrated using the collected field data. These models were analyzed in view of wedge failures along the crest of the simulated slope. The analysis resulted in mostly small wedges; only a few larger wedges were found, which indicates a low probability for wedges similar to the wedges observed on site. The probability of failure for wedges that form along the slope crest was evaluated as high, but only a small average number of wedge failures along the slope crest were calculated.

4 Conclusions for the Fleurimont rock slope

The investigated rock slope along a highway cut has experienced two large wedge failures during the construction of the road in 1995. The wedge analysis was carried out with the aim to assess the slope stability for wedge failures, and to determine frequency and failure probability for wedges along the slope crest. The necessary analysis data was collected on site. The stability analysis was carried out as limit equilibrium analysis using deterministic and probabilistic analysis tools.

The two large wedge failures observed in 1995 were back-analyzed using the structural data collected for both wedges. The deterministic analysis was performed as sensitivity analysis for joint shear parameters. The results show the potential instability of both wedges.

The slope stability is controlled by three joint sets that were identified on site and with the collected structural data. The probabilistic analysis of individual wedges was carried out using the structural data of all three joint sets as well as the statistical distribution of the orientation data. Only wedges formed from two joints for a given slope crest configuration were taken into account. The results confirmed the assumption that wedges are formed mainly from joint combination 1-2 and indicated a moderate probability of wedge failures (37 %), but a high probability of sliding (96 %). Since mean joint trace lengths were used for the analysis, only small wedges were formed.

The probable occurrence of wedges along the slope crest was investigated with a probabilistic 3D joint system analysis. 3D joint system models were generated and calibrated using the collected field data. These models were analyzed for frequency and failure probability of wedges along the crest of a simulated slope of 100 m length. The results confirmed that wedges can form along the slope crest, mainly formed from joint combinations 1-2. They also indicate a high probability of failure (92 %) for wedges out of joint combination 1-2, while the probability of failure for wedges out of all joint combinations is moderate (57 %). The average number of probable failures (2 wedges) along a crest of 100 m length was evaluated as low. An even lower average number (0.02

wedges) was evaluated for probable large wedge failures (wedges > 1.0 m^3).

Summarizing the results, a good reproduction of the field rock conditions and the wedge failure mechanism was reached with the different analysis tools, although some limitations are recognized. It can be assumed that wedge failures could have been predicted during the construction of the road in 1995, but the prediction would have included mainly small-size wedges along the slope crest. No information was available whether also smaller wedges occurred during the road construction. Based on the observations on site and on the structural data analysis it seems possible that a few small wedge failures occurred along the slope crest.

The results indicate that the stability of the slope is not critical; this especially since the investigated slope is at a distance of about 12 m from the highway and away from any other structure. However, the results also demonstrate that a comprehensive data analysis using various analysis tools is required to reach a reliable judgment of the rock behaviour. Apart from the choice of the analysis tools, mainly the data quality significantly influences the analysis results. A comprehensive and reliable data base is necessary to reach reliable results. In this work some shortcomings in the data may result in a limitation of their significance:

- For several joints no information was recorded for trace length, spacing, and joint termination. This influences the determination of analysis parameters like mean trace length and mean spacing.

- In areas of pronounced schistosity only one joint was measured exemplarily. This leads to a misrepresentation of the total number of joints, and has an influence on the determination of various analysis parameters like mean orientation values and mean trace length and spacing.

- Mapping was performed only along a horizontal scanline, which does not record well the subhorizontal joint set 3. Due to the unavailable data the orientation bias within the collected field data could not be corrected. In this work this shortcoming is of minor relevance. As confirmed with the data analysis, the affected joint set 3 is not crucial for

wedges forming along the investigated slope.

- The data collection along scanline 3 and 4 was hindered by the vegetation. The access to the rock was difficult, and particularly the determination of the intersection distance but also a continuous measuring was hindered. As a result some joints along the scanline may be not or wrongly recorded.

Further shortcomings in this work result from the available analysis tools. Although it is difficult to classify their impact, they may lead to a limitation of the significance of the results:

- The used analysis tools allow only the analysis of wedges along the slope crest. Neither the probabilistic analysis of single wedges nor the 3D joint system analysis account for wedges within the slope face, formed from three different joints.

- A difference between input and output variability was noted during the calibration of the 3D joint system models. This should be considered in future work.

- Although the results in this work conform to the reliability criterion used within the 3D joint system analysis, the criterion may be unsuitable for cases with even smaller average numbers of wedges, since the requested threshold may not be satisfied. A way of handling small numbers of wedges could be to consider a more robust estimate of the average number of wedges.

Outlook and future work

For the previously described wedge analysis various analysis tools of different complexity were used, but several limitations remain in the analysis results. Apart from several restrictions that result from the available analysis tools, the main factor of influence on the results is the analysis data, which was mapped on site. For a more consistent analysis a more extensive and comprehensive data collection would be helpful. A better quality of field data will arguably improve the analysis results.

5 Drifts in fractured rock at the LaRonde underground mine

In this chapter a case study is presented that addresses the stability of underground drifts in a fractured rock mass. It was carried out at the LaRonde underground mine, where certain excavations display severe wall deformations. These rock displacements affect the safety in the mine, lead to temporary closures of parts of the mine, and can cause expensive and time-consuming rehabilitation work and production downtimes.

The large wall deformations at LaRonde are caused by squeezing of rock. According to Barla, 1995 squeezing of rock can be defined as a "time dependent large deformation, which occurs around the tunnel (…), and is essentially associated with creep caused by exceeding a limiting shear stress. Deformations may terminate during construction or continue over a long time period". The term "tunnel" refers thereby to excavations in general.

Rock squeezing is a complex problem, and the influencing factors are manifold. Potvin and Hadjigeorgiou, 2008 report about the conditions usually associated with squeezing ground. Their conclusions are based on field data from different underground mines in Australia and Canada. Accordingly in all investigated mines with squeezing rock a prominent structural feature, e.g. highly layered rock or a shear zone, was found, whereby a parallel orientation of structural feature and excavation was promoting the ground deformations. In addition the intact rock strength of the squeezing rocks was usually rather weak (less than 60 MPa), while the in situ stresses were significantly high. A further factor of influence is the degree of alteration of the affected rock, since a highly altered rock leads to an additional decrease of rock strength. An indication for the alteration of a rock is usually the presence of characteristic alteration minerals like e.g. mica or montmorillonite. Steiner, 1996 furthermore mentions water pressure, support system, and the selected construction procedure as factors influencing squeezing ground conditions.

In accordance with the above mentioned factors, which promote the occurrence of squeezing ground conditions, the following conditions can be found at the LaRonde mine site (Mercier-Langevin and Turcotte, 2006): Squeezing occurs usually within the

pyroclastic rocks (especially tuff), i.e. in altered rock with a pronounced foliation. However, not all tuff dominated areas are equally affected. Depending on the grade of alteration, which is associated with the mineral composition of the rock, some areas show no or only slight signs of squeezing. Especially tuff with a relatively high content of silica (quartz) and only less sericite seems to be more resistant against squeezing. Since squeezing occurs in excavations in great depth, high stress conditions are given. Furthermore the squeezing phenomenon is dependent on the orientation of excavation to foliation. It could be observed that squeezing occurs mainly in drifts, where the excavation axes have the same strike like the foliation planes (Mercier-Langevin and Turcotte, 2006).

In contrast to most cases reported in Potvin and Hadjigeorgiou, 2008 is the aspect of weak intact rock strength at LaRonde. In Mercier-Langevin and Turcotte, 2006 the average strength of the rock associated with squeezing problems is given with σ_{ci} =140 MPa (intact rock strength for intermediate tuff). However, the foliation in the rock mass results in low values for the rock mass strength, which arguably is the controlling parameter.

The result of the wall deformations caused by squeezing rock is the convergence of the drift walls, i.e. after the excavation the rock moves into the drift opening and causes a reduction of the cross-section. At worst the drifts become inaccessible for mining equipment. At LaRonde wall convergence of more than one meter was observed in some areas of the mine (Mercier-Langevin and Turcotte, 2007). Aydan et al., 1993 distinguish three different failure types to describe the nature of the rock movement into the opening: a) complete shear failure, b) buckling failure, and c) shearing and sliding failure. These failure types are illustrated in Figure 44.

| a | b | c |
| Complete shear failure, | buckling failure, | tensile splitting shearing and sliding |
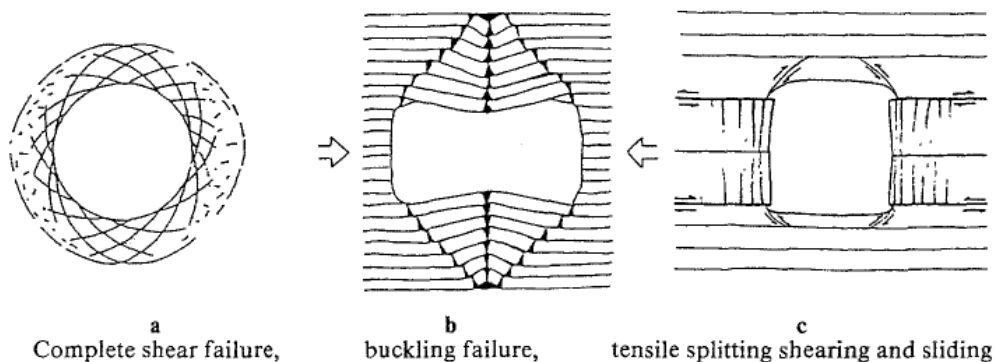
Figure 44: Classification of failure types of tunnels in squeezing rock (Aydan et al., 1993)

The failure mode observed in LaRonde's heavily foliated rock can be classified as the buckling failure type, that is usually associated with thinly layered rock (Aydan et al., 1993). A characteristic deformation profile observed at LaRonde is shown in Figure 45. With their nearly vertical dip the orientation of the rock layers in relation to the drift walls favours buckling failure, since according to Steiner, 1996 "overbreak due to buckling of schistose layers will occur mainly where the schistosity is parallel to the tunnel perimeter".

Figure 45: Drift wall deformation due to squeezing, observed at LaRonde on level 236 (Feb. 2008)

The large wall deformations observed in certain areas at LaRonde, and the different factors of influence on these deformations were of interest in this second case study. The aim was to develop a numerical model of the affected excavations and the surrounding rock, and to reproduce the failure mechanism and the resulting deformations with the aid of numerical modelling. A reliable model of the deforming ground could contribute to understand the squeezing rock at the mine. The focus was on the investigation of three drifts on different underground levels that have experienced large deformations following their excavation. In the following sections of chapter 5 the investigated areas are described, followed by a convergence analysis in chapter 6.

5.1 Site description

In this section information about the LaRonde mine and the regional geology is provided, followed by a detailed description of the rock mass, the ground control problems and the investigated drifts.

5.1.1 Location

The LaRonde underground mine is located in the region of Abitibi-Témiscamingue in the western part of the province of Québec between Val-d'Or and Rouyn-Noranda near the village of Cadillac (see Figure 46).
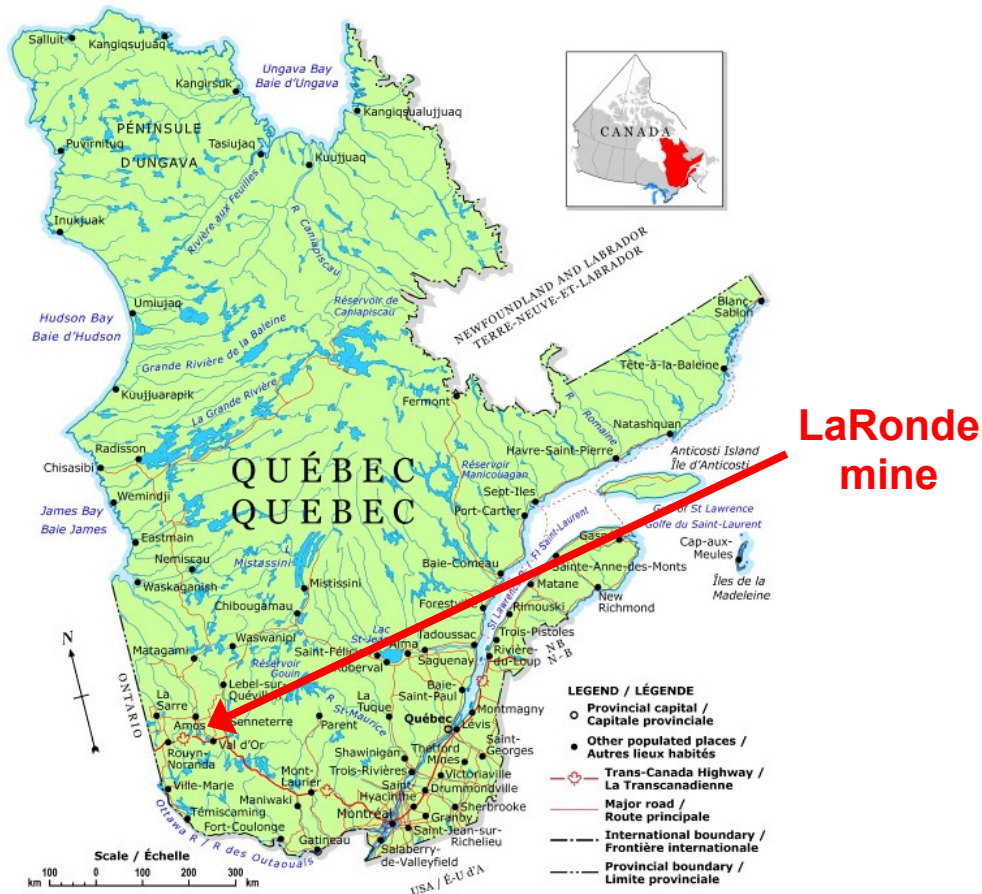
Figure 46: Location of the LaRonde underground mine (www.atlas.nrcan.gc.ca)

5.1.2 Geology

Most of Québec's bedrock north of the St.-Lawrence River belongs to the Precambrian rocks of the Canadian Shield, i.e. the rocks were formed during the period from 4.5 billion

to 540 million years ago. The province of Québec is divided into different geological provinces as shown in Figure 47. The north-western part of Québec is related to the Superior Province, which forms the central part of the Canadian Shield, and is subdivided into several sub provinces. The region of Abitibi-Témiscamingue with the LaRonde mining area in western Québec belongs to the Abitibi sub province (www.mrnf.gouv.qc.ca).
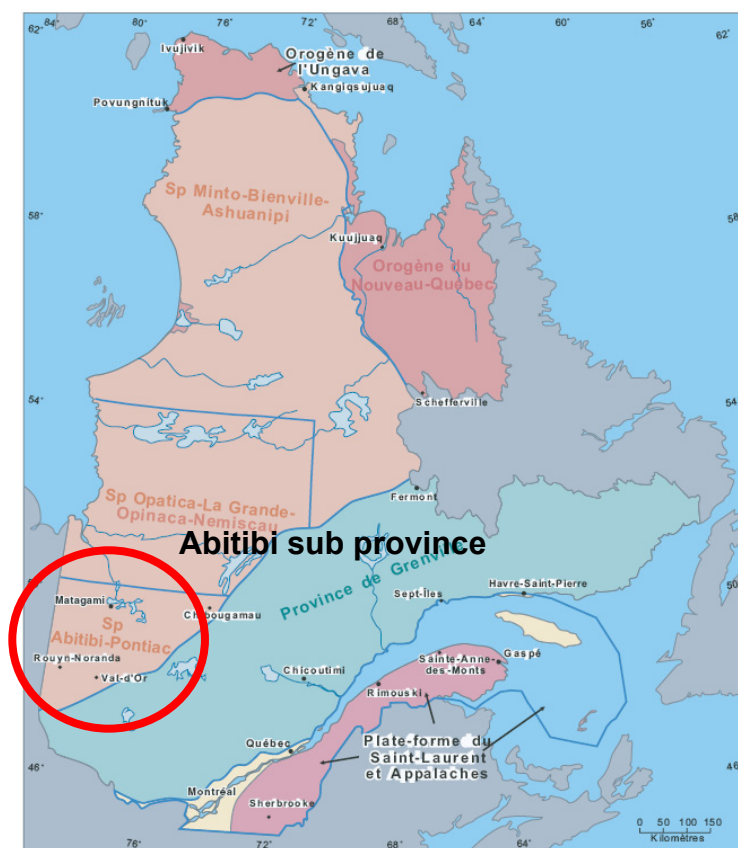
Figure 47: Geological provinces of Québec

The Abitibi sub province is part of the Abitibi Greenstone Belt, an about 2,800 million years old greenstone belt, which spans across the border of Ontario and Québec. Greenstone belts are elongated areas with sequences of variably metamorphosed or altered volcanic rocks, and sedimentary rocks. ″Greenstone″ refers to compact, dark-green, altered or metamorphosed mafic igneous rock, like basalt or gabbro. The green hue is caused by the specific minerals the rock consists of (Mitchell, 1985). In the southern part of the Abitibi Greenstone Belt lies the Blake River Group, a sub aqueous caldera system. Figure 48 illustrates the location of the mine as part of the Doyon-Bousquet-LaRonde Mining camp and the geology in this mining area.
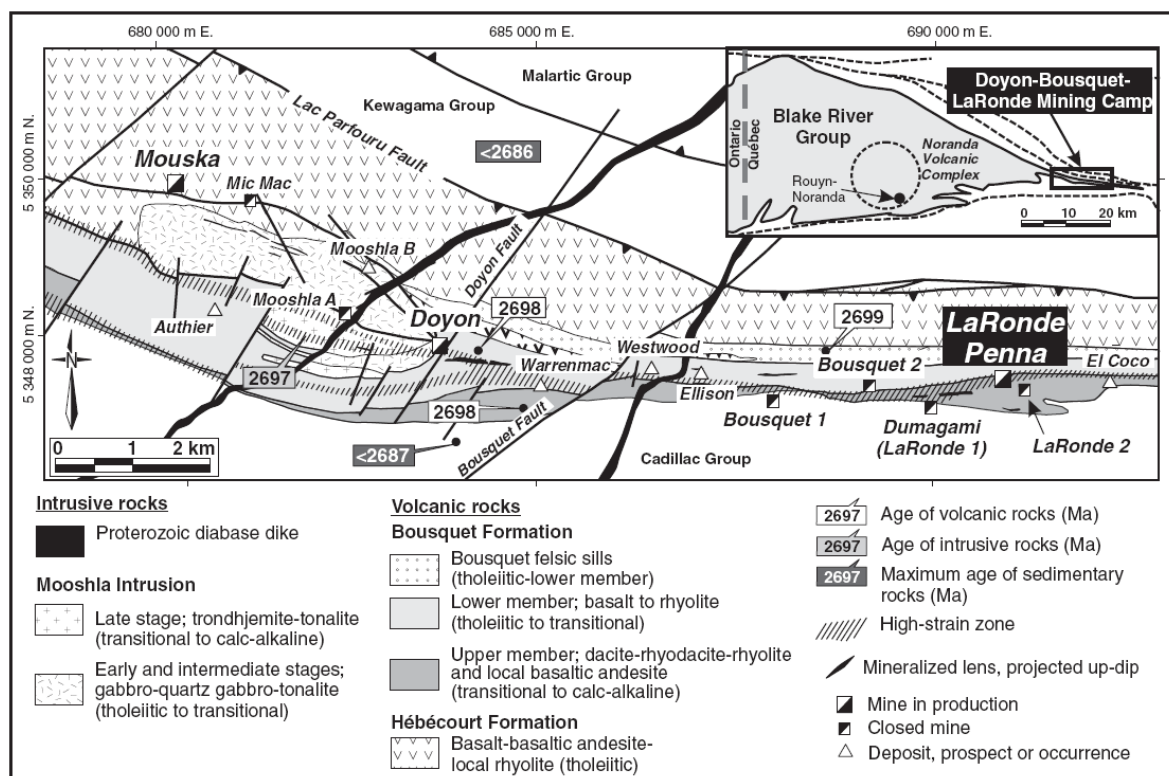
Figure 48: Simplified geologic map of the Doyon-Bousquet-LaRonde mining camp (Mercier-Langevin et al., 2007a)

According to Mercier-Langevin et al., 2007a the region of the Doyon-Bousquet-LaRonde Mining camp is divided into two volcanic formations, whose rocks differ particularly in their silica content: the Hébécourt formation in the north, with its mainly mafic rocks, and the Bousquet formation in the south, which is subdivided into an upper member (south) and a lower member (north). While the lower member is composed of mafic to felsic rocks, the upper member consists mainly of intermediate to felsic rocks. In Table 20 the silica content of the different rock types is given.

Table 20: Rock types defined by silica content (Le Bas and Streckeisen, 1991 and Hyndman, 1972)

Rock type	Ultramafic (ultrabasic)	Mafic (Basic)	Intermediate	Felsic (Acid)
Silica content	< 45%	45 - 52%	52 - 63%	> 63%

Figure 49 represents the stratigraphic settings of the Doyon-Bousquet-LaRonde Mining camp. The adjacent groups northwards and southwards of the volcanic formations consist

of sedimentary rocks. Since these areas are not relevant for the present case study, they are not described further.
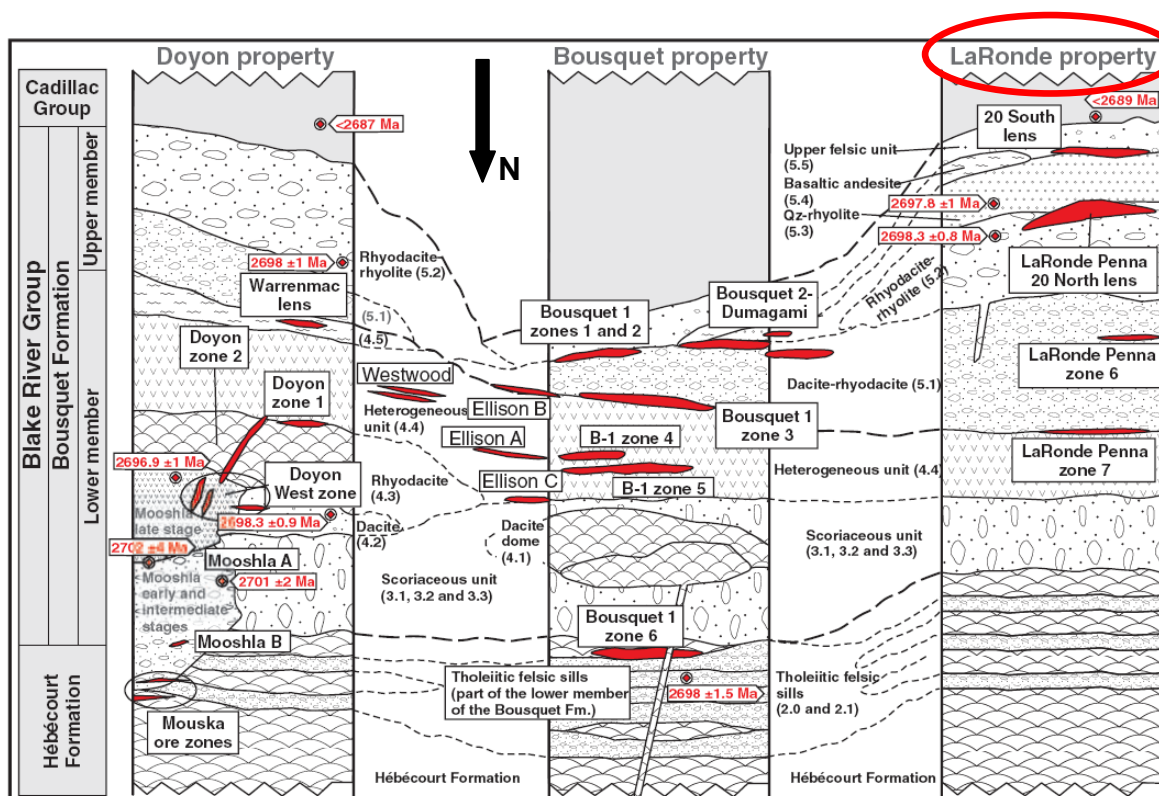
Figure 49: Simplified stratigraphic setting of mineral lenses of the Doyon-Bousquet-LaRonde mining camp (Mercier-Langevin et al., 2007b)

According to Mercier-Langevin et al., 2007a the mineral deposit at LaRonde is a volcanogenic massive sulphide (VMS) orebody that consists of semi-massive to massive sulphide lenses of varying size. A VMS deposit can be defined as a massive accumulation of sulphide minerals of tabular or lens-like shape, parallel to volcanic stratigraphy or bedding, and consisting of at least 60% sulphide minerals (Franklin et al., 1981). At LaRonde the mineralized sulphide lenses are found in the upper member of the Bousquet formation, which consists of five stratigraphic units, and is characterized mainly by quartz- and feldspar-porphyritic rhyodacite to rhyolitic flows and pyroclastic rocks (www.agnico-eagle.com).

Due to movements of the continental plates the mine area, a former seafloor region, has undergone large displacements. The previously horizontal layers straightened up from north

until the present inclination of about 70° to 80° towards south. The once lower (older) formations are now located in the northern mine area, while the former upper (younger) regions can be found in the south. The mineralized zones, that have been thin horizontal layers at their formation, are now nearly vertical zones. At present, five different zones belonging to LaRonde are known (zones 6, 7, 19, 20 and 21), but mainly two zones are currently mined out (zones 7 and 20).

5.1.3 The LaRonde underground mine

The LaRonde mine with its 2240 m deep Penna shaft is an Gold-Silver-Zinc-Copper underground mine, whose reserves extend from the surface to a depth of 3110 m (Mercier-Langevin and Turcotte, 2007). In Figure 50 an overview of the LaRonde orebody is given. Presently production takes place between level 98 and 236, i.e. between 980 and 2360 meters below surface, whereby the access to the lower part of the mine is enabled by a ramp. In March 2008 the ramp reached a depth of about 2400 m below surface.
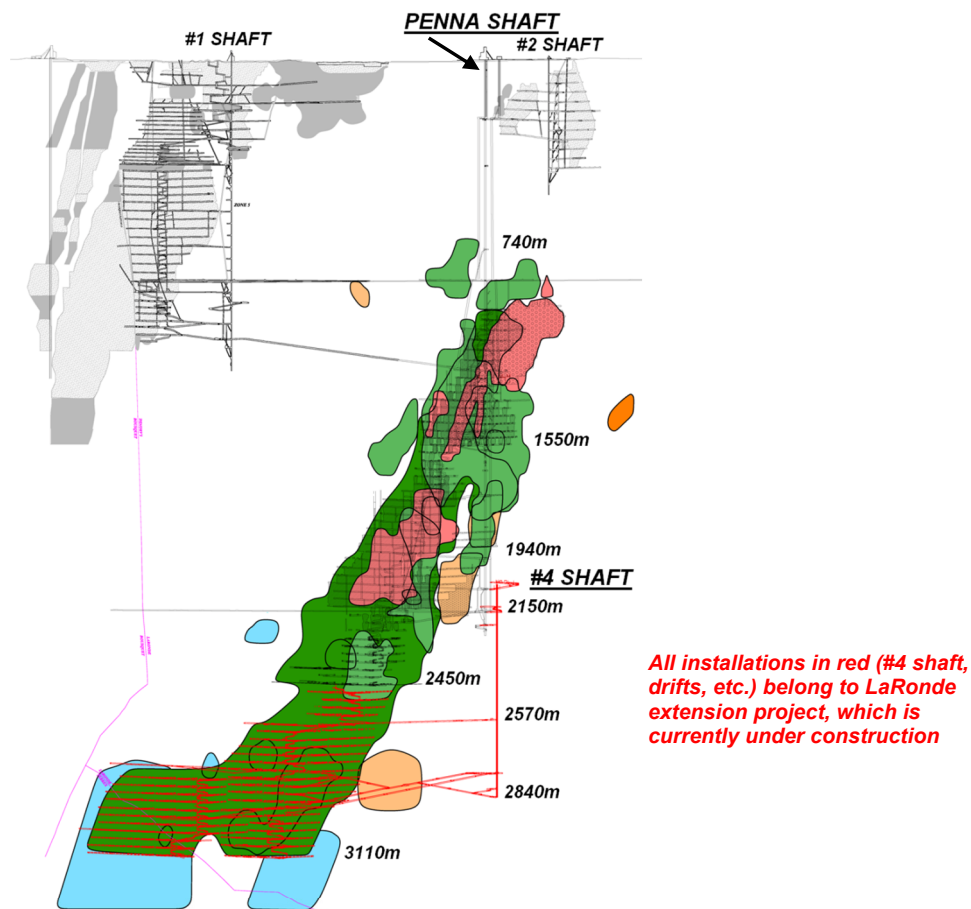
Figure 50: Longitudinal view of the LaRonde mine and orebody (after Mercier-Langevin, 2008)

5.2 Material and methods

For the present case study the convergence in three different drifts on three different underground levels was investigated. Especially the side walls of these excavations had experienced large deformations and considerable closure of the openings.

The crucial data to develop realistic models of the deforming drifts was information about the deformations, like size and development with time. Hence it was necessary that the investigated underground excavations provide both pronounced deforming of rock as well as available convergence measurements. The mine identified three haulage drifts on three different underground levels for this study (drift no. 218-35-W, 227-43-E, and 233-41-W). Long-term convergence measurements were available for all three drifts, carried out during several months following each drift excavation.

For this work a series of site visits was undertaken in February and March 2008 in order to collect information on the three drifts. This included especially information about the rock foliation, like dip, dip direction, and spacing of the layers. Furthermore, drift heights, condition of walls, etc. were recorded, whereby the drift heights were measured either with the aid of a measuring tape or with a portable laser measuring device. Dip and dip direction of the foliation were determined with the aid of a Brunton compass.

Table 21: Description of the collected data

Kind of data:	Collected data/information:	Source
Structural data	Rock types and geological structure	Mapped / prov. by mine
	Orientation (dip, dip direction) and spacing of foliation	Mapped
	General information (alteration, condition of rock, etc.)	Mapped
Rock mass data	Field stress	Provided by mine
	E-modulus, Poisson's ratio and uniaxial compressive strength of intact rock	Provided by mine
Ground control data	Seismicity (number, location, magnitude of seismic events)	Provided by mine
	Squeezing (occurrence, location, dimension, etc.)	Provided by mine
Specific data for investigated drifts	Geometry and orientation of drifts	Mapped
	Rock support measures (initial and additional support)	Provided by mine
	General information (condition of walls, signs of deformation, location of deformation, etc.)	Mapped
	Seismic events in drift areas	Provided by mine
	Convergence measurements (drift width measurements)	Provided by mine

Table 21 summarizes the collected data. Convergence data, rock mass data as well as general information about the ground control problems at LaRonde were provided by the mine. The convergence measurements, carried out by technicians of the ground control group of the LaRonde division, were taken at different time intervals, varying from several days up to several weeks.

5.2.1 Convergence measurements

The mine used the following process for the convergence measurements. The convergence of the drift walls was determined by measuring the width of the opening, i.e. the distance between hanging wall and footwall, at varying time intervals. The difference between two measurements gives the total wall displacement within a time interval. Within each drift the measurements were carried out for several drift profiles. For each profile the opening width was measured twice. One measurement was carried out in the upper part of the profile; a second measurement was taken in the lower part as shown in Figure 51 (without scale). The drift widths were measured using either a measuring tape or a portable laser measuring device. The indicated measuring heights above drift floor are approximate values. They were determined out of the measuring information provided by the mine.
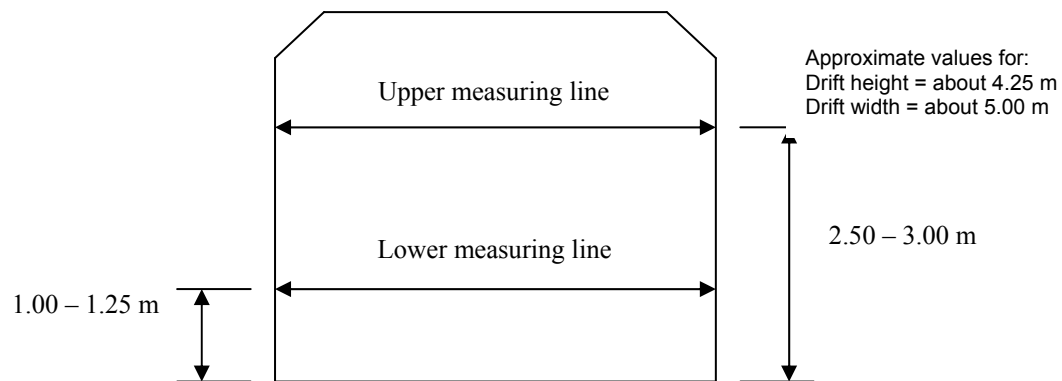
Figure 51: Position of convergence measurements within the drift profiles at the LaRonde mine (without scale)

The applied measuring method allows only the determination of the total lateral convergence of the opening, i.e. the total displacement of both sidewalls together. No measurements to define the displacement of hanging wall and footwall separately were performed. Possible displacements of roof and floor were also not measured.

In drift 218-35-W measurements with a total station were carried out three times (Nov. 23, 2007 (initial measurement), Dec. 18, 2007, and March 04, 2008). Available were only the measured drift profiles as shown in Figure 52, but not the measured data. According to Turcotte, 2008 only very small displacements of the roof were determined, and the measured uplift of the floor was considered as accumulation of stoped material, dropped from transport vehicles. For the purposes of this thesis it was felt that the quality of the total station measuring data was not adequate. This was based on the fact of repeated rehabilitation work especially at the drift roof. Furthermore, since no measuring data was available the results could not be compared with the above mentioned convergence measurements. Hence, the total station measurements were not used further.
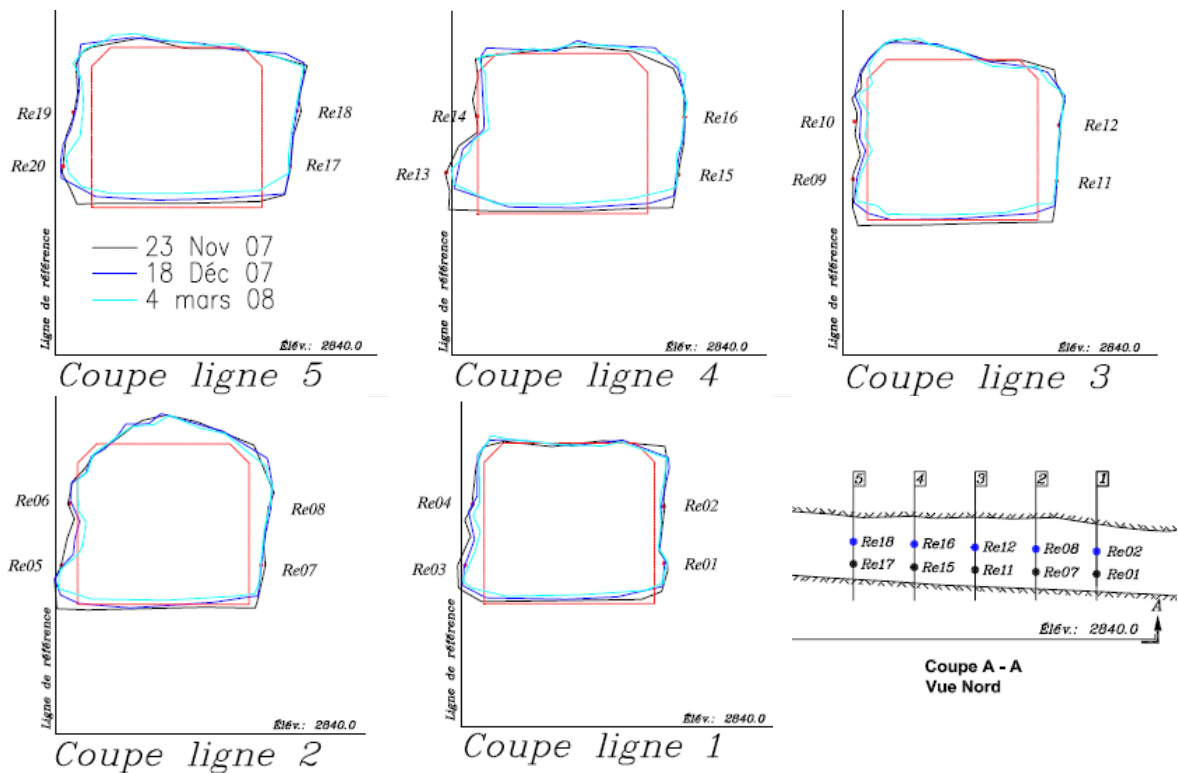
Figure 52: Drift profile measurements in drift 218-35-W (LaRonde mine), carried out with total station

5.3 Description of the rock mass and the investigated areas

This section summarizes the available rock mass and drift information collected at the LaRonde mine in February and March 2008.

5.3.1 Geological structure

The geology in the immediate mine area is dominated mainly by two different rock types. While the northern parts of the mine are mostly formed from basalt, the southern areas are dominated by tuff of different mineral compositions and with different grades of alteration (Mercier-Langevin and Turcotte, 2006). The two main rock types, i.e. basalt and tuff, can be described as follows:

- **Basalt** is a dense, fine-grained, igneous extrusive rock formed from lava. With its rather low silica content, but high content of magnesium and iron, basalt belongs to the mafic rocks (Mitchell, 1985, Fenton and Adams Fenton, 1940).

- **Tuff** is a pyroclastic volcanic (igneous extrusive) rock formed from volcanic ash, a fine-grained volcanic pyroclastic material. Volcanic ash is produced by explosive eruptions of volcanoes, and created by shattering of solid rock and separation of magma. It consists of small rock and mineral fragments, and dust-sized particles, which can be extremely small (particle diameter less than 0.063 mm). The settling of this material results in beds or layers of volcanic ash (Mitchell, 1985, Fenton and Adams Fenton, 1940).

Caused by the genesis of the geological formations, the alteration as well as the mineralization increases from the older rocks (today in the northern mine area) to the younger rocks (today in the southern mine area). As a result, at LaRonde the tuff formations are younger but more altered than the basalt formations, and the mineral lenses are found mostly within tuff. In Figure 53 an overview of the approximate location of the different rock types is given, exemplarily for level 218. The boundaries between the different rock types cannot be precisely defined, since they are irregular within one underground level and also different on each level.
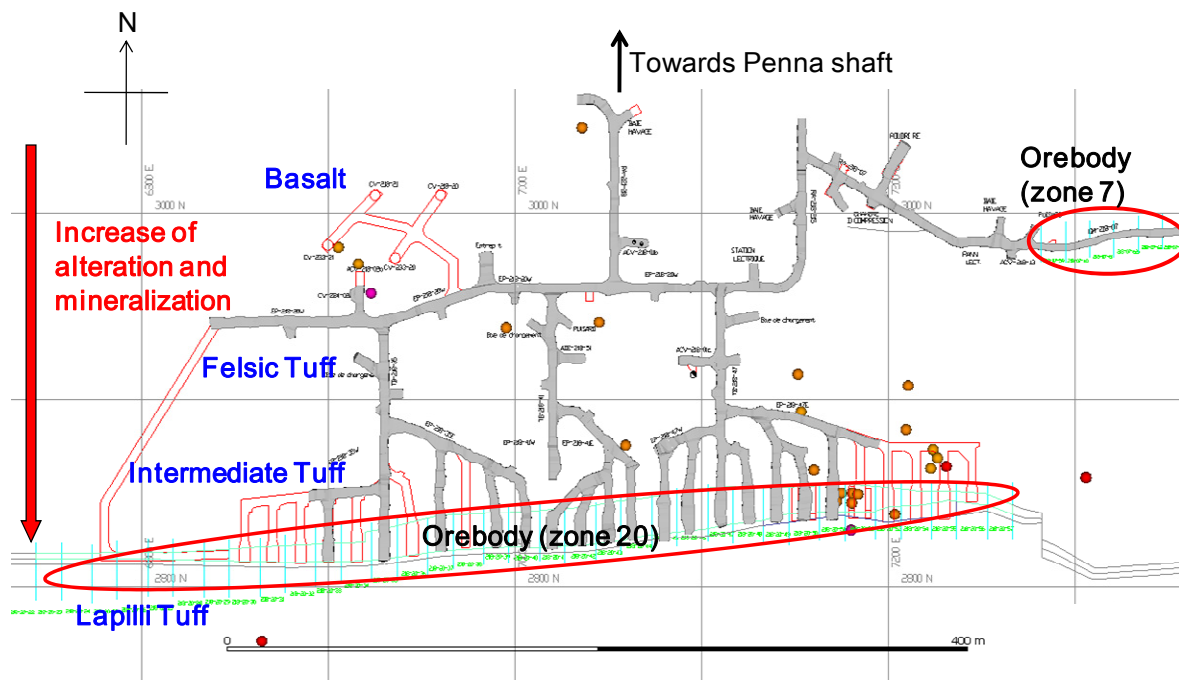
Figure 53: Plan view of level 218 with location of different rock types (LaRonde mine)

According to Mercier-Langevin and Turcotte 2006 all permanent excavations like shaft, ramp, and permanent drifts are located in basalt in the northern part of the mine. The orebody as well as most of the temporary excavations developed to access the ore are located in tuff with a varying grade of alteration, and a varying content of silica (felsic to intermediate tuff). These areas are situated in the southern part of the mine.

5.3.2 Foliation

As the most significant structural feature of the rock, associated with both basalt and tuff, but more pronounced within the latter (Mercier-Langevin and Turcotte, 2007), a foliation with a small spacing can be made out. The thickness of the layers varies from one centimeter to some decimeters. The foliation of the rock is a result of factors like pressure and deformations caused by the forces that formed the upright layers, but also given by the original stratification of the rock. Since tuff is by nature a layered rock type, the foliation is more pronounced in tuff dominated areas than in basalt areas. The inclination (dip) of the foliation varies between about 70° and 80° with an orientation (dip direction) approximately towards south (see Figure 54).

Figure 54: Foliation of rock (tuff) in drift 218-35-W and 227-43-E at the LaRonde mine

5.3.3 Mechanical properties of intact rock

Several different rock units were found at the LaRonde mine site. In Table 22 the main rock types and their average mechanical properties are shown as provided in Mercier-Langevin and Turcotte 2007. The variation of the given data was not available.

Table 22: Mechanical properties of intact rock at the LaRonde mine (Mercier-Langevin and Turcotte, 2006, Mercier-Langevin and Turcotte, 2007)

Rock type	Uniaxial compressive strength σ_c [MPa]	E-modulus E [GPa]	Poisson's ratio ν [-]
Andesite / Basalt	100	50	0.30
Intermediate Tuff	140	48	0.16
Massive Sulphide	100	53	0.28
Semi-massive Sulphide	85	47	0.16
Mineralized Felsic Tuff	140	58	0.15
Lappilli Block Tuff	150	47	0.13

In Mercier-Langevin and Turcotte, 2007 the equations given in Table 23 are provided for the estimation of the in-situ stresses within the intact rock mass at LaRonde. Herein σ_1, σ_2, and σ_3 are the principal stresses, while z represents the depth below surface. The principal stress σ_1 runs normal to the foliation approximately in north-south direction. It is the main force that causes the uplift of the formerly horizontal rock layers. The principal stress σ_2 runs perpendicular to σ_1, while principal stress σ_3 is the vertically oriented stress component. It is recognized that there are variations in the resulting stresses. Hence, the equations provide only general guidelines.

Figure 55 shows the principal stress development with increasing depth below surface, resulting from the given equations. The resulting stress values for the three investigated underground levels are given in Table 24.

Table 23: In-situ stress equations for the rock mass at the LaRonde mine (Mercier-Langevin and Turcotte, 2007)

Stress component	Equation
σ_1 [MPa]	8.62 + 0.04z
σ_2 [MPa]	5.39 + 0.0262z
σ_3 [MPa]	0.0281z
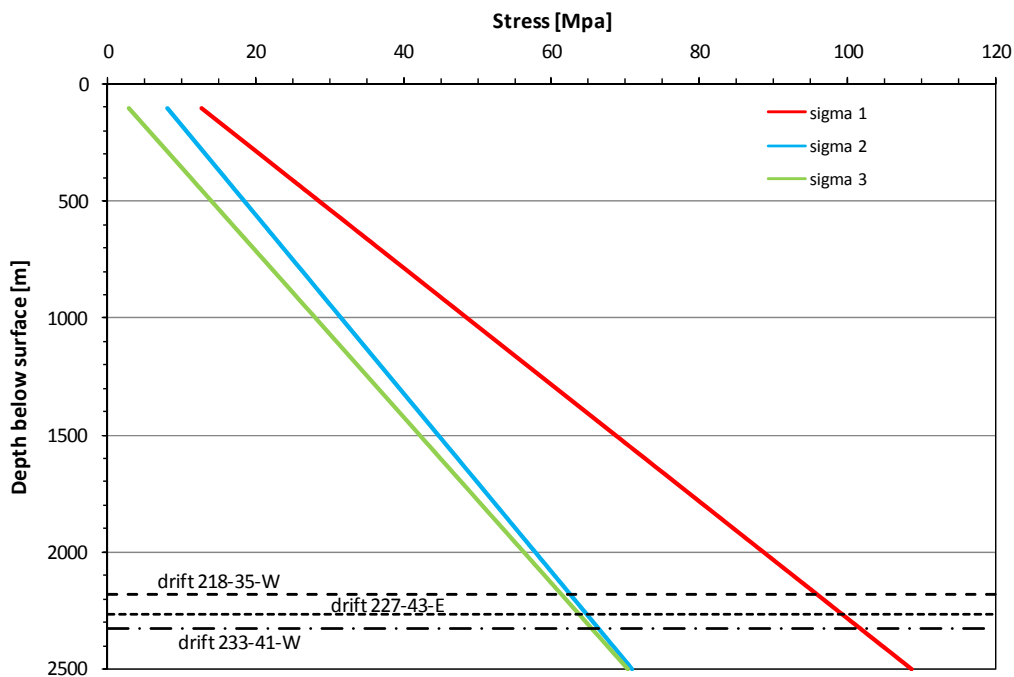
Figure 55: Principal stress estimates with increasing depth (LaRonde mine)

Table 24: In-situ stresses on different underground levels (LaRonde mine)

Stress component	Underground level		
	2180 m	**2270 m**	**2330 m**
σ_1 [MPa]	96	99	102
σ_2 [MPa]	63	65	66
σ_3 [MPa]	61	64	65

5.3.4 Ground control problems

Two main ground problems associated with the geological settings occur in the LaRonde mine area. Apart from the above described rock squeezing the mine has to deal with the occurrence of seismic events. In general, these two problems do not occur in the same areas, though there are transition zones where both phenomena exist. While squeezing of rock can be observed usually within the more altered rock formations, seismic events are associated rather with hard, less altered rock. Affected by seismicity are in particular the northern basalt areas of the mine, containing most of the permanent excavations.

There is no major seismicity in the investigated drifts. Due to the geological settings, no or only a few small seismic events occurred within the immediate area of these drifts. Therefore, seismicity is not relevant for the present case study and is not discussed further.

5.3.5 Investigated drifts

For the present case study the deformations of three haulage drifts were investigated (drifts no. 218-35-W, 227-43-E, and 233-41-W), located on three different underground levels (level 2180, 2270 and 2330 meters below surface). All three drifts are located within intermediate tuff with a varying mineral composition and a different grade of alteration, and serve to access the ore. The major ground problem in these drifts is the convergence of the sidewalls due to rock squeezing, which causes problems in the accessibility of stopes. In all three drifts during several months after their excavation convergence measurements were carried out. In the following sections the three drifts as well as the results of convergence measurements are described in detail. A summary of the collected drift data is provided in Annex M, N, and O. The results of the convergence measurements are presented in Annex P, Q, and R.

Drift 218-35-W

Haulage drift 218-35-W is located 2180 m below the surface (level 218) and enables the access to several stopes in the south-western part of the mine (see Figure 56). The drift is approximately east-west oriented (trend of 85°). The investigated drift length is about 25 m.
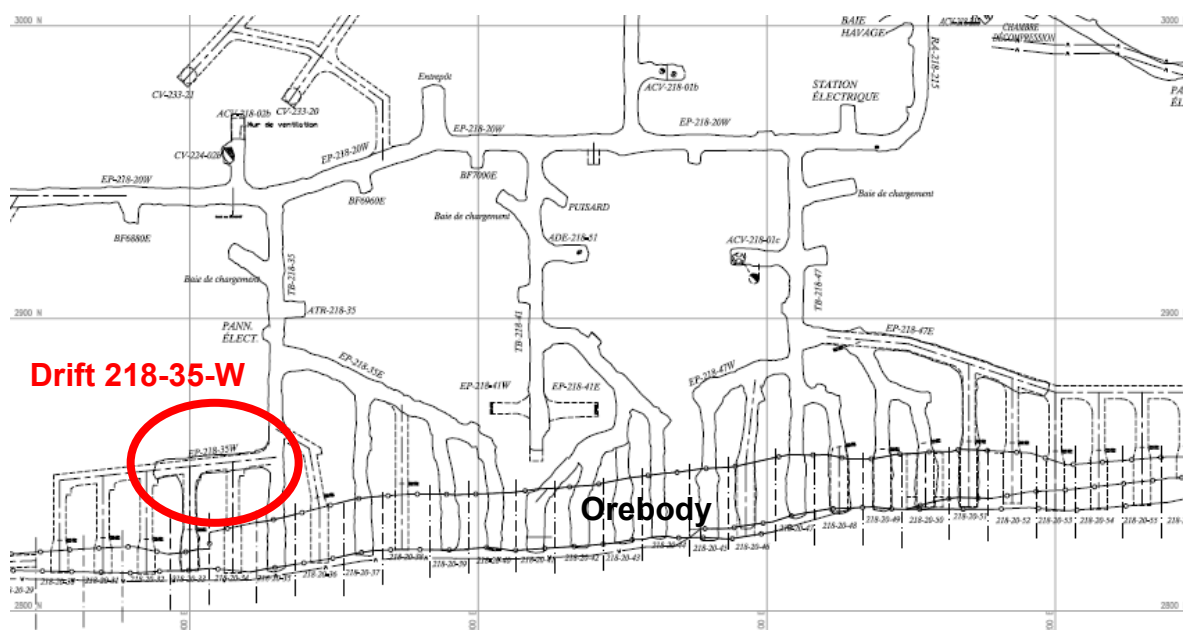
Figure 56: Location of drift 218-35-W (LaRonde mine)

The drift was excavated during October/November 2007 with opening widths varying between 5.05 m and 6.10 m. The widths were measured in November 2007 subsequently to the drift excavation in five profiles over a drift length of 16 m. No initial drift height measurements were available. The height was determined during an underground visit in March 2008 in five drift profiles. Thereby, values between 3.85 m and 4.93 m were measured. Table 25 provides the evaluated drift geometry.

Table 25: Opening geometry of drift 218-35-W (LaRonde mine) along a drift length of 16 m

	Opening width (Nov. 2007)		Opening height (March 2008)
	Upper part of drift	Lower part of drift	
Range measured in five drift profiles [m]	5.05 – 5.91	5.07 – 6.10	3.85 – 4.93
Mean (stdev) [m]	5.47 (0.31)	5.54 (0.44)	4.23 (0.41)

The support, consisting of bolts and mesh (sidewalls with friction sets 6′6″, roof with resin grouted rebars 7′6″/9′6″; both in combination with 6-gauge weld mesh) was installed immediately after the excavation of the drift. The support standard for this drift is shown in Figure 57.

Different rehabilitation work had to be done since the excavation of drift 218-35-W. Additional roof support had to be installed in November 2007 (cable bolts and mesh straps). Due to rock falls in January 2008 the section was closed, and hybrid bolts were installed on both sidewalls. Hybrid bolts consist of resin grouted rebars installed inside friction bolts. They were developed at LaRonde as a measure to handle the large wall deformations due to the squeezing rock (Mercier-Langevin and Turcotte, 2007). Furthermore, additional cable bolts and mesh straps were installed at the roof. In February 2008, damaged mesh at the roof was replaced and installed with friction bolts.
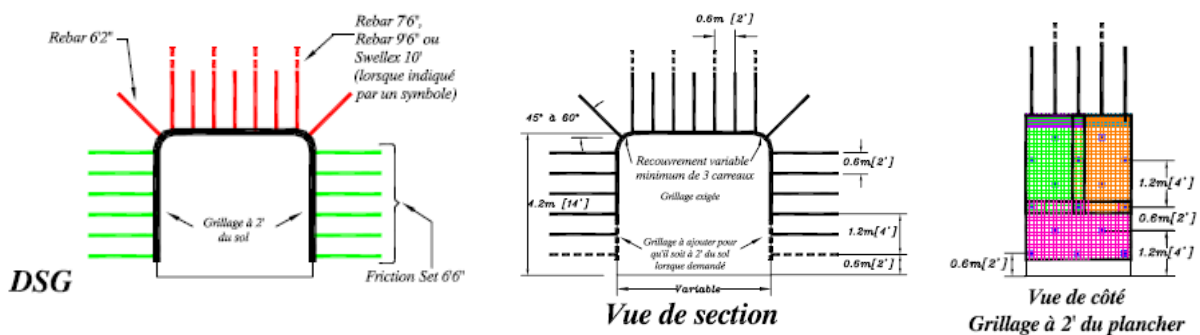
Figure 57: Support standard for drift 218-35-W at the LaRonde mine (DSG = Devis Standard Grillage)

The rock mass in drift 218-35-W consists of intermediate tuff, whereby the mineral composition of the rock changes from the footwall (north wall) to the hanging wall (south wall). The rock in the north contains a relatively high proportion of silica (quartz) and is rather blocky, whereas the rock in the south is schistose and consists of more sericite. According to the mine staff the transition zone runs almost parallel to the drift, approximately in the middle of the opening. This, however, could not be verified during the site visit. Furthermore, the footwall has a less pronounced foliation and is less altered than the hanging wall.

The rock foliation has a dip of 80° with a dip direction of 175° (strike parallel to drift trend). The spacing of the foliation varies slightly from the hanging wall (approximately 1 to 5 cm) to the footwall (about 5 cm up to 25 cm). While the hanging wall shows large displacements, especially in the upper part of the wall, the footwall is stable without signs of large deformation. The mine staff reports that due to the large deformations the hanging wall was scaled some time after the drift excavation. Consequently it was difficult to identify the original rock profile of the hanging wall in March 2008. The wall surface was heavily fragmented, and the installed mesh was bulging and filled with broken rock. In Figure 58 the condition of the drift walls during the visit in March 2008 is shown, together with the initial deformation profile, as described by the mine staff.

Figure 58: Hanging wall (left) and footwall (right) of drift 218-35-W (LaRonde mine, March 2008)

Between November 23, 2007 and February 28, 2008 convergence measurements were carried out in drift 218-35-W. During this time altogether nine measurements were taken. Measured was the opening width in the upper and in the lower part of five drift profiles as shown in the outline in Figure 59. The distance between each profile was approximately four meters. The measurements in the upper part of the drift were taken at a height of about

2.60 m from the floor, and in the lower part at a height of 1.00 m. Table 26 provides a summary of the measured convergence. The convergence percentage is given with reference to the initially measured drift widths. Since only the total width of the drift opening was measured, the values provide the total reduction of the opening width after a certain time. It is not possible to quantify the individual side wall deformation. However, it is a reasonable assumption that most of the measured convergence is associated with deformation of the hanging wall.
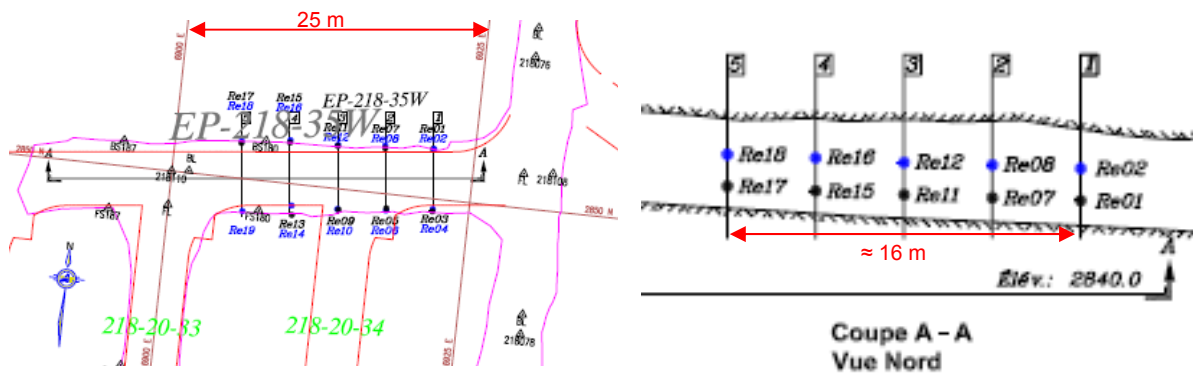
Figure 59: Measuring profiles for drift 218-35-W, LaRonde mine (without scale): plan view (left), longitudinal section (right)

Table 26: Convergence measured in drift 218-35-W (LaRonde mine) along a drift length of 16 m

	Upper part of wall (H = 2.60 m above floor)		Lower part of wall (H = 1.00 m above floor)	
	Mean (stdev)		Mean (stdev)	
	[m]	[%]*	[m]	[%]*
Total convergence after 9 measurements between Nov. 23, 2007 and Feb. 28, 2008	0.34 (0.07)	6.16 (1.29)	0.19 (0.09)	3.40 (1.50)

*in % of initial drift opening widths

There is nearly no seismic activity in the region of drift 218-35-W (see Figure 60). In the closer area only three minor seismic events were registered, all of them with a magnitude of less than -0.8 on the local scale (corresponding to a magnitude of about 0.2 on the Nuttli scale).

Figure 60: Seismic events during the years 2006 and 2007 on level 218 (left) and close to drift 218-35-W (right) (LaRonde mine)

All available information concerning drift 218-35-W is given in Annex M, and the detailed results of the convergence measurements are provided in Annex P.

Drift 227-43-E

Haulage drift 227-43-E is situated 2270 m below the surface (level 227) and enables the access to three stopes in the eastern part of the mine (see Figure 61). The drift is approximately east-west oriented (trend of 85°). The investigated drift length is about 20 m.

Figure 61: Location of drift 227-43-E at the LaRonde mine

The drift was excavated during July 2007 with an opening width varying between 4.51 m and 6.14 m. The width was measured in August 2007 in 11 drift profiles over a drift length of 20 m. No initial drift height measurements were available. The height was determined during a site visit in March 2008 in eight drift profiles. Thereby, values between 4.04 m and 5.05 m were measured. Table 27 provides the evaluated drift geometry.

Table 27: Opening geometry of drift 227-43-E (LaRonde mine) along a drift length of 20 m

	Opening width (August 2007)		Opening height (March 2008)
	Upper part of drift	Lower part of drift	
Range measured in 11 (width) and 8 (height) drift profiles [m]	4.15 – 5.59	4.56 – 6.14	4.04 - 5.05
Mean (stdev) [m]	4.91 (0.37)	5.25 (0.43)	4.32 (0.35)

The first support was installed immediately after the drift was excavated. The side wall support consisted of friction sets and mesh (friction sets 6′6″ and 6-gauge weld mesh) as well as hybrid bolts (hybrid bolt = resin grouted rebar installed inside a friction bolt). The support standard for drift 227-43-E is shown in Figure 62. In this location no mesh straps were installed with the hybrid bolts. The back was supported with resin grouted rebars 7′6″/9′6″ and 6-gauge weld mesh. Friction sets in the east part of the hanging wall, which were damaged by mine equipment, were replaced in November/December 2007.

The rock mass in drift 227-43-E consists of intermediate tuff. The rock is schistose and contains a relatively high amount of sericite. Both hanging wall and footwall are strongly altered. The rock foliation has a dip of 75° and a dip direction of 180° (strike parallel to the drift trend). The spacing of the foliation is about 1 to 5 cm. The footwall shows deformed and broken layers of the foliation about 60 cm from the floor. Both side walls show signs of great displacements (deformed foliation, broken rock, etc.). The wall surfaces are completely broken, and, as stated by the mine staff, the hanging wall had to be scaled to keep the drift accessible. Figure 63 shows the state of the drift in March 2008. As a result of scaling and rehabilitation work it was not possible to establish the original deformation profile as described by the mine staff and outlined in Figure 63. According to the mine staff, the footwall had less displacement than the hanging wall.
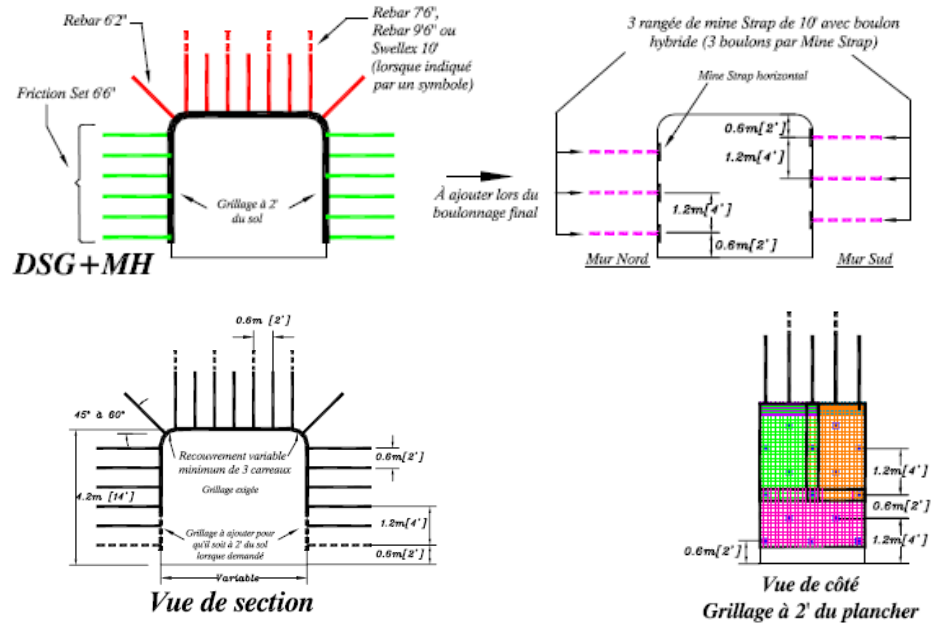
Figure 62: Support standard for drift 227-43-E at the LaRonde mine (DSG+MH = Devis Standard Grillage + Mine strap et boulon Hybride)
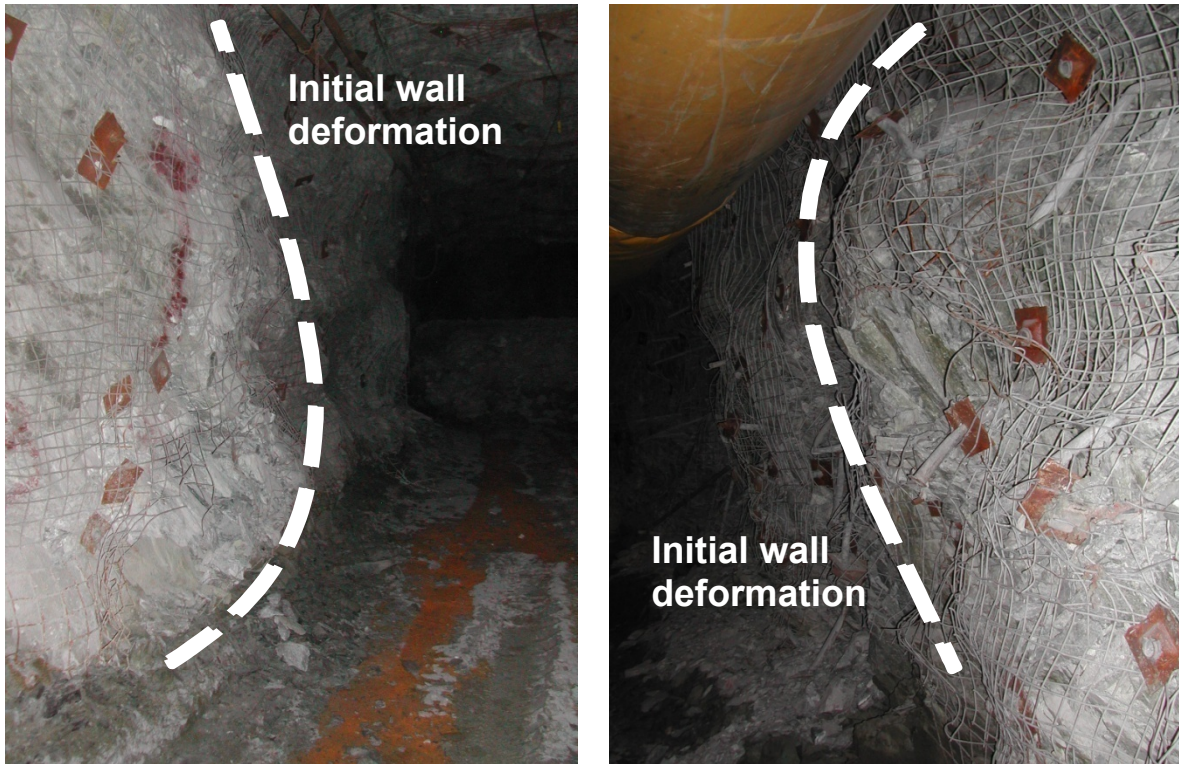
Figure 63: Footwall (left) and hanging wall (right) of drift 227-43-E (LaRonde mine, March 2008)

Between August 22, 2007 and November 30, 2007 altogether 10 measurements were taken in drift 227-43-E along a length of 20 m. The opening width was measured in 11 drift profiles in the upper and in the lower part of the drift with a distance of two meters between each profile. The position of the measuring lines is shown in Figure 64. The measuring points at the sidewalls were located 3.00 m and 1.25 m respectively above the floor. As a result of rock falls most of the measuring points were destroyed a few months after the drift excavation, and the monitoring program was abandoned.
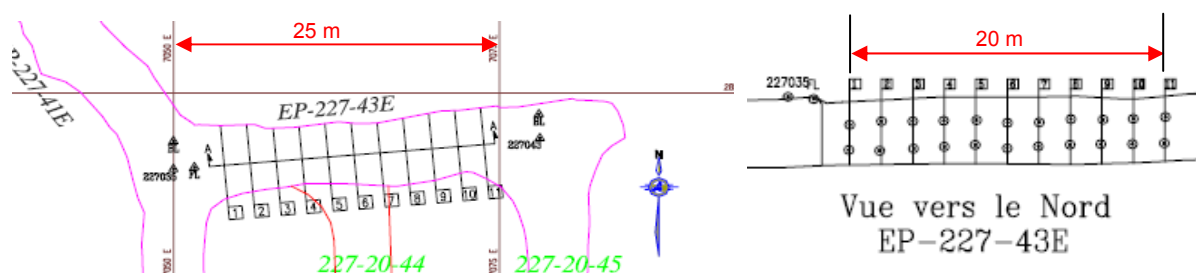
Figure 64: Measuring profiles for drift 227-43-E, LaRonde mine (without scale): plan view (left), longitudinal section (right)

In Table 28 a summary of the convergence measuring results is provided. The convergence percentage was determined based on the initially measured drift widths. The mean convergence was calculated only for the measuring profiles 1 to 7 since for the profiles 8 to 10 no more measurements were carried out after two months, and profile 11 was measured only sporadically.

Table 28: Convergence measured in drift 227-43-E (LaRonde mine) along a drift length of 20 m

	Upper part of wall (H=3.00 m above floor)		Lower part of wall (H=1.25 m above floor)	
	Mean (stdev)		Mean (stdev)	
	[m]	[%]*	[m]	[%]*
Total convergence after 11 measurements between Aug. 22 and Nov. 30, 2007	0.15 (0.09)	3.06 (1.99)	0.21 (0.22)	3.81 (4.05)

*in % of initial drift opening widths

Although a cluster of seismic events was registered a short distance eastwards from drift 227-43-E, there is only low seismic activity in the immediate region of drift 227-43-E (see Figure 65). Only two minor seismic events were registered in the west part since the drift

was excavated, both with a magnitude of less than -1.5 on the local scale (corresponding to a magnitude of about -0.5 on the Nuttli scale). Two events in the surrounding of the drift had a local magnitude of about -0.5 (about 0.5 on Nuttli scale).
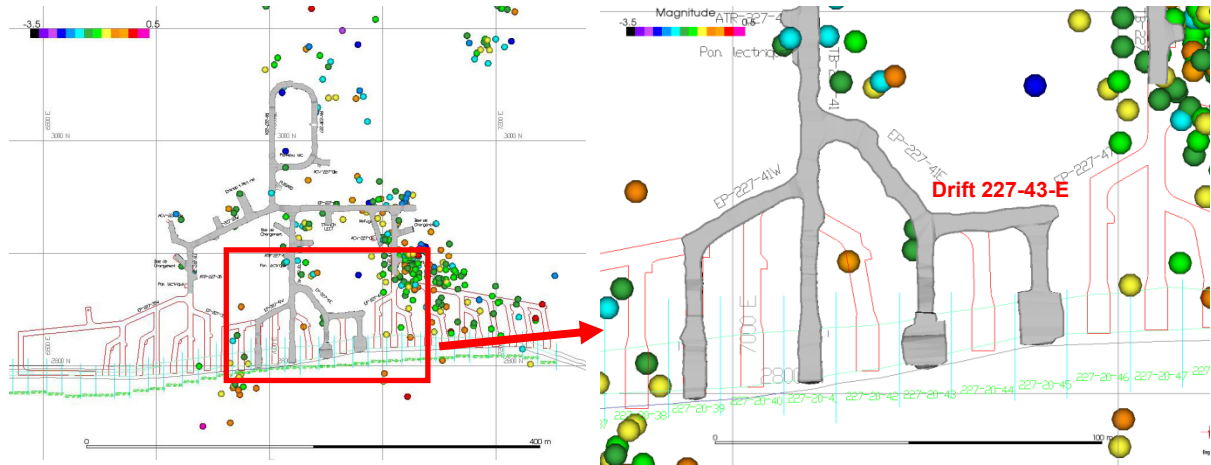
Figure 65: Seismic events during the years 2006 and 2007 on level 227 (left) and close to drift 227-43-E (right) (LaRonde mine)

All information about drift 227-43-E is summarized in Annex N. The detailed results of the convergence measurements are given in Annex Q.

Drift 233-41-W

Haulage drift 233-41-W is situated 2330 m below the surface (level 233). Of interest was the eastern part of the drift, which enables the access to three stopes (see Figure 66). The drift runs approximately from north-east to south-west (trend of 60°). The investigated drift length is about 25 m.

The drift was excavated during May 2007 with an opening width varying between 4.35 m and 6.20 m. The widths were measured in June 2007 in 13 drift profiles over the investigated drift length of 25 m. No initial drift height measurements were available. The drift height was determined during a site visit in March 2008 in six drift profiles. Thereby, values between 4.00 m and 4.30 m were measured. In Table 29 the evaluated drift geometry is given.
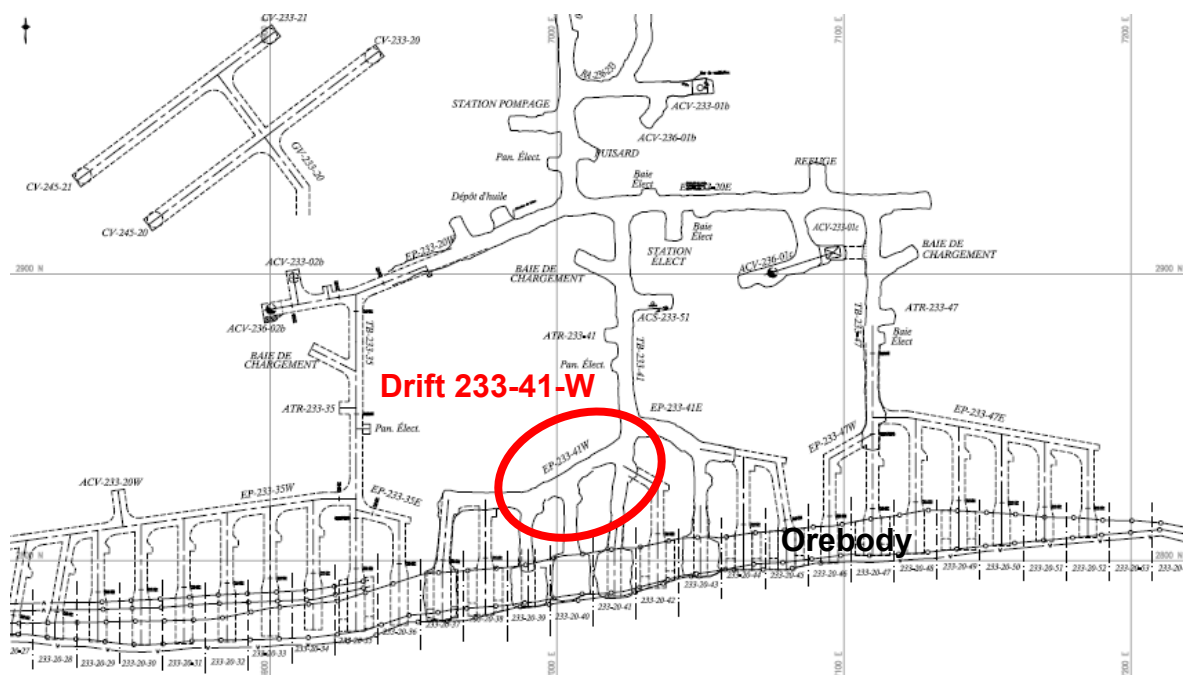
Figure 66: Location of drift 233-41-W at the LaRonde mine

Table 29: Opening geometry of drift 233-41-W (LaRonde mine) along 25 m drift length

	Opening width (June 2007)		Opening height (March 2008)
	Upper part of wall	**Lower part of wall**	
Range measured in 13 (width) and 6 (height) drift profiles [m]	4.35 – 6.06	4.82 – 6.20	4.00 – 4.30
Mean (stdev) [m]	4.97 (0.50)	5.29 (0.40)	4.15 (0.12)

The first support was installed immediately after the excavation of the drift. The side walls were supported with friction sets and mesh (friction sets 6′6″ and 6-gauge weld mesh) and hybrid bolts. The support standard for this drift is shown in Figure 67. No mesh straps but 6-gauge mesh were installed with the hybrid bolts. The back was supported with resin grouted rebars 7′6″/9′6″ and 6-gauge weld mesh.
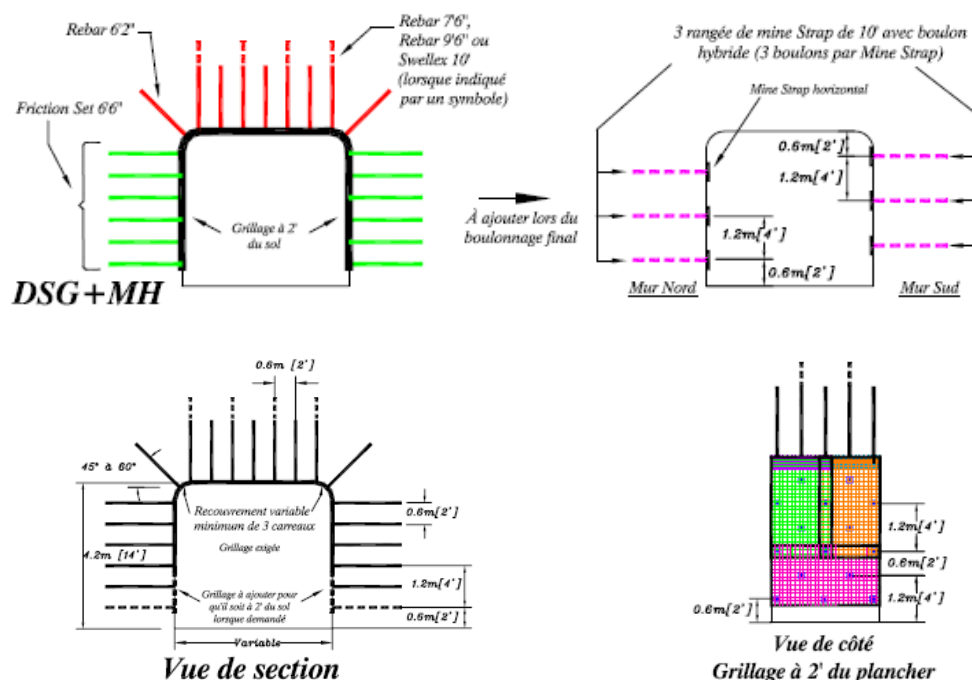
Figure 67: Support standard for drift 233-41-W at the LaRonde mine (DSG+MH = Devis Standard Grillage + Mine strap et boulon Hybride)

Various rehabilitation work was carried out in drift 233-41-W. In September 2007 the footwall support in the western part of the drift was repaired, and near stope 233-20-40 broken friction sets and damaged mesh were replaced. In November 2007 additional mesh and friction sets were installed on the footwall close to stope 233-20-40 to provide a better support during the excavation of this stope. At the eastern drift entrance the first 6 m of the hanging wall were shotcreted (see Figure 68, left side). No information was available about the date of installation.

The rock mass in drift 233-41-W consists of intermediate tuff. As in drift 227-43-E the rock is schistose and contains sericite. Both the hanging wall and the footwall are strongly altered. The rock foliation has a dip of about 75° and a dip direction of 175°. Since the drift has a trend of 60°, the foliation does not run parallel to the drift. The angle between drift trend and strike of foliation is about 25°. The spacing of the foliation is about 5 cm. On the lower footwall locally deformed and broken rock layers are visible. Both sidewall surfaces are heavily broken and show signs of great displacements (deformed foliation, broken rock, etc.), but in places the initial deformation profile with large displacements in the upper hanging wall and in the lower footwall is still visible (see Figure 68). According to the

mine staff, the hanging wall and the footwall had shown approximately the same amount of displacement.
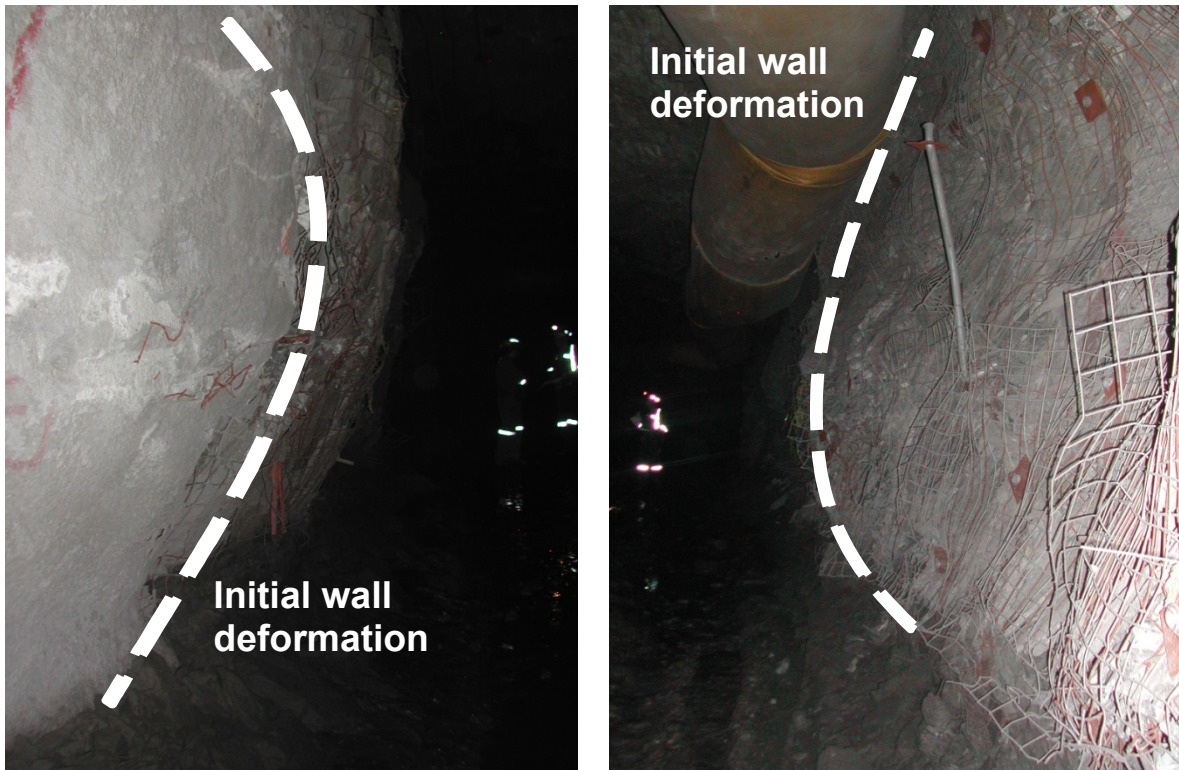
Figure 68: Hanging wall (left) and footwall (right) of drift 233-41-W (LaRonde mine, March 2008)

Between June 06, 2007 and November 05, 2007 altogether 14 convergence measurements were carried out in haulage drift 233-41-W over a length of about 25 m. As shown in the outline in Figure 69, a total of 13 profiles with a distance of two meters between each profile were measured. In each profile the opening width in the upper and in the lower part of the drift was measured, taken at a height of 2.50 m and 1.10 m respectively. As a result of large deformations the measuring points installed on the side walls were destroyed a few months after the drift was excavated, and all measurements were stopped. In Table 30 a summary of the measured convergence in drift 233-43-E is given. The convergence percentage was calculated with reference to the initially measured opening widths.
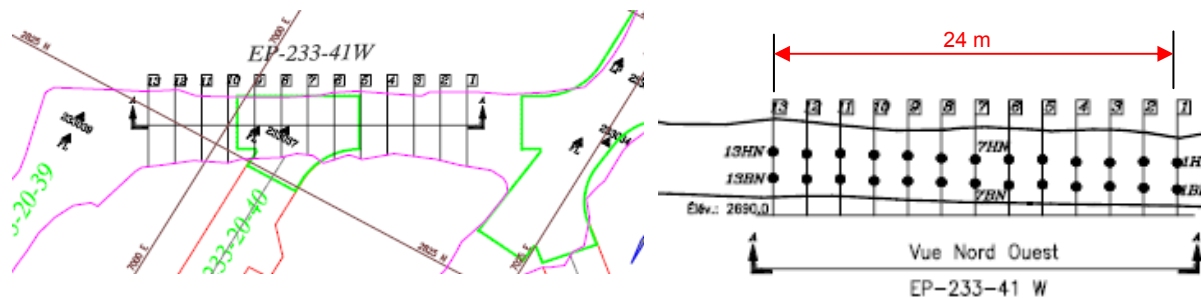
Figure 69: Measuring profiles for drift 233-41-W at the LaRonde mine (without scale): plan view (left), longitudinal section (right)

Table 30: Convergence measured in drift 233-41-W (LaRonde mine) along 25 m drift length

	Upper part of wall (H = 2.50 m above floor)		Lower part of wall (H = 1.10 m above floor)	
	Mean (stdev)		Mean (stdev)	
	[m]	[%]*	[m]	[%]*
Total convergence after 14 measurements between June 06 and Nov. 05, 2007	0.26 (0.11)	5.05 (1.96)	0.19 (0.19)	3.52 (3.53)

*in % of initial drift opening widths

In comparison with the two drifts described above the seismic activity in the area of drift 233-41-W is slightly higher (see Figure 70). Especially during the excavation of stope 233-20-39 several seismic events were registered, but most of them with a small magnitude of less than -1.2 on the local scale, and three events with a local magnitude of less than -0.8 (corresponding to a magnitude of about -0.2 and 0.2 respectively on the Nuttli scale). One event with a local magnitude of -0.5 (about 0.5 on the Nuttli scale) occurred close to stope 233-20-40. Nevertheless, when compared with other regions of the mine the occurrence of seismic events is relatively low.

Detailed information about drift 233-41-W is provided in Annex O, and the complete convergence measurements results are given in Annex R.
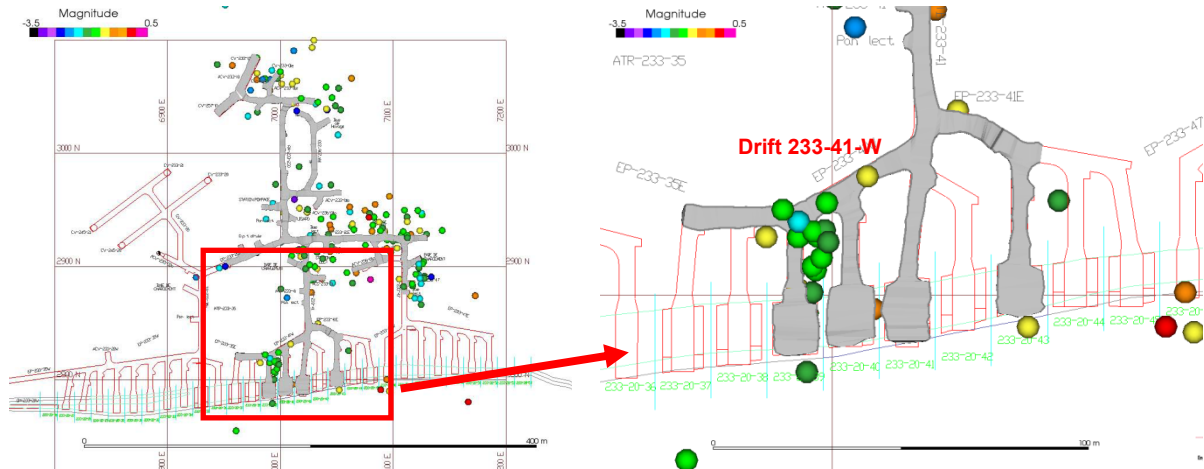
Figure 70: Seismic events during the years 2006 and 2007 on level 233 (left), and close to drift 233-41-W (right) (LaRonde mine)

5.4 Summary

In this chapter a stability problem of underground excavations in fractured rock is discussed. Three drifts at the LaRonde underground mine were investigated that displayed pronounced convergence as a result of rock squeezing. Squeezing is usually associated with specific rock conditions. At LaRonde the following factors lead to squeezing conditions: altered rock with pronounced foliation, high stresses due to excavations at great depth, and drift axes parallel to the strike of the foliation, whereby the nearly vertical foliation planes run parallel to the drift walls. The rock displacements usually lead to typical deformation profiles with pronounced bulging in the upper hanging wall and in the lower footwall.

In this chapter a detailed description of the rock mass and of the investigated drifts is given. Furthermore, the data that was necessary for the analysis of the observed convergence is specified. This data was either collected on site or provided by the mine. The convergence analysis is presented in the following chapter 6.

6 Convergence analysis of underground drifts

The large wall deformations observed in certain drifts at LaRonde, caused by geologic factors and stress conditions in the mine area, were of interest in this second case study. The aim was to develop a numerical model to describe the deformations observed in certain drifts. It was intended to reproduce the observed failure mechanism with the aid of numerical modelling using the finite element method.

6.1 Numerical modelling application for squeezing rock

Several publications deal with the problem of modelling excavations in squeezing rock. Hoek, 2001 discusses civil engineering tunnels under squeezing conditions. He used the results of numerical experiments, carried out with a 2D finite element model (PHASE2, Rocscience Inc., Toronto), to link resulting strain to rock mass strength and in-situ stresses. In his axi-symmetric numerical model Hoek, 2001 assumed a circular tunnel cross section with a diameter of 8 m, exposed to equal horizontal and vertical in-situ stresses. The applied stresses are relatively low (12 MPa). The rock mass in this model was homogeneous and without any specific structure, and had an elastic-plastic material behaviour. Hoek, 2001 developed a relationship between the percentage strain ε and the ratio of rock mass strength σ_{cm} to in situ stress p_o, whereby he considered different rock masses, in situ stresses, and internal support pressures. Strain was thereby defined as ratio of either tunnel wall or tunnel face deformation δ to tunnel radius r. A comparison of the modelling results with field observations showed an acceptable agreement. From this results Hoek, 2001 developed a curve of ground response related to rock mass strength, as shown in Figure 71, which provide the possibility for a first estimation of tunneling problems that have to be expected in squeezing ground.

Although applicable to a wide range of cases, these results are not directly transferable to the case study discussed in this work. As shown in chapter 5 the investigated drifts at LaRonde are rectangular, and they are in a mining environment under anisotropic high stress. Furthermore, the rock mass is inhomogeneous with a prominent structure. However, in the present case study also a 2D finite element model was used since the approach by Hoek, 2001 shows that this is a useful tool to analyze the behaviour of squeezing ground by

means of strain, i.e. in this case by using the measured deformation of the squeezing rock.
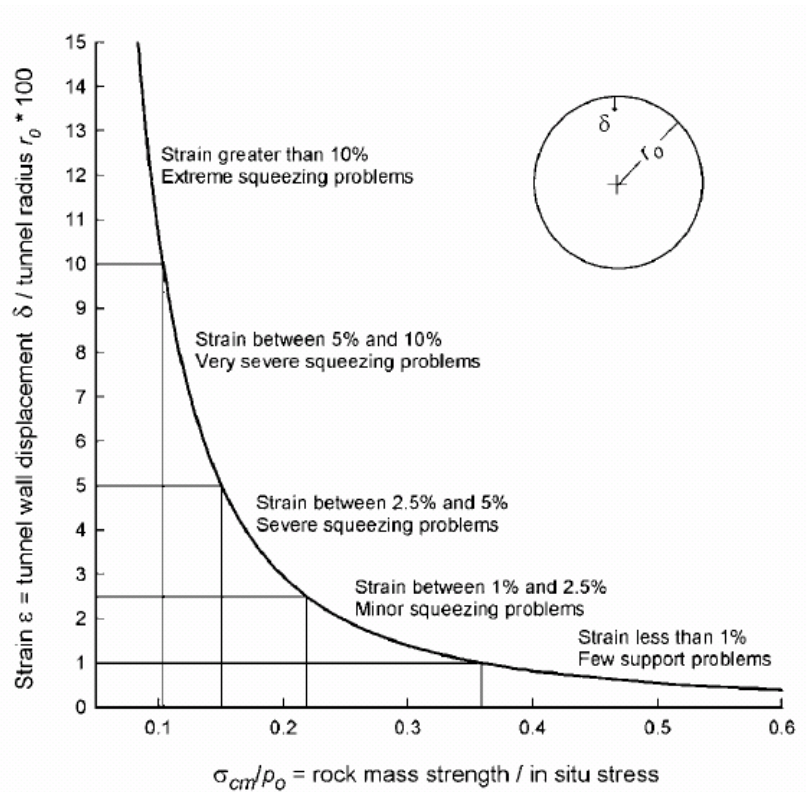
Figure 71: Tunneling problems associated with different levels of strain (Hoek, 2001)

Another approach of modelling the influence of squeezing ground conditions on civil engineering tunnels is provided by Barla et al., 2007. These authors used a more complex numerical model (FLAC2D, Itasca Consulting Canada Inc., Sudbury), which accounts for viscoelastic-plastic material behaviour, to simulate the time-dependent behaviour of squeezing ground around a circular tunnel. A comparison of the resulting deformations with long term field measurements showed that at least for the early stages the modelled and measured values were in good agreement.

Malan, 2002 investigated different numerical approaches to simulate the time-dependent behaviour of tabular excavations, whereby his focus was on the long term development of fracture zones around an excavation. This approach was not considered in the present work, since the emphasis was not on fracture development but on the resulting wall deformations due to squeezing ground.

Sandy et al., 2007 discuss tabular mining excavations that are affected by squeezing ground conditions using two different numerical models: a 2D finite element model (PHASE2, Rocscience Inc., Toronto) and a 3D finite difference model (FLAC3D, Itasca Consulting Canada Inc., Sudbury). The two models are shown in Figure 72 and Figure 73. Sandy et al., 2007 suggested that the 2D finite element model can be used to show the probable location of shearing on foliation (see Figure 72). Since no reference to any site data is given, this model is regarded as a conceptual model.
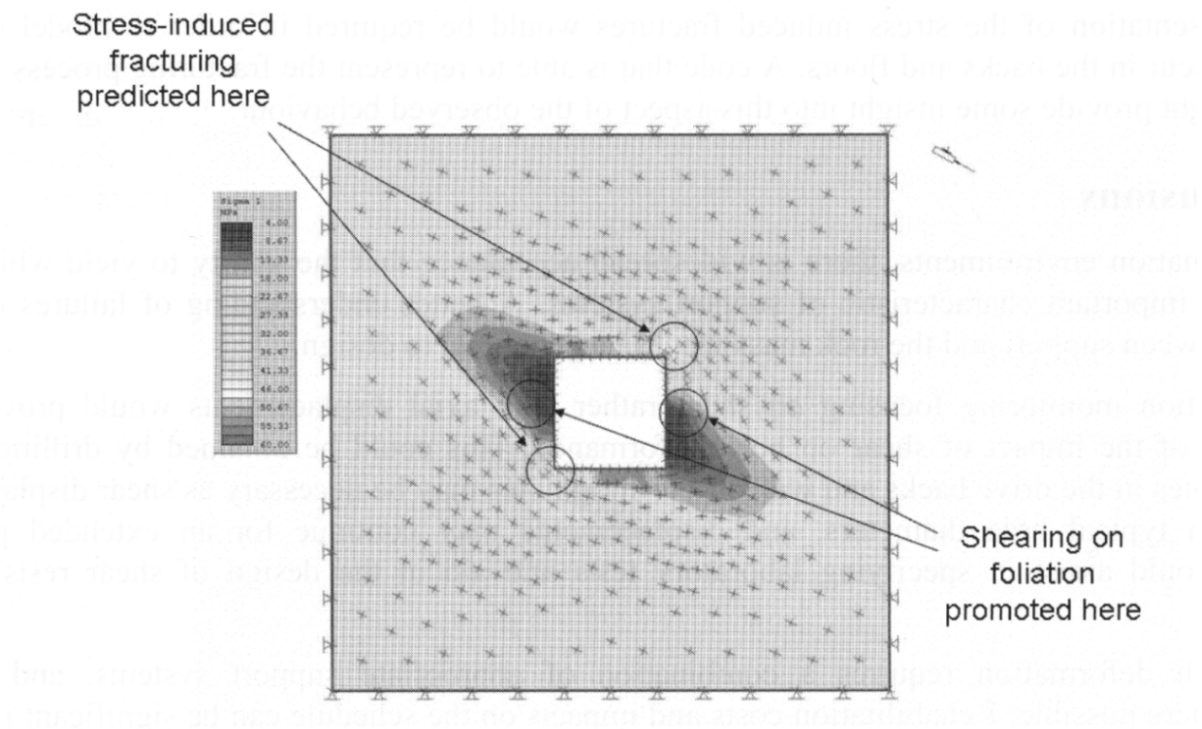
Figure 72: Numerical modelling of squeezing ground with PHASE2 (after Sandy et al., 2007)

In another numerical modelling study in the same publication Sandy et al., 2007 used FLAC3D. The 2D representation of their 3D model is shown in Figure 73. Information about the investigated site is not given. Sandy et al., 2007 state, that this model localized the shearing zones in good agreement with the field observations. Modelled or measured deformations are not provided.
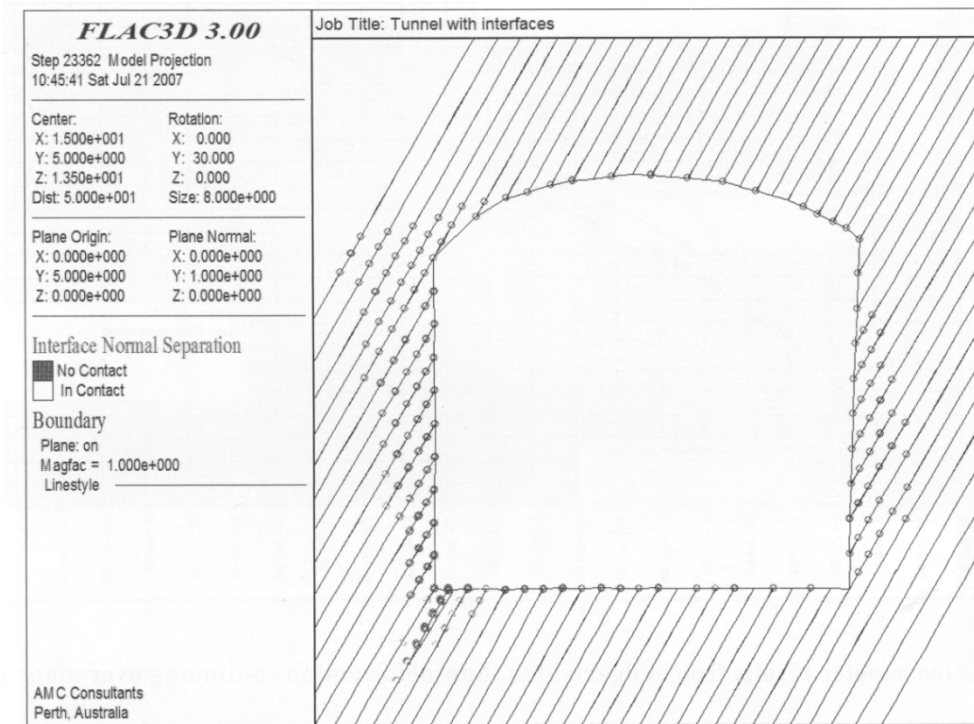
Figure 73: Numerical modelling of squeezing ground with FLAC3D (after Sandy et al., 2007)

Mercier-Langevin and Turcotte, 2007 present results of numerical modelling of squeezing ground conditions at LaRonde (see Figure 74). They also used a 2D finite element model (PHASE2) to simulate the squeezing conditions. In their case study the pronounced foliation of the rock was introduced explicitly into the model. The model reproduced the typical sidewall deformation profile based on observations in certain haulage drifts at LaRonde as shown in Figure 74. These were not related to any particular drift. Measured deformation magnitudes are not given.

Different numerical approaches investigating strain, rock fracturing, or slip on foliation were presented by different authors as discussed above. The approach followed in this work was similar to Hoek, 2001, and focused on the deformations due to squeezing rock conditions. As in Mercier-Langevin and Turcotte, 2007 the 2D finite element program PHASE2, version 6.0 (Rocscience, 2008b) was applied for the numerical analysis considering elasto-plastic material behaviour. The objective was to develop representative deformation models based on field data that was provided by the mine.
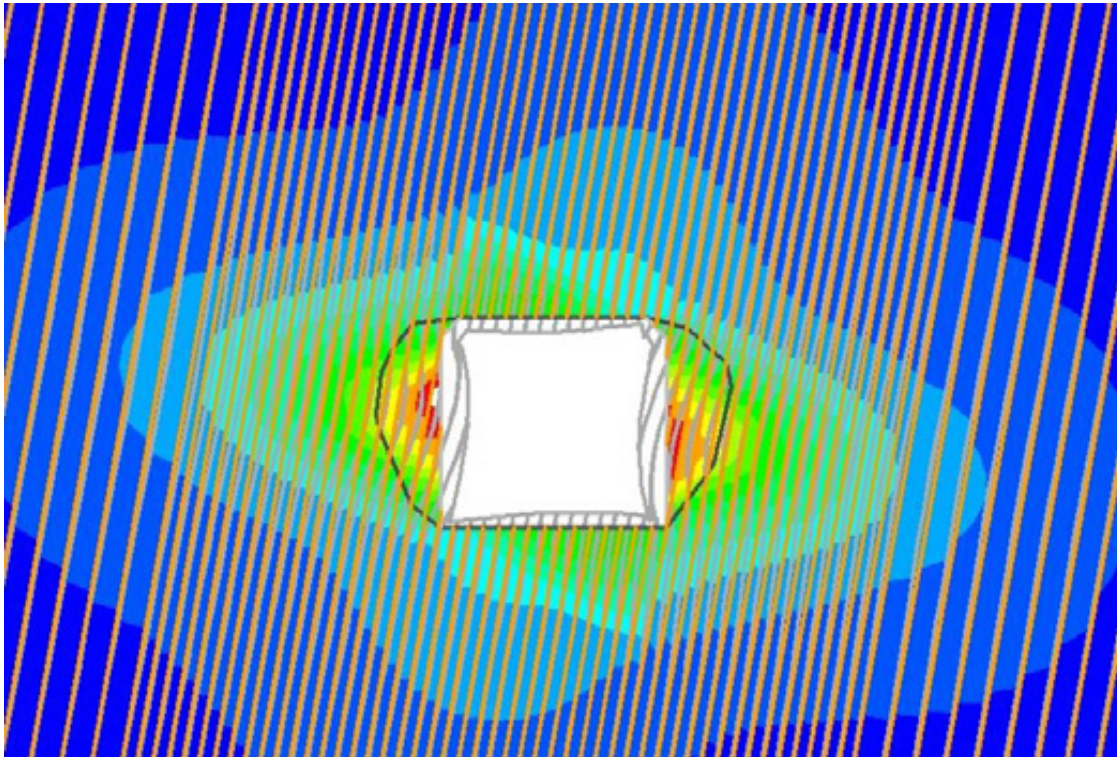
Figure 74: Numerical modelling of squeezing ground at LaRonde using PHASE2 (after Mercier-Langevin and Turcotte, 2007)

In the following sections the numerical analysis of drift wall convergence is presented that was carried out for three investigated mine areas (drift 218-35-W, 227-43-E, and 233-41-W). All available input data and reference data for the numerical models as well as the modelling results are described, including model development and model calibration.

6.2 Failure mechanism

The postulated failure mechanism at LaRonde is shearing along the joint planes, as shown schematically in Figure 75. In drifts where the foliation runs parallel to the drift trend the rock mass starts to deform and to move into the opening once the drift is excavated. This mechanism is driven by high stresses perpendicular to the foliation, and often accompanied with a break of the outer layers.
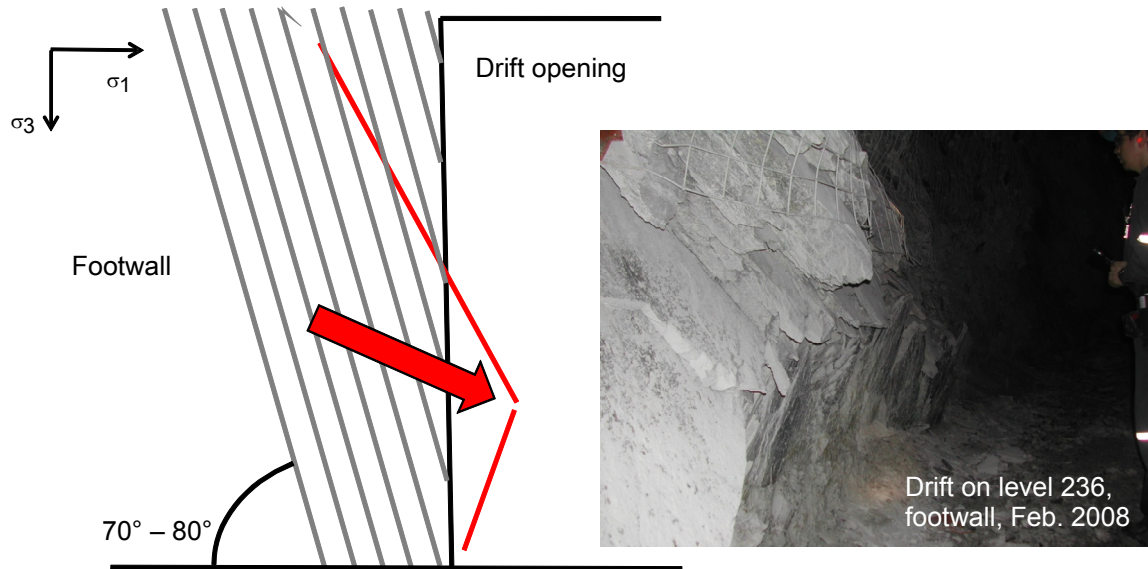
Figure 75: Failure mechanism observed in certain drifts at the LaRonde mine (schematic and on site)

6.3 Analysis data

The objective of the numerical convergence analysis was the reproduction of the observed failure mechanism with the aid of numerical models. Two types of data were necessary for the analysis: input data for the model development, and reference data for the model calibration. Table 31 summarizes all data that was used for the performance of the convergence analysis.

Table 31: Analysis data

Input data	
- In-situ stresses of intact rock - Elastic properties of the rock mass	Data provided by the mine
- Structural parameters	Measured data
- Strength parameters for rock mass and joints	Extrapolated data
Reference data	
- Convergence measurements - Drift profiles	Data provided by the mine

6.3.1 Input data for model development

Based on the available information three drift models were generated. The external boundaries of all three models were chosen with respect to the influence zone of an

underground excavation on the adjacent ground. According to Hoek and Brown, 1980 the influence of a circular tunnel opening on the stresses in the rock tends to zero in a distance of three times the radius of the excavation, measured from the center of the excavation. Hoek and Brown, 1980 suggest that the minimum size of a model should be three to four times the maximum dimension of an excavation. Considering a maximum excavation width of 5.50 m and a maximum height of 4.30 m, the model dimensions were set to 35 x 35 m, to get a sufficiently large model with minimum external boundary disturbance.

In Table 32 the model configurations are summarized. The foliation was introduced explicitly into the model. Based on preliminary analysis it was recognized that the models had to be simplified in order to allow for model execution. In particular a spacing of 15 cm was used in all models to specify the foliation. This was a simplification of the observed spacing of in places 1 to 5 cm.

Table 32: Input data: model generation

		215-35-W	227-43-E	233-41-W
External boundaries	[m]	35 x 35	35 x 35	35 x 35
Opening geometry:				
Height	[m]	4.20	4.30	4.15
Width	[m]	5.50	5.10	5.25
Foliation:				
Spacing	[cm]	15	15	15
Inclination (Dip)	[°]	80	75	75

The small spacing of the foliation resulted in the generation of a finite element mesh with elements having very small interior angles. According to Rocscience, 2008b these long thin elements, defined as of "poor quality" (see Annex S, T, and U) "can have adverse effects on the analysis results". However, due to the introduction of the foliation these elements could not be avoided and were accepted within this work.

The in-situ stresses of the intact rock were calculated with the equations provided in section 5.3.3, Table 23. The resulting stresses for the three investigated underground levels are given in Table 33. All investigated drifts are located in intermediate tuff. The elastic properties of this rock type are provided in Table 34.

There were no further field data available for the constitutive rock and joint properties at LaRonde. The choice of these parameters was made through an iterative process within a plausible range. The chosen values are provided in the following sections.

Table 33: Input data: in-situ stress

Stress component		215-35-W	227-43-E	233-41-W
σ_1	[MPa]	96	99	102
σ_2	[MPa]	63	65	66
σ_3	[MPa]	61	64	65

Table 34: Input data: elastic properties

	Young modulus E [MPa]	Poisson's ratio ν [--]
Intermediate tuff	48,000	0.16

Figure 76: Rock support on level 218 and 227 (LaRonde mine, March 2008)

As a further simplification of the developed models the influence of the applied rock support elements was not considered. It is recognized that the support elements influence the level of deformations. However, because of the partly destroyed and replaced bolts and

the meanwhile irregular bolt pattern due to additionally installed support (see Figure 76) it was not possible to introduce these elements correctly into the model. Furthermore, no precise date of support installation was available, that would be necessary to determine the influence of support on the measured deformations.

6.3.2 Reference data for model calibration

As reference data the results of convergence measurements as well as the deformation profiles were available. In Table 35 the measured total drift convergence is given in meters and as a percentage of the initial mean opening width. The mean values were determined out of the measurements taken in the particular drift profiles (see convergence data in Annex P, Q, and R).

Table 35: Reference data: measured drift convergence (LaRonde mine)

	218-35-W mean (stdev)		227-43-E mean (stdev)		233-41-W mean (stdev)	
	[m]	[%]	[m]	[%]	[m]	[%]
Upper part of wall	0.34 (0.07)	6.16* (1.29)	0.15 (0.09)	3.06* (2.00)	0.26 (0.11)	5.05* (1.96)
Lower part of wall	0.19 (0.09)	3.40* (1.50)	0.21 (0.22)	3.81* (4.05)	0.19 (0.19)	3.52* (3.53)

*in % of initial opening widths

Only the total convergence of the opening was measured (see section 5.1.1). This does not allow for the determination of different displacement rates on hanging wall and footwall. A rough allocation can be made only for drift 218-35-W. Since in this drift the footwall deformations are clearly smaller than the hanging wall deformations, most of the measured convergence can be associated with the hanging wall. The footwall displacement, even though small, is approximately the same over the total drift height. The displacements in drift 227-43-E and 233-41-W were considered as equal for both sidewalls.

Regarding the convergence development over time as shown in Figure 77, Figure 78, and Figure 79 the tendency of increasing sidewall deformations can be recognized. However, it has to be noticed that for all drifts, but especially for the drifts 227-43-E and 233-41-W, the development is erratic with several "negative convergence" values, implying an enlargement instead of a reduction of the opening width. Part of the variations of closure

and expansion of the drifts are probably attributed to scaling of the drift walls. According to the mine staff the hanging walls in drift 218-35-W and 227-43-E were scaled. However, no information about the date of scaling was available. Another possible explanation is the ongoing mining process that has an influence on the sidewalls. According to the monitoring results (see Annex Q and R) some of the measuring points were damaged by mine equipment, and different rehabilitation work was carried out in the drifts. Furthermore, some of the up-and-down movements in several measuring profiles could be measurement errors. Since the individual measurements were taken without repetition, possible measuring inaccuracies could not be detected.
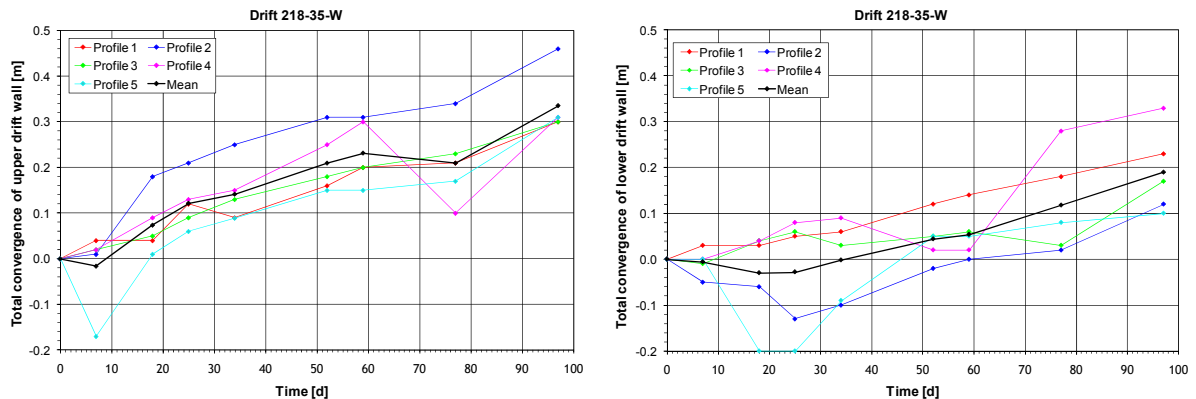
Figure 77: Convergence in drift 218-35-W, measured on upper wall (left) and lower wall (right)
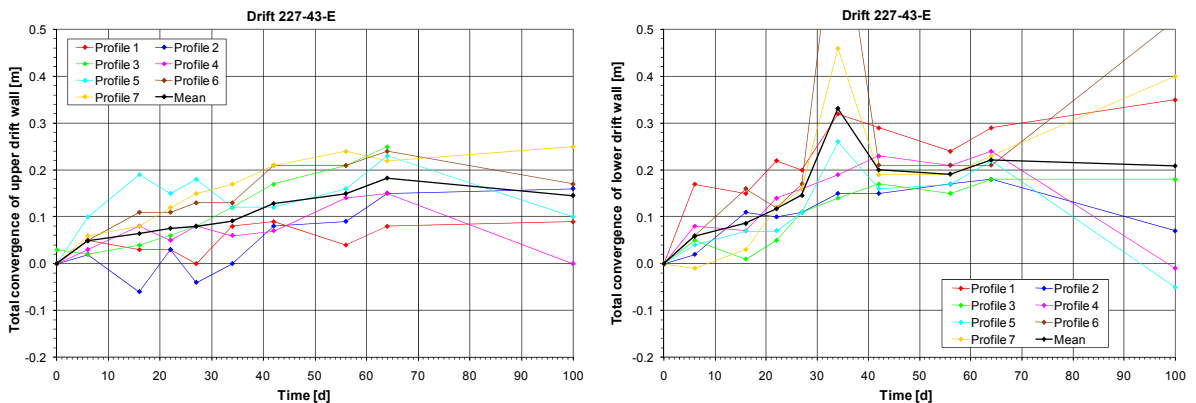
Figure 78: Convergence in drift 227-43-E, measured on upper wall (left) and lower wall (right)
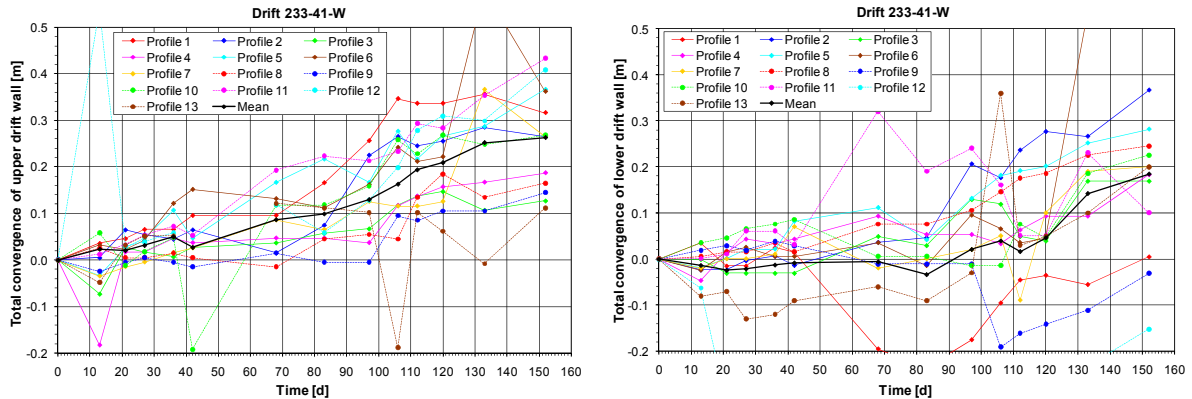
Figure 79: Convergence in drift 233-41-W, measured on upper wall (left) and lower wall (right)

On average the greatest convergence was measured in drift 218-35-W, although in this drift only the hanging wall had large deformations. The potentially smallest convergence was measured in drift 233-41-W. However, due to the above mentioned factors of influence on the measurements, and since the monitoring program did not start at the same point in time after completion of the excavations, it is difficult to compare the convergence in the three drifts.

It is recognized that the available convergence data has limitations. Therefore, it can be used only as a general guideline. It was assumed that modelled deformation values within the range of the standard deviation of the mean deformations are sufficient accurate for the model calibration.

Simplified characteristic deformation profiles observed at LaRonde are shown schematically in Figure 80. As presented in Figure 80 a, the deformations of the hanging wall are more pronounced in the upper part of the wall, and the footwall deformations are more distinctive in the lower part of the wall. This pattern corresponds to the deformation profiles observed in drifts 227-43-E and 233-41-W. A different deformation profile was observed in drift 218-35-W. While the hanging wall in this drift shows the usual deformation with bulging in the upper part of the wall, the footwall has only small deformations over the whole drift height without pronounced bulging (see Figure 80 b).

a) Deformation profile in drift 227-43-E and 233-41-W   b) Deformation profile in drift 218-35-W
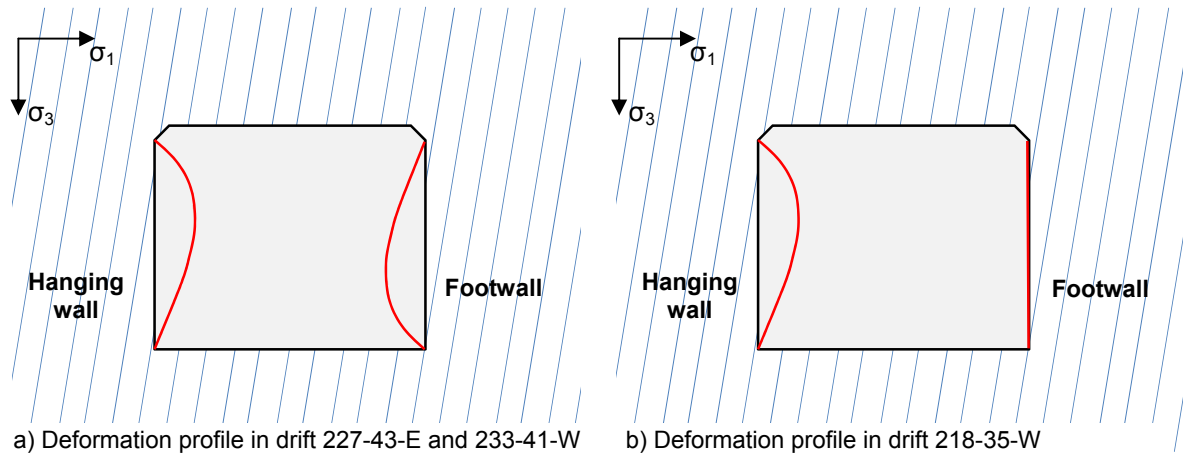
Figure 80: Simplified characteristic deformation profiles observed at LaRonde (without scale)

6.4 Generation and calibration of drift models

In this section the generation and calibration of the three drift models is described. Out of the geometric and structural data from Table 32, Table 33, and Table 34 three models were generated with outer model boundaries of 35 x 35 m. The model of drift 218-35-W is shown in Figure 81. The drift model calibration was carried out in several steps. The first step was a pre-calibration with the aim to define the order of magnitude of the rock mass properties and joint properties. The values for these parameters, selected after a sensitivity analysis and through an iterative process within a plausible range, are provided in Table 36 and Table 37.

Detail drift opening
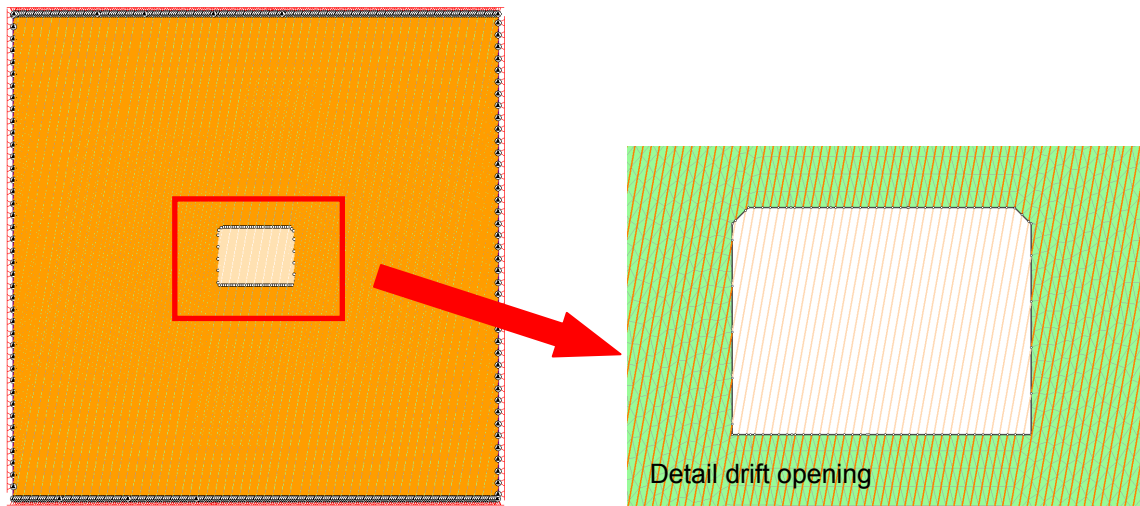
Figure 81: Model of drift 218-35-W

Table 36: Selected data for rock mass properties (first calibration step)

Material properties		Input value
Elastic properties		
Young-modulus E	[MPa]	48,000
Poisson's ratio ν	[-]	0.16
Strength properties (failure criterion = Mohr-Coulomb; elastic-plastic material)		
Tensile strength	[MPa]	0
Friction angle (peak) φ_p	[°]	35
Cohesion (peak) c_p	[MPa]	8
Dilation angle	[°]	0
Friction angle (residual) φ_r	[°]	20
Cohesion (residual) c_r	[MPa]	2

Table 37: Selected data for joint properties (first calibration step)

Joint properties		Input value
Strength properties (slip criterion = Mohr-Coulomb)		
Tensile strength	[MPa]	0
Friction angle φ	[°]	10
Cohesion c	[MPa]	0
Joint stiffness		
Normal stiffness	[MPa/m]	100,000
Shear stiffness	[MPa/m]	10,000

The pre-calibration results are presented in Figure 82, Figure 83, and Figure 84 as well as in Table 38. For each model the total wall deformation profiles are shown, and the size of the sidewall deformations is given with reference to the initial opening widths.

It can be noted that the modeled deformation profiles for drift 227-43-E and 233-41-W correspond well to the profiles observed in these drifts. Both modeled profiles show large sidewall displacements with pronounced deformations of the upper hanging wall and of the lower footwall. On the other side the modelled profile of drift 218-35-W differs from the observed deformation profile. In the model both sides have approximately the same displacements, while on site the footwall is clearly less deformed than the hanging wall and has no pronounced bulging in the lower part of the wall.
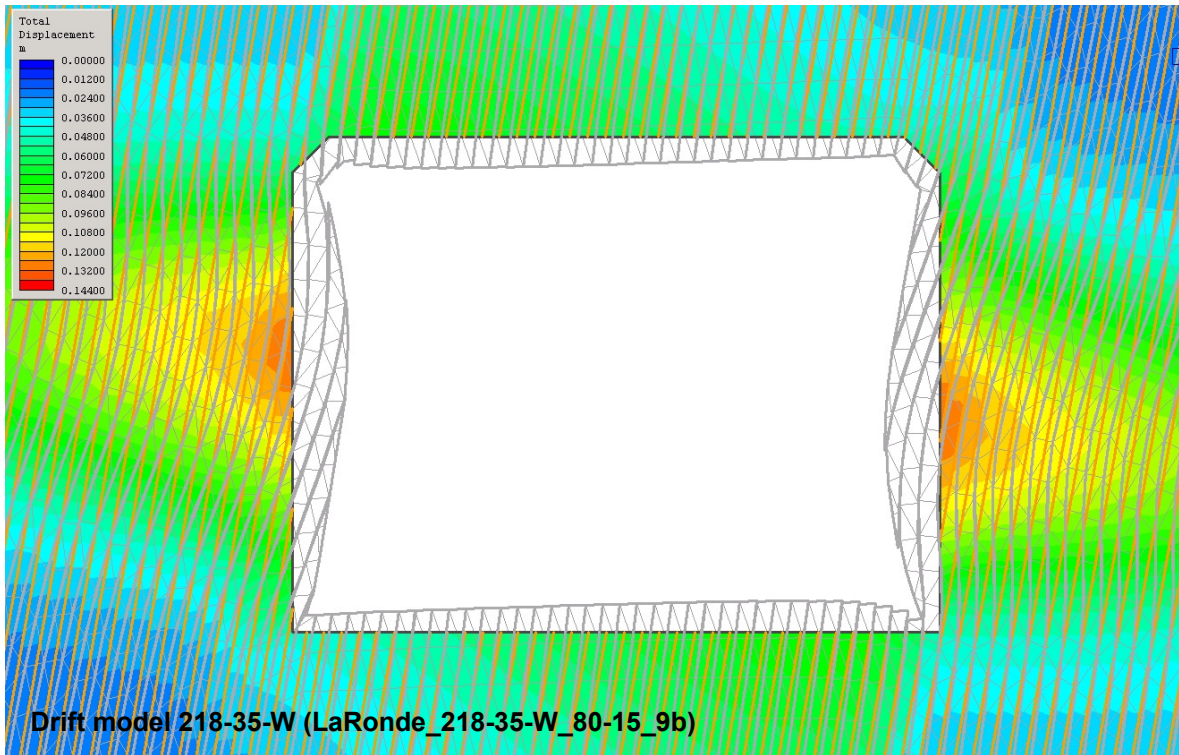
Figure 82: Drift model 218-35-W with resulting deformation profile (first calibration step)
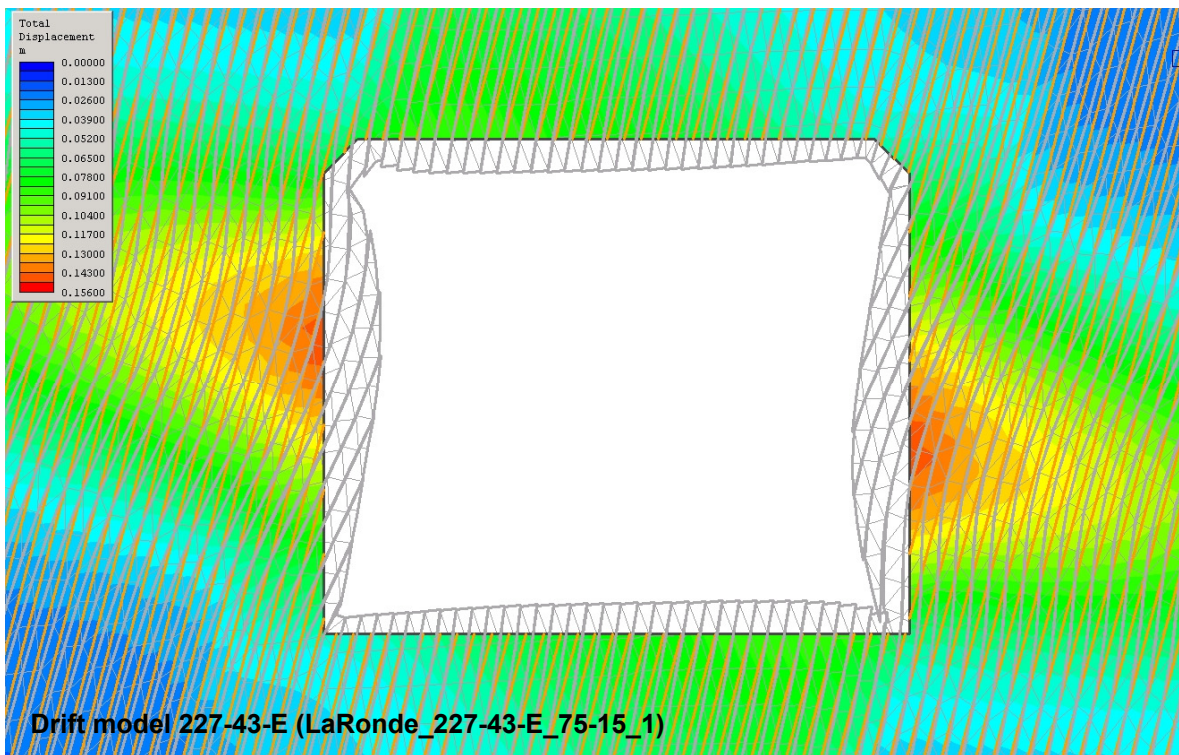
Figure 83: Drift model 227-43-E with resulting deformation profile (first calibration step)
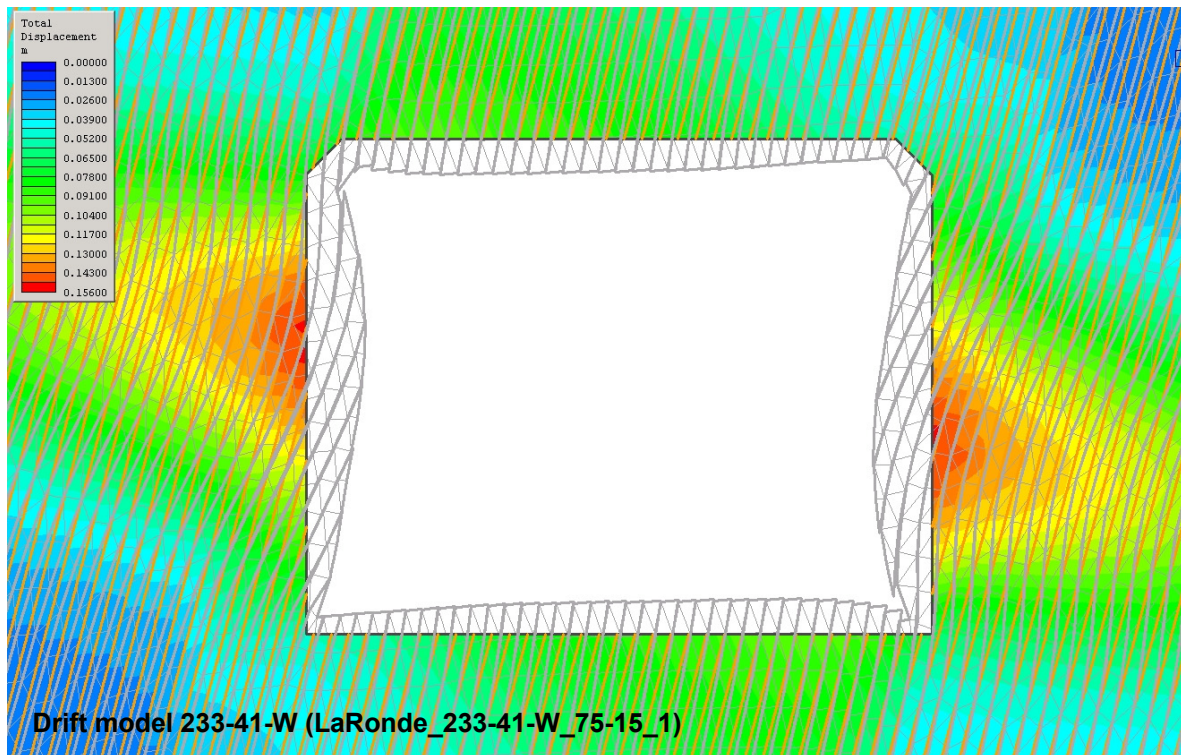
Figure 84: Drift model 233-41-W with resulting deformation profile (first calibration step)

A similar result was obtained for the modelled displacement values. Table 38 summarizes and compares the measured and the modelled convergence. For drift 227-43-E and 233-41-W the magnitude of the modelled deformations, i.e. the resulting total convergence, is within the range of the standard deviation of the measured mean values, both for the upper part and for the lower part of the drift. Agreement between measured and modelled convergence was obtained also for the lower wall in drift 218-35-W. For the upper part of the sidewalls the modelled deformation lies outside the range of the standard deviation of the measured mean value. It follows that the modelled deformations in the upper drift profile are too small.

The generated models of drift 227-43-E and 233-41-W are plausible regarding both the deformation profiles and the deformation magnitude. Further calibration will not lead to higher reliability, and is not justified based on the available reference data. Therefore, the calibration of drift 227-43-E and 233-41-W was concluded after this first calibration step.

Table 38: Measured and modelled convergence (first calibration step)

		218-35-W		227-43-E		233-41-W	
		measured mean (stdev)	modelled	measured mean (stdev)	modelled	measured mean (stdev)	modelled
Upper part of wall (H=2.6m)	**[m]**	0.34 (0.07)	0.24	0.15 (0.09)	0.24	0.26 (0.11)	0.28
	[%][*]	6.16[*] (1.29)	4.40[*]	3.06[*] (2.00)	4.79[*]	5.05[*] (1.96)	5.25[*]
Lower part of wall (H=1.5m)	**[m]**	0.19 (0.09)	0.20	0.21 (0.22)	0.25	0.19 (0.19)	0.25
	[%][*]	3.40[*] (1.50)	3.72[*]	3.81[*] (4.05)	4.85[*]	3.52[*] (3.53)	4.70[*]

[*]in % of initial opening widths

In contrast, the calibration of drift 218-35-W was less successful. While the simulated deformation profile of the hanging wall and the simulated convergence magnitude in the lower drift profile were in accordance with the observed deformation on site, no agreement was reached for the deformation profile of the footwall and the deformation magnitude in the upper drift profile.

Calibration of drift 218-35-W

As described in chapter 5 squeezing is associated with the shear strength of rock. At LaRonde the postulated failure mechanism is a shearing along joint planes. Therefore, the shear strength parameters were considered as the relevant parameters for the observed displacements. Considering the different behaviour of hanging wall and footwall in drift 218-35-W, it was assumed that both sides have different joint shear strength, while the rock mass properties were assumed as equal. Since the displacements of the footwall were smaller than the displacements of the hanging wall, the shear strength of the joints in the footwall is obviously higher. Consequently further calibration of drift model 218-35-W was carried out as sensitivity analysis for the joint shear strength parameters (friction angle and cohesion) in the footwall. These parameters were varied within the range given in Table 39. The emphasis was placed in generating a numerical model that accurately captures the deformation profiles, even if it meant using somewhat exaggerated joint properties. Since the modelled deformation profile for the hanging wall was in agreement with the observed profile, the strength parameters on this side were not further changed, and the values extrapolated in the first calibration step were used. For all other input parameters the pre-calibrated values given in Table 36 and Table 37 were used.

Table 39: Variation of joint shear parameters for drift model 218-35-W (second calibration step)

	Hanging wall	Footwall
Friction angle φ [°]	10	10 - 50
Cohesion c [MPa]	0	0 - 10

The results of the sensitivity analysis are provided in Figure 85. It can be seen that both parameters influence the wall deformations, while the influence of cohesion is clearly higher. Already the introduction of a small cohesion of c = 1 MPa leads to an immediate reduction of wall displacements. The strong influence of even small cohesion is caused by the extensive lengths of the joints within the generated model. With c = 8 MPa the minimum displacement is reached, a further increase in cohesion causes no further decrease of wall displacement. The friction angle has the widest influence when no cohesion is implemented in the model. As soon as cohesion is introduced, the influence of a varying friction angle decreases rapidly. With cohesion of c ≥ 8 MPa a variation in friction angle has no further influence.
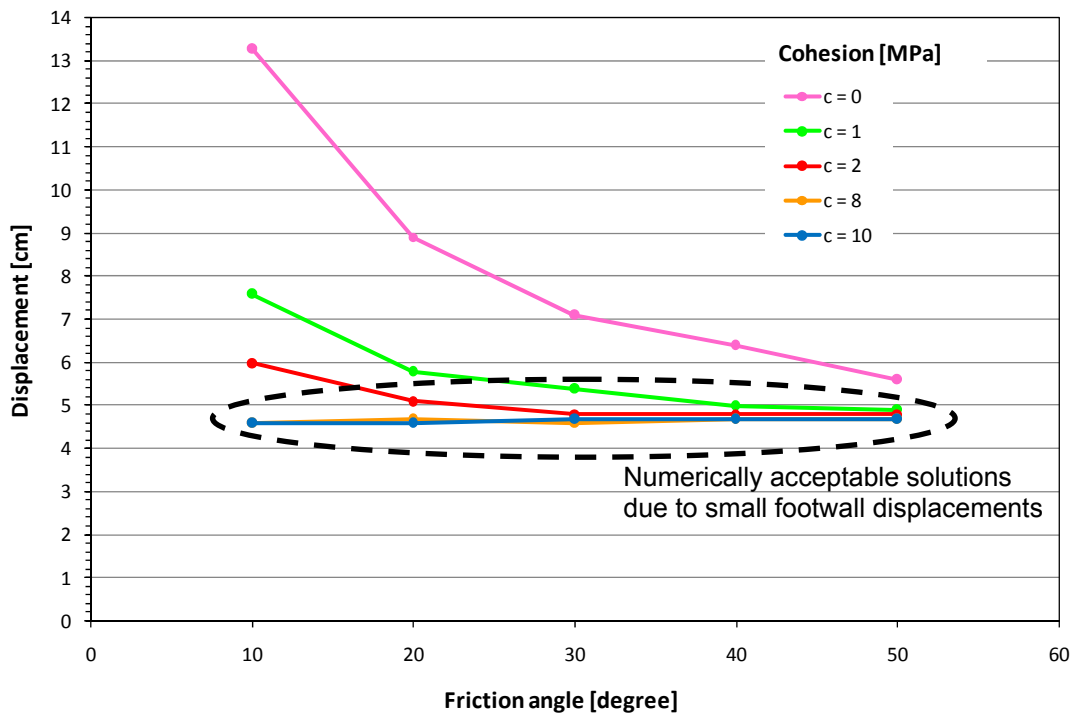
Figure 85: Maximum footwall displacement for varying joint shear strength (second calibration step)

Since the intention of this calibration step was the reduction of the footwall displacements, the parameter combinations indicated in Figure 85 are numerically acceptable solutions, although it is recognized that they are not all plausible. Unlikely is for example a friction angle of 50°. One of the plausible solutions is presented in Figure 86 with a combination of friction angle $\varphi = 20°$ and cohesion c = 2 MPa (see Table 40). Figure 86 shows the resulting deformation profile. In comparison with the first calibration step the footwall has clearly reduced deformations with approximately the same magnitude over the total drift height, while the hanging wall deformations are the same as after the first calibration step, i.e. the magnitude is generally greater, and the displacements are pronounced in the upper part of the wall.
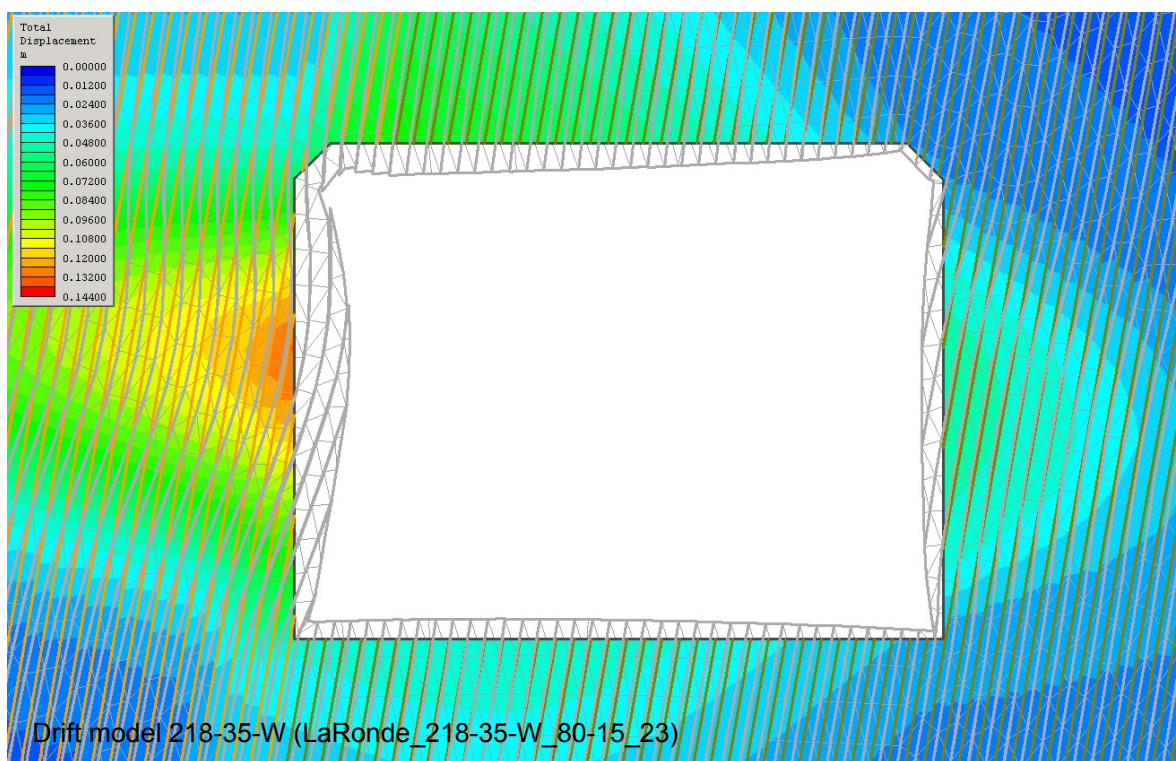
Figure 86: Drift model 218-35-W with resulting deformation profile (second calibration step, plausible solution)

Table 40: Joint shear parameters for drift model 218-35-W (second calibration step)

	Hanging wall	**Footwall**
Friction angle φ [°]	10	20
Cohesion c [MPa]	0	2

There is still a variation between measured and modelled displacements, as can be seen from the convergence values given in Table 41. While the modelled convergence in the lower drift profile is still within the standard deviation of the measured mean value, the modelled convergence of the upper wall is clearly too small. In Figure 87 the resulting total deformations of upper and lower wall are shown for all parameter variations. Indicated are also the measured mean values with their standard deviation. It can be noticed that for the upper wall no agreement between modelled and measured convergence was reached for all parameter combinations, whereas for the lower wall the modeled displacements for all combinations are within the range of the measured standard deviation.

Table 41: Measured and modelled convergence for drift 218-35-W (second calibration step)

Drift 218-35-W		measured convergence mean (stdev)	modelled convergence
Upper part of wall (H=2.60 m above floor)	**[m]**	0.34 (0.07)	0.18
	[%][*]	6.16[*] (1.29)	3.23[*]
Lower part of wall (H=1.00 m above floor)	**[m]**	0.19 (0.09)	0.13
	[%][*]	3.40[*] (1.50)	2.38[*]

[*]in % of initial opening width
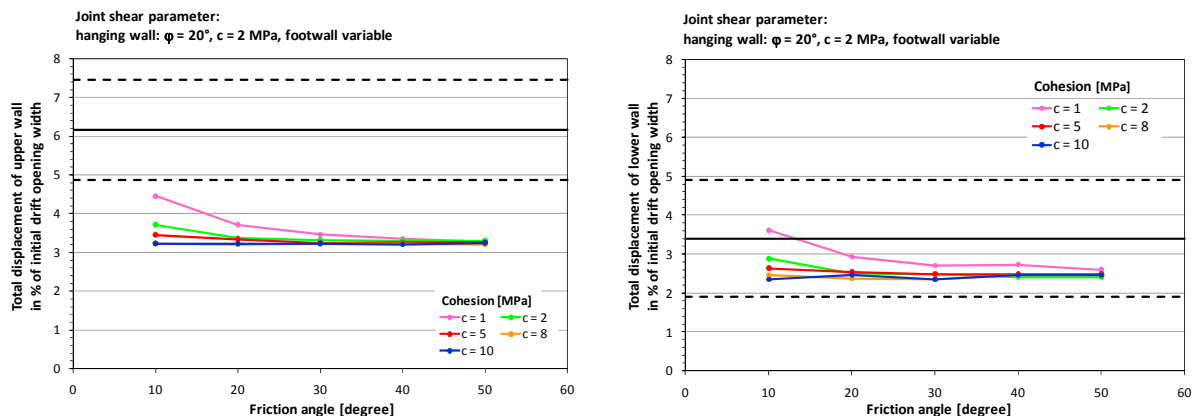
Figure 87: Relation between modelled and measured convergence for drift 218-35-W (second calibration step): for upper drift profile (left) and lower drift profile (right)

A further calibration step was necessary with the aim to determine parameters that result in an increase of upper hanging wall deformations without influencing the results for the footwall deformations. The sensitivity of different parameters to hanging wall deformations was analyzed in a sensitivity analysis. Since the joint properties were already evaluated in

the previous calibration step, the focus was now on rock mass properties. The investigated parameters were varied by ± 50 %, i.e. each initial parameter value was diminished as well as augmented by 50%. This relatively high percentage leads partly to values that are not plausible, but it allows capturing and comparing the influence of all investigated parameters on the resulting deformation. Although it is recognized that there is a connection or dependency between some parameters, each parameter was analyzed separately to evaluate its influence. In Table 42 the investigated parameters with their initial value as well as the chosen variation are provided. Only the values for the hanging wall were changed. For the footwall the same parameter values as in the previous calibration step were used. In addition, the influence of dilation was evaluated, although according to Barla, 1995 squeezing does not imply volume increase except for rocks with dilatant behaviour. A dilation angle was introduced into the model as a general rock mass property, i.e. with the same value for both side walls (see Table 43).

Table 42: Rock mass properties for sensitivity analysis for drift model 218-35-W (third calibration step)

Rock mass properties		Initial value = footwall parameters	Variation for hanging wall (± 50% of initial values)
Young modulus E	[MPa]	48,000	24,000 / 72,000
Poisson's ratio ν	[--]	0.16	0.08 / 0.24
Peak friction angle φ_p	[°]	35	17.5 / 52.5
Peak cohesion c_p	[MPa]	8	4 / 12
Residual friction angle φ_r	[°]	20	10 / 30
Residual cohesion c_r	[MPa]	2	1 / 3

Table 43: Dilation values for sensitivity analysis for drift model 218-35-W (third calibration step)

Rock mass properties		Initial value	Variation for hanging wall and footwall
Dilation	[°]	0	5 / 10

The results of the sensitivity analysis and of the introduction of dilation are shown in Figure 88 and Figure 89. It can be noted that the resulting total convergence varies for all parameter variations, but mostly the changes are relatively small. For the lower drift wall the modelled convergence values are all within the range of the measured standard

deviation. In contrast the results for the upper drift profile: For nearly all varied parameters no agreement between measured and modelled total convergence was determined. Only an extremely decreased Young modulus for the hanging wall causes a large increase of wall displacements, and leads to agreement between modeled and measured convergence.

Similar results were reached with the introduction of dilation. Generally, dilation causes an increase of wall displacement, but while measured and modelled lower wall deformations are in agreement, in the upper profile the range of the measured values could not be modelled.
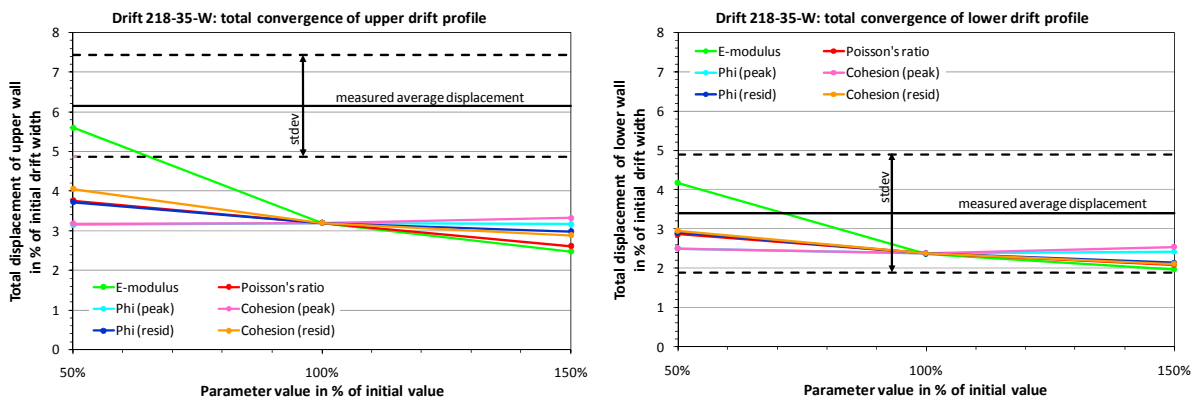
Figure 88: Parameter study results for rock mass properties in drift 218-35-W (third calibration step)
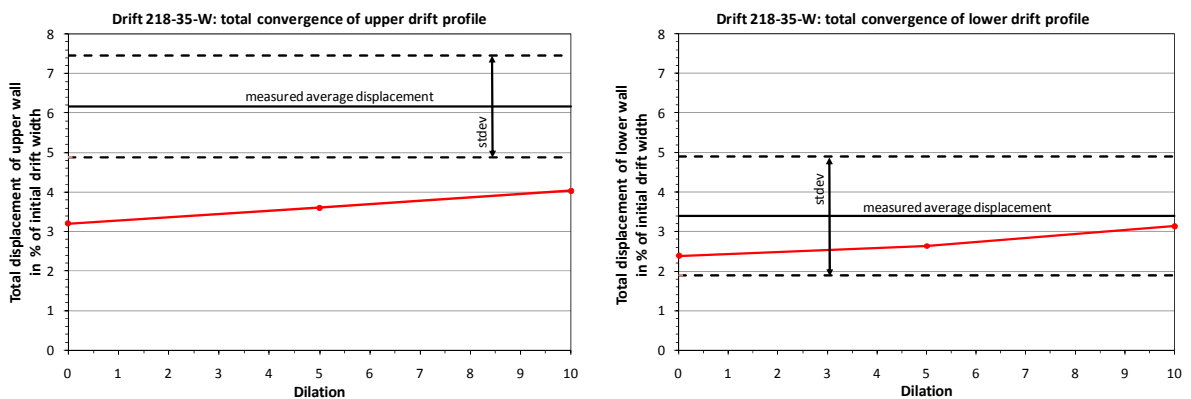
Figure 89: Influence of dilation on wall displacements in drift 218-35-W (third calibration step)

The calibration results show that the drift convergence at LaRonde is controlled not by any single parameter within a plausible range, but by a combination of several ones. A plausible solution for a combination of several varied parameters is shown in Figure 90. For this

parameter combination the resulting convergence for the upper wall and for the lower wall are within the range of the measured convergence (see Table 44). The chosen parameter values are given in Table 45. As for the joint properties, only the rock mass shear parameters for both side walls were slightly varied. As mentioned before, the available input data and especially the reference data is too imprecise to allow the determination of only one definite drift model with a clearly defined set of rock mass and joint properties. However, the model presented in Figure 90 is one plausible solution.
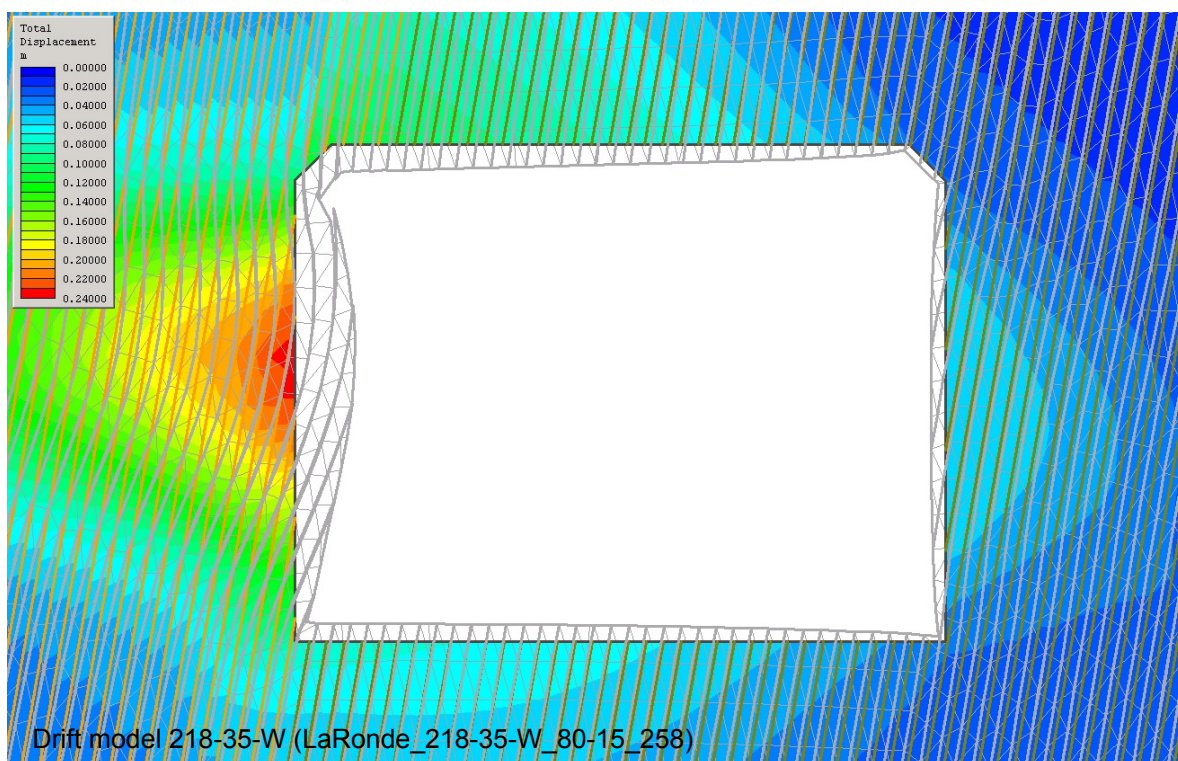
Figure 90: Calibrated drift model 218-35-W (third calibration step; plausible solution)

Table 44: Measured and modelled convergence in drift 218-35-W (third calibration step; plausible solution)

Convergence in drift model 218-35-W		measured mean (stdev)	modeled
Upper part of wall (2.60 m above floor)	**[m]**	0.34 (0.07)	0.29
	[%][*]	6.16[*] (1.29)	5.31[*]
Lower part of wall (1.00 m above floor)	**[m]**	0.19 (0.09)	0.22
	[%][*]	3.40[*] (1.50)	4.00[*]

[*]in % of initial opening widths

Table 45: Rock mass and joint properties for calibrated drift model drift 218-35-W (third calibration step; plausible solution)

Rock mass properties		Hanging wall	Footwall
Young modulus E	[MPa]	48,000	48,000
Poisson's ratio ν	[--]	0.16	0.16
Peak friction angle φ_p	[°]	30	35
Peak cohesion c_p	[MPa]	5	8
Tensile strength	[MPa]	0	0
Residual friction angle φ_r	[°]	20	20
Residual cohesion c_r	[MPa]	1	2
Dilation	[°]	8	8
Joint properties		Hanging wall	Footwall
Friction angle φ	[°]	10	20
Cohesion c	[MPa]	0	2
Tensile strength	[MPa]	0	0
Normal stiffness	[MPa/m]	100,000	100,000
Shear stiffness	[MPa/m]	10,000	10,000

In Annex S, T, and U the PHASE2 analysis information for the three calibrated drifts is provided.

6.5 Summary

In the previous sections the investigated underground drifts were analyzed regarding sidewall convergence due to rock squeezing. The numerical analysis was carried out using the 2D finite element program PHASE2. The intention was the generation of representative numerical models of the three investigated drifts, and the reproduction of failure mechanism and resulting wall deformations. The necessary data was collected on site. As reference data convergence measurements and typical deformation profiles were available. Since the convergence data had several limitations, it could be used only as general guidelines for the modelled deformation magnitude. It was assumed that modelled convergence values within the range of the standard deviation of the measured mean convergence constitute sufficient accurate results.

At LaRonde usually the drift deformations are characterized by pronounced bulging of the upper hanging wall and the lower footwall. This could be observed in two of the three investigated drifts. Due to changing rock conditions the deformation profile in the third drift showed the characteristic form only on the hanging wall. The footwall had only small displacements without pronounced bulging.

For each drift a numerical model was generated using the specific structural and geometric data. The models were calibrated using the available reference data. After the calibration all three models were in good agreement with the observed deformation profiles as well as with the measured deformation magnitudes. Due to the limitations of the available field data it was not possible to define one exclusive numerical solution for each investigated drift. However, since realistic input parameter values were chosen, and good agreement was reached between modelled and measured/observed convergence, the calibrated models are plausible solutions of the observed drift deformations. It could be demonstrated that the applied finite element method is appropriate to model the observed failure mechanism and the resulting wall deformations due to squeezing rock.

7 Conclusions for the LaRonde underground drifts

Three drifts at the LaRonde underground mine were investigated due to their large sidewall deformations as a result of rock squeezing. The drifts were selected by the mine based on the available convergence measuring data. The measured total convergence was in the range of 3 to 6 % of the initial drift opening width, corresponding to approximately 15 to 34 cm of rock displacement. Although the convergence data had limitations, it was adequate as guidelines for reference purposes.

The rock squeezing at LaRonde leads to characteristic drift deformation profiles with pronounced bulging of the upper hanging wall and the lower footwall. This could be observed in two of the investigated drifts (drift 227-43-E and 233-41-W). It was assumed that in these drifts the deformation magnitude is equal for both sidewalls. Due to changing rock conditions the deformation profile in the third drift (drift 218-35-W) shows the characteristic form only on the hanging wall. The footwall has only small deformations without pronounced bulging. In this drift most of the measured total convergence was associated with the hanging wall.

For each investigated drift a 2D finite element model was generated and calibrated. The pronounced foliation was introduced explicitly into the models. The modelling results showed that the observed deformations are not controlled by a single parameter, but by a combination of several ones. Therefore, the finally calibrated models provide one possible solution, using plausible parameter values. For these models both deformation profile and deformation magnitude were in good agreement with the field data.

Numerical modelling in rock mechanics always means a simplification of the real situation. The problem has to be reduced and simplified to enable the analysis. Numerical modelling results are, therefore, always an approximate solution of the given problem, and do not allow the determination of one exclusive or right solution. However, since the necessary assumptions were made in agreement with the observed situation on site, and a good agreement was reached between modelled and measured/observed convergence, the generated models presented in this work are plausible solutions. It could be demonstrated that the applied numerical model is appropriate for the analysis of the investigated

squeezing rock. The results show that an approximate reproduction of the observed conditions at LaRonde is possible with the used 2D finite element model, both in terms of deformation profile and deformation size. More validation experiments should be carried out, but the method can potentially be used to develop better mine development strategies in similar conditions.

A limitation of this work is the available convergence data, which allows no accurate model calibration. More precise reference data would lead to more reliable drift models. It is not necessarily required to use extensive measuring equipment with extensometers, etc. as described e.g. in Barla et al., 2007, who reports a case study of a tunnelling project. Reliable results can also be reached with small equipment, which is especially important in mining environments with its restrictions. The important points are the accuracy and the systematic method of the performed measurements, and, probably as the most crucial factor, the instructions and information given to the personnel, who perform the measurements. It would be useful for mine operation to develop a comprehensive, cost effective instruction program.

As a simplification in this work no support measures were taken into account. For a more comprehensive analysis the introduction of the installed rock support into the model would be necessary. This would require more precise data (e.g. support installation dates) that allows the consideration of support elements in relation to measured deformations.

Furthermore, the time-dependent behaviour of the squeezing rock was not considered in this work. The available data allows only a rough determination of the deformation profile at a certain point in time. For a realistic reproduction of time-dependent deformations more precise and systematically collected data is necessary.

As a general limitation the applied 2D analysis cannot account for the dependency of drift orientation and strike of foliation.

Outlook and future work

The previously described analysis of the squeezing rock conditions and the resulting wall deformations is only one part of the work that is necessary to describe and understand the

complex failure mechanism due to squeezing rock. Although a good reproduction of the observations on site was reached, there are several limitations in the generation and calibration of the models, especially in view of the available reference data. Therefore, it would be of interest to carry out more precise measurements that show the variation in the measured values and reflects the possibly different behaviour and the different deformation size of both sidewalls. In addition, measurements of possible roof and floor displacements could be helpful. With more accurate measurements more reliable drift models could be developed. Furthermore, a more reliable model would allow evaluating the influence of support measures on the deformations.

Finally, a more comprehensive analysis showing the relation between drift orientation, orientation of foliation, and resulting convergence would require the construction of three dimensional models.

8   General conclusions

Two case studies of excavations in fracture rock were presented. The first case study investigated potential wedge failures at a surface excavation in a rock mass with three defined joint sets. The second case study explored the stability of underground excavations in a strongly layered rock mass that experienced large wall deformations due to squeezing rock.

Rock slope in fractured rock: The investigated rock slope along a highway cut near Fleurimont is situated in layered schist and had experienced wedge failures during the construction of the road in 1995. The objective of the investigation was to determine if the reported wedge failures could have been predicted and to assess the probability of failure for wedges along the slope crest. A wedge stability analysis, focusing on the representation of the structural field data, was carried out as limit equilibrium analysis using various deterministic and probabilistic analysis tools such as i) deterministic back-analysis of observed wedge failures using the software SWEDGE, ii) a probabilistic approach for single wedges also using SWEDGE, and iii) a second probabilistic method for 3D joint system models using Fracture-SG and Fracture-Slope. The required data was collected on site.

The deterministic back-analysis of two observed wedge failures indicated the potential instability of both wedges. The probabilistic approaches were applied to investigate the potential occurrence of wedge failures along the slope crest, their frequency and their failure probability. The results of both methods (SWEDGE and Fracture-Slope) confirmed that wedges can form along the slope crest and indicated a high failure probability for these wedges. However, only a low frequency for wedge failures along the whole slope length was calculated. These wedges are mainly small; the probability for large wedges was very low.

Underground drifts in fractured rock: The stability of the three investigated underground drifts at Agnico Eagle's LaRonde mine is affected by large sidewall deformations caused by squeezing rock. The analysis focused on the generation of 2D finite element models using PHASE2 to reproduce the observed drift convergence. The emphasis

was on developing models that capture the observed deformation profiles and the measured deformation magnitudes. The approach necessitated several simplifying assumptions about material properties and influence of support. The calibration process succeeded in developing models that are in good agreement with the observations on site. Deformation profiles and magnitudes were adequately reproduced.

Comparison: Both case studies investigated the influence of discontinuities inherent in the rock mass, and the necessity to take them into account within a stability analysis when designing excavations. Therefore, reliable structural data was the essential basis for both case studies. The Fleurimont case had to deal with slope instabilities caused by the rock structure, whereas the LaRonde case investigated a problem of large but manageable drift wall deformations caused essentially by an interaction of stress and rock structure.

All analyses in the Fleurimont case were based on the limit equilibrium method and allowed the determination of the potential for wedge failures for the investigated slope. The results of the different analysis approaches (deterministic and probabilistic) signified that in principal a prediction of wedge failures is possible, but that the applied methods influence the conclusions. The use of different methods allows a better understanding of a given problem. The finite element models used for the LaRonde case allowed a good reproduction of the observed drift deformations, and the results provide important information for future development of underground excavations and required support measures.

The applied numerical modelling approaches proved to give insights into the behaviour of fractured rock masses. However, both case studies signified the limitations of current approaches, mainly the availability, quality, and representation of data. For the Fleurimont case the choice of analysis tools and the available data had an important influence on the results. For the LaRonde case the results were essentially influenced by the quality of the available data.

9   References

Aydan, Ö., Akagi, T. and Kawamoto, T. (1993) The Squeezing Potential of Rocks Around Tunnels; Theory and Prediction. Rock Mechanics and Rock Engineering 26(2), 137-163.

Barla, G. (1995) Squeezing rocks in tunnels. Int. Soc. Rock Mech., News Journal 2(3-4), 44-49.

Barla, G., Bonini, M. and Debernardi, D. (2007) Modelling of tunnels in squeezing ground. Shahriar, K. (ed), pp. 1267-1285, 3rd Iranien Rock Mechanics Conference, 2007, Amirkabir University of Technology, Tehran, Iran.

Barton, N.R. (1973) Review of a new shear-strength criterion for rock joints. Engineering Geology 7, 287-332.

Barton, N.R. and Choubey, V. (1977) The Shear Strength of Rock Joints in Theory and Practice. Rock Mechanics 10, 1-54.

Barton, N.R., Lien, R. and Lunde, J. (1974) Engineering classification of rock masses for the design of tunnel support. Rock Mechanics and Rock Engineering 6(4), 189-239.

Bieniawski, Z.T. (1989) Engineering rock mass classification, Wiley, New York, USA.

Brown, E.T. (ed) (1981) Rock Characterization, Testing and Monitoring, ISRM Suggested Methods, Pergamon Press, Oxford, UK.

Deere, D.U. and Deere, D.W. (1988) The Rock Quality Designation (RQD) Index in Practice. Rock Classification Systems for Engineering Purposes, ASTM STP 984, Louis Kirkaldie, ED., American Society for Testing and Materials, 91-101.

Dershowitz, W.S. and Einstein, H.H. (1988) Characterizing Rock Joint Geometry with Joint System Models. Rock Mechanics and Rock Engineering 21, 21-51.

Fenton, C.L. and Adams Fenton, M. (1940) The rock book, Dover Publications, Inc., Mineola, N.Y., USA.

Franklin, J.M., Lydon, J.W. and Sangster, D.F. (1981) Volcanic-Associated Massive Sulfide Deposits. Economic Geology 75th Anniversary Volume, 485-627.

Goodman, R.E. and Bray, J.W. (1976) Toppling of rock slopes. Rock Engineering for foundations and slopes 11.

Grenon, M. (2007) Personal communication.

Grenon, M. and Hadjigeorgiou, J. (2008a) A design methodology for rock slopes susceptible to wedge failure using fracture system modelling. Engineering Geology 96(1-2), 78-93.

Grenon, M. and Hadjigeorgiou, J. (2008b) Fracture-SG. A fracture system generator software package. Version 2.17.

Grenon, M. and Hadjigeorgiou, J. (2008c) Fracture-Slope. A fracture system based rock slope wedge stability analysis software package. Version 1.25.

Grenon, M., Mellies, G. and Hadjigeorgiou, J. (2008) Structural analysis along a highway rock exposure: The Fleurimont road cut. Locat, J., Perret, D., Turmel, D., Demers, D. and Leroueil, S. (eds), 4th Canadian Conference on Geohazards, May 2008, Québec, Canada.

Hadjigeorgiou, J. and Grenon, M. (2005) Rock slope stability analysis using fracture systems. International Journal of Surface Mining, Reclamation and Environment 19(2), 87-99.

Hoek, E. (2001) Big tunnels in bad rock. ASCE Journal of Geotechnical and Geoenvironmental Engineering 127(9), 726-740.

Hoek, E. and Bray, J.W. (1981) Rock Slope Engineering, Revised third edition, E & FN Spon, London.

Hoek, E. and Brown, E.T. (1980) Underground Excavations in Rock, The Institution of Mining and Metallurgy, London, UK.

Hudson, J.A. and Harrison, J.P. (1997) Engineering Rock Mechanics - An Introduction to the Principals, Elsevier Ltd., Oxford, UK.

Hyndman, D.W. (1972) Petrology of igneous and metamorphic rocks, New York, USA.

ISRM (1978) Suggested methods for the quantitative description of discontinuities in rock masses. International Journal of Rock Mechanics and Mining Sciences and Geomechanics Abstracts 15, 319-368.

Kulatilake, P.H.S.W. and Wu, T.H. (1984) Estimation of Mean Trace Length of Discontinuities. Rock Mechanics and Rock Engineering 17, 215-232.

Laslett, G.M. (1982) Censoring and edge effects in areal and line transect sampling of rock joint traces. Journal of the international association for mathematical geology 14(2), 125-140.

Le Bas, M.J. and Streckeisen, A.L. (1991) The IUGS systematics of igneous rocks. Journal of the Geological Society 148, 825-833.

Malan, D.F. (2002) Simulating the Time-dependent Behaviour of Excavations in Hard Rock. Rock Mechanics and Rock Engineering 35(4), 225-254.

Marinos, P. and Hoek, E. (2001) Estimating the geotechnical properties of heterogeneous rock masses such as flysch. Bulletin of Engineering Geology and the Environment 60, 82-92.

Marinos, V., Marinos, P. and Hoek, E. (2005) The geological strength index: applications and limitations. Bulletin of Engineering Geology and the Environment 64, 55-65.

Mercier-Langevin, F. (2008) Stope Performance Under Post-Peak Conditions. Hadjigeorgiou, J. (ed), Strategic vs Tactical Approaches in Mining, November 2008, Québec, QC, Canada.

Mercier-Langevin, F. and Turcotte, P. (2006) Expansion at Depth at Agnico-Eagle's LaRonde Division - Meeting Geotechnical Challenges without Compromising Production Objectives, Deep and High Stress Mining, 2006, Québec, QC, Canada.

Mercier-Langevin, F. and Turcotte, P. (2007) Evolution of ground support practices at Agnico-Eagle's LaRonde Division - Innovative solutions to high-stress yielding ground, in: Rock Mechanics, Meeting Society's Challenges and Demands. Eberhardt, E., Stead, D. and Morrison, T. (eds), pp. 1497-1504, Taylor & Francis Group, London, Vancouver, BC, Canada.

Mercier-Langevin, P., Dubé, B., Hannington, M.D., Davis, D.W., Lafrance, B. and Gosselin, G. (2007a) The LaRonde Penna Au-Rich Volcanogenic Massive Sulfide Deposit, Abitibi Greenstone Belt, Quebec: Part I. Geology and Geochronology. Economic Geology 102(4), 585-609.

Mercier-Langevin, P., Dubé, B., Lafrance, B., Hannington, M.D., Galley, A., Marquis, R., Moorhead, J. and Davis, D.W. (2007b) A Group of Papers Devoted to the LaRonde Penna Au-Rich Volcanogenic Massive Sulfide Deposit, Eastern Blake River Group, Abitibi Greenstone Belt, Quebec: Preface. Economic Geology 102(4), 577-583.

Meyer, T. (1999) Geologic stochastic modeling of rock fracture systems related to crustal faults. Masters Thesis, Massachusetts Institute of Technology, Cambridge, USA.

Mitchell, R.S. (1985) Dictionary of rocks, Van Nostrand Reinhold Company Inc., New York, USA.

Norrish, I.N. and Wyllie, D.C. (1996) Landslides: Investigation and Mitigation, Special report 247. Turner, A.K. and Schuster, R.L. (eds), National Academy Press, Washington, D.C.

Potvin, Y. and Hadjigeorgiou, J. (2008) Ground support strategies to control large deformations in mining excavations. SIAMM - Journal of The South African Institute of Mining and Metallurgy 108(7).

Priest, S.D. (1993) Discontinuity analysis for rock engineering, Chapman & Hall, London, UK.

Priest, S.D. and Hudson, J.A. (1981) Estimation of Discontinuity Spacing and Trace Length Using Scanline Survey. International Journal of Rock Mechanics and Mining Science and Geomechanics Abstracts 18, 182-197.

Rocscience (2008a) DIPS software information, Rocscience Inc., Toronto, Canada.

Rocscience (2008b) Phase2 software information, Rocscience Inc., Toronto, Canada.

Rocscience (2008c) RocData software information, Rocscience Inc., Toronto, Canada.

Rocscience (2008d) Swedge software information, Rocscience Inc., Toronto, Canada.

Sandy, M.P., Gibson, W. and Gaudreau, D. (2007) Canadian and Australian ground support practices in high deformation environments. Potvin, Y. (ed), pp. 297-311, Australian Centre for Geomechanics, Deep Mining 07, Perth, Australia.

Steiner, W. (1996) Tunnelling in Squeezing Rock: Case Histories. Rock Mechanics and Rock Engineering 29(4), 211-246.

Tremblay, A. (1992) Géologie de la région de Sherbrooke (Estrie). ET 90-02 Gouvernement du Québec, Ministère de l'Énergie et des Ressources, Canada.

Turcotte, P. (2008) Personal communication.

Ulusay, R. and Hudson, J.A. (eds) (2007) The complete ISRM suggested methods for rock characterization, testing and monitoring:1974-2006, ISRM, Ankara, Turkey.

Villaescusa, E. and Brown, E.T. (1992) Maximum Likelihood Estimation of Joint Size from Trace Length Measurements. Rock Mechanics and Rock Engineering 25, 67-87.

Warburton, P.M. (1980) A Stereological Interpretation of Joint Trace Data. International Journal of Rock Mechanics and Mining Sciences and Geomechanics Abstracts 17, 181-190.

Wyllie, D.C. and Mah, C.W. (2004) Rock slope engineering: civil and mining, Spon Press, New York, NY.

Wyllie, D.C. and Norrish, I.N. (1996) Landslides: Investigation and Mitigation, Special report 247. Turner, A.K. and Schuster, R.L. (eds), National Academy Press, Washington, D.C.

Zhang, L. and Einstein, H.H. (1998) Estimating the Mean Trace Length of Rock Discontinuities. Rock Mechanics and Rock Engineering 31(4), 217-235.

10 Glossary

In this thesis several specific terms and definitions were used to describe the rock mass and its specific features. These terms were chosen in accordance with the ISRM suggested methods to characterize rock (Ulusay and Hudson, 2007). In particular for the description of "breaks" in the rock the following terms recommended by Ulusay and Hudson, 2007 were used.

Discontinuity   General term for any mechanical discontinuity in a rock mass (e.g. joints, faults, bedding planes, etc.)

Joint   Break of geological origin in the continuity of a body of rock

Joint set   Group of parallel joints

Joint system   Intersecting joint sets

Annex A: Joint data (scanline mapping)

Joint data scanline 1 and 2

Joint No	Dip	Dip direct.	Dip direct. 16o W decl	Scanline	Set	Trace length [m]	Intersection distance [m]	Comment	Rough-ness	Ending	Aperture	Filling	Water
1	89	168	152	1	1	1.3	3.9		0	2			
2	86	123	107	1	1	0.5	4.7		0	2			
3	85	120	104	1	1	1.3	4.75		0	1			
4	75	88	72	1	2	4.5	5.55		0	0			
5	79	89	73	1	2	1.2	4.9		0	2			
6	74	96	80	1	2	3	5.95		0	1			
7	75	89	73	1	2	5	6.58		0	0			
8	90	152	136	1	1		3 - 6.8	schistosity 5-10cm	0				
9	89	334	318	1	1		8.5		0				
10	72	71	55	1	2	3.1	6.8		0	1			
11	79	177	161	1	1	2.3	9.7		0	1			
12	80	148	132	1	1	0.8	11.1		0	2			
13	82	71	55	1	2	3	9.6		0	1			
14	80	55	39	1	2	3.8	11.75		0	1			
15	89	42	26	1	2	5	12.4		0	0			
16	65	155	139	1	1	3.2	13.65		0	1			
17	83	12	356	1	random	1.9	13.55		0	2			
18	82	70	54	1	2	8	14.5		0	1			
19	77	48	32	1	2	3	15.95		0	1			
20	70	144	128	1	1	2	17.5		0	1			
21	21	342	326	1	3	10-15m	16.5	subhorizontal	0				
22	74	168	152	1	1	8	19.3		rough	2			
23	63	180	164	1	1	3.2	19.3		0	1			
24	80	152	136	1	1	2.3	20.15		0	1			
25	72	222	206	1	2	3.5	19.4		0	1			
26	71	177	161	1	1	4.5	20.4		rough	1			
27	70	144	128	1	1	3	20.7		0	1			
28	77	129	113	1	1		20.7 - 23.6	schistosity	0				
29	77	129	113	1	1	2.2	21.6		0	1			
30	69	150	134	1	1	5	23.6		0	1			
31	69	149	133	1	1	2	24.3		0	1			
32	71	149	133	2	1	4	0 - 2.0	schistosity 5-10cm	0		2mm		
33	67	146	130	2	1	5	2.7		0-1				
34	65	152	136	2	1	4	4.1		0				
35	80	144	128	2	1	3	5.6		0				
36	70	150	134	2	1	2	6.7		0				
37	68	214	198	2	2	4	4.5	wedge A	0	1			
38	69	142	126	2	1	4.2	7.8	wedge A	0	0			
39	68	142	126	2	1	4	8.3		0				
40	68	142	126	2	1	4	8.5		0				
41	68	142	126	2	1	4	8.8		0				
42	84	229	213	2	2	8	11.05		0				
43	71	227	211	2	2	8	10.7		0				
44	35	340	324	2	3	3	8	subhorizontal	0				
45	55	136	120	2	1	1	12.7		0	1			
46	64	142	126	2	1	7	15.3		0				
47	75	144	128	2	1	1	14.5		0				
48	80	238	222	2	2	2	15.5	schistosity 5-10cm	0				
49	69	138	122	2	1	7	18.1		0				
50	79	144	128	2	1	2.5	19		0				
51	70	150	134	2	1	1.5	19.7		0				
52	70	146	130	2	1	3	20.8		0				
53	65	224	208	2	2	8	21.5	wedge B	0	0			
54	63	146	130	2	1	8	24.5	wedge B	0	0			
55	90	239	223	2	2	4	24.8		0	1			
56	84	152	136	2	1	1	26		0				

Joint data scanline 3 and 4

Joint No	Dip	Dip direct.	Dip direct. 16o W decl	Scanline	Set	Trace length [m]	Intersection distance [m]	Comment	Rough-ness	Ending	Aperture	Filling	Water
57	80	146	130	3	1	1	0.8	folded	0	1	0		
58	78	142	126	3	1	1	1.7		0	2	0		
59	36	333	317	3	3	4	3.2	subhorizontal	1	1	2mm		
60	89	244	228	3	2	2	5.4	light undulation	1	1	-		
61	73	145	129	3	1	1	6.6	folded	1	0	0		
62	55	142	126	3	1	1	9.4		0	1	3mm		
63	66	226	210	3	2	3	14.3	excavated surface?		0			
64	80	209	193	3	2	1	19	wedge	0	1	0		
65	64	142	126	3	1	2	25.2	wedge	0	1	0		
66	43	357	341	3	3	1	13.2	subhorizontal, spacing 5-20cm	1	1	<10mm	?	a bit
67	63	229	213	3	2	4	9.4		1	2	2mm	Quartz	
68	30	322	306	3	3	0.3 ?	10.4	subhorizontal	1	1	?		
69	75	149	133	3	1	2	8.1	undulation	1	1	?	? Veget.	
70	79	249	233	3	2	1	4		1	2	10mm		
71	80	144	128	3	1	0.3	2.2		0	2	1mm		
72	80	146	130	3	1	1	9	folded, convex	1	1	1mm		
73	52	146	130	3	1	3	13.1	undulated	1	0	2-3mm		
74	80	248	232	3	2	2	12.8	undulated	1	0	-		
75	59	138	122	3	1	2	18.2		1	0	-		
76	51	142	126	3	1	1	19.4		1	1	1mm		
77	46	149	133	3	1	1	24.2		1	0	?		
78	86	235	219	4	2	2	0.4	{spacing 20-50cm	0	1	0		
79	88	241	225	4	2	2	0.2	{	0	1	0		
80	89	250	234	4	2	3	1.2	{maybe no natural surface	0	0	-		
81	50	316	300	4	3	2		subhorizontal, spacing 20-50cm	-	1	1mm		
82	74	139	123	4	1	2	2.9		1	1	1mm		
83	89	270	254	4	2	5	1.7		0	0	?		
84	76	346	330	4	random	1	?	subhorizontal	1	0	?		
85	74	150	134	4	1	1.5	11.9		1	0	?		
86	74	145	129	4	1	1	13.2		1	2	1mm		
87	90	242	226	4	2	1	12.65	wedge	1	1	3mm		
88	81	136	120	4	1	1	16.1	wedge	1	1	3mm		
89	83	238	222	4	2	2	17.2		1	1	0		
90	70	136	120	4	1	1	20.3		1	2	0		
91	72	139	123	4	1	1	20.1		1	2	2mm		
92	74	142	126	4	1	1.5	21.4		1	1	0		
93	84	142	126	4	1	4	24.2	undulated	1	1	0		
94	75	144	128	4	1	3	25.2		1	1	0		
95	69	232	216	4	2	1	26.6		1	2	0		
96	76	144	128	4	1	2	26.6		1	0	0		
97	85	62	46	4	2	3	29.3		1	0	0		
98	61	135	119	4	1	3	30.3		0	0	0-2mm		

Annex B: Slope data (field measurements)

Slope inclination measurements [degrees]

	scanline 2	scanline 1	all
	68	69	68
	68	61	68
	71	68	71
	69	62	69
	67	66	67
	67	67	67
	70	70	70
	70	65	70
	68	70	68
	72	78	72
	75		75
	70		70
	67		67
	65		65
	68		68
	70		70
	66		66
	66		66
	67		67
	67		67
	66		66
	68		68
	68		68
	69		69
	63		63
	70		70
	66		66
	64		64
	66		66
	66		66
	65		65
	69		69
	66		66
	70		70
	65		65
	66		66
	66		66
	69		69
	81		81
	82		82
	75		75
	85		85
	83		83
	70		70
	68		68
	70		70
	72		72
			69
			61
			68
			62
			66
			67
			70
			65
			70
			78
mean	**69**	**68**	**69**
stdev	**5**	**5**	**5**
min	**63**	**61**	**61**
max	**85**	**78**	**85**

Slope dip direction measurements [degrees]
(no declination considered)

	182
	182
	184
	181
mean	182
stdev	1

	mean	stdev
Area of wedge A	69	3
Area of wedge B	67	2

Annex C: Joint compressive strength (Schmidt hammer)

Rebound numbers measured with Schmidt hammer (joint sets 1 and 2)

No	Rebound numbers r [-]			
	Joint set 1		Joint set 2	
	A	B	A	B
1	51	52	33	46
2	38	50	48	48
3	45	50	43	48
4	36	50	45	50
5	46	50	42	45
6	44	52	49	45
7	46	51	52	54
8	44	54	48	46
9	52	48	44	53
10	40	48	42	44

Mean rebound number (joint sets 1 and 2)

No	Rebound numbers r [-]			
	Joint set 1		Joint set 2	
	A	B	A	B
1	51	52		
2			48	48
3	45	50		48
4			45	50
5	46			
6		52	49	
7	46	51	52	54
8		54	48	
9	52			53
10				
mean r [-]	48	51.8	48.4	50.6
STDEV [-]	3.24	1.48	2.51	2.79
mean r A+B [-]	49.9		49.5	
STDEV [-]	2.7		1.6	
mean r set1+set2 [-]	49.7			
STDEV [-]	0.3			

Annex D: DIPS analysis information

Dips Document Information

Document Name: Dips_all joints_dec16west_2008-09-02.dip
Document Title:
Document Setup:
Traverses: 4
ID# 1:Linear Traverse oriented; 256/0, Traverse 1
ID# 2:Linear Traverse oriented; 256/0, Traverse 2
ID# 3:Linear Traverse oriented; 256/0, Traverse 3
ID# 4:Linear Traverse oriented; 256/0, Traverse 4

Data is DIP/DIPDIRECTION format
Magnetic Declination (E pos): -16 degrees
Multiple Data Flag (Quantity) is OFF
10 Extra Data Columns
98 Poles from 98 Entries

Global Mean Vector:
Unweighted TREND/PLUNGE = 317.901/29.7494
Weighted TREND/PLUNGE = 314.203/29.5628
Unweighted DIP/DIPDIRECTION = 60.2506/137.901
Weighted DIP/DIPDIRECTION = 60.4372/134.203

Added Planes (via Add Plane Option):

ID	TREND/PLUNGE	DIP/DIPDIRECTION	LABEL
1	346/21	69/166	

Set Planes (via Add Set Options):

ID	TREND/PLUNGE	DIP/DIPDIRECTION	LABEL
1m	309.863/18.2946	71.7054/129.863	
1w	311.982/18.5359	71.4641/131.982	
2m	44.9409/3.31036	86.6896/224.941	
2w	43.5764/4.23106	85.7689/223.576	
3m	138.433/55.0306	34.9694/318.433	
3w	139.874/55.782	34.218/319.874	

Set Statistics
Set: 1m (UNWEIGHTED)
59 Poles from 59 Entries
Fisher's K = 33.0573
68.26% Variability Limit = 15.1413 degrees
95.44% Variability Limit = 24.9616 degrees
99.74% Variability Limit = 34.9211 degrees
68.26% Confidence Limit = 1.99549 degrees
95.44% Confidence Limit = 3.27356 degrees
99.74% Confidence Limit = 4.54556 degrees

Set: 1w (WEIGHTED)
59 Poles from 59 Entries
Fisher's Kw = 32.4017
68.26% Variability Limit = 15.2946 degrees
95.44% Variability Limit = 25.217 degrees
99.74% Variability Limit = 35.2841 degrees
68.26% Confidence Limit = 2.0162 degrees
95.44% Confidence Limit = 3.30755 degrees
99.74% Confidence Limit = 4.59277 degrees
Set: 2m (UNWEIGHTED)
31 Poles from 31 Entries
Fisher's K = 14.5986
68.26% Variability Limit = 22.8698 degrees
95.44% Variability Limit = 37.956 degrees
99.74% Variability Limit = 53.6815 degrees
68.26% Confidence Limit = 4.22364 degrees
95.44% Confidence Limit = 6.93087 degrees
99.74% Confidence Limit = 9.62823 degrees
Set: 2w (WEIGHTED)
31 Poles from 31 Entries
Fisher's Kw = 13.9853
68.26% Variability Limit = 23.3728 degrees
95.44% Variability Limit = 38.8119 degrees
99.74% Variability Limit = 54.9429 degrees
68.26% Confidence Limit = 4.32204 degrees
95.44% Confidence Limit = 7.09246 degrees
99.74% Confidence Limit = 9.85298 degrees
Set: 3m (UNWEIGHTED)
6 Poles from 6 Entries
Fisher's K = 35.6798
68.26% Variability Limit = 14.5711 degrees
95.44% Variability Limit = 24.0125 degrees
99.74% Variability Limit = 33.5736 degrees
68.26% Confidence Limit = 6.00587 degrees
95.44% Confidence Limit = 9.85932 degrees
99.74% Confidence Limit = 13.7044 degrees
Set: 3w (WEIGHTED)
6 Poles from 6 Entries
Fisher's Kw = 39.1884
68.26% Variability Limit = 13.9001 degrees
95.44% Variability Limit = 22.8971 degrees
99.74% Variability Limit = 31.9931 degrees
68.26% Confidence Limit = 5.72434 degrees
95.44% Confidence Limit = 9.39649 degrees
99.74% Confidence Limit = 13.0597 degrees

Set Window Limits

ID	TREND1/PLUNGE1	TREND2/PLUNGE2	WRAPPED
1	274/49	168/3	YES
2	6/40	263/21	YES
3	111/75	170/33	NO

Annex E: Censoring bias correction

Determination of unbiased trace lengths
(after Villaescusa and Brown (1992))

no	exposed ends	Trace lengths set 1			Trace lengths set 2			Trace lengths set 3		
		2	1	0	2	1	0	2	1	0
1		1.3	1.3	4.2	1.2	3.0	4.5		4.0	
2		0.5	2.3	8.0	4.0	3.1	5.0		1.0	
3		0.8	3.2	1.0	1.0	3.0	5.0		0.3	
4		8.0	2.0	3.0	1.0	3.8	8.0		2.0	
5		1.0	3.2	2.0		8.0	3.0			
6		0.3	2.3	1.0		3.0	2.0			
7		1.0	4.5	1.5		3.5	3.0			
8		1.0	3.0	2.0		4.0	5.0			
9		1.0	2.2	3.0		4.0	3.0			
10			5.0			2.0				
11			2.0			2.0				
12			1.0			2.0				
13			1.0			1.0				
14			1.0			2.0				
15			2.0			1.0				
16			2.0							
17			1.0							
18			1.0							
19			2.0							
20			1.0							
21			1.5							
22			4.0							
23			3.0							
sum trace lengths	[m]	14.9	51.5	25.7	7.2	45.4	38.5	0.0	7.3	0.0
no of joints	[-]	9	23	9	4	15	9	0	4	0
unbiased trace length	**[m]**	**2.25**			**3.96**			**1.83**		

Annex F: Joint shear parameters

Determination of friction angle [°] and cohesion [MPa]

Friction angle [°]								Cohesion [Mpa]	
phi r [°]	25	26	27	27.5	28	29	30	phi r [°]	25 - 30
JRC = 0, JCS = 73	25.0	26.0	27.0	27.5	28.0	29.0	30.0	JRC = 0, JCS = 73	0
JRC = 1, JCS = 73	27.3	28.3	29.3	29.8	30.3	31.3	32.3	JRC = 1, JCS = 73	0.001
JRC = 2, JCS = 73	29.6	30.6	31.6	32.1	32.6	33.6	34.6	JRC = 2, JCS = 73	0.002
JRC = 0, JCS = 123	25.0	26.0	27.0	27.5	28.0	29.0	30.0	JRC = 0, JCS = 123	0
JRC = 1, JCS = 123	27.6	28.5	29.5	30.0	30.5	31.5	32.5	JRC = 1, JCS = 123	0.001
JRC = 2, JCS = 123	30.1	31.1	32.1	32.6	33.1	34.0	35.0	JRC = 2, JCS = 123	0.002
JRC = 0, JCS = 173	25.0	26.0	27.0	27.5	28.0	29.0	30.0	JRC = 0, JCS = 173	0
JRC = 1, JCS = 173	27.7	28.7	29.7	30.2	30.7	31.7	32.7	JRC = 1, JCS = 173	0.001
JRC = 2, JCS = 173	30.4	31.4	32.4	32.8	33.3	34.3	35.3	JRC = 2, JCS = 173	0.002

Annex G: Swedge deterministic analysis information (wedge A)

Swedge Analysis Information

Document Name: Swedge_wedge A_2008-06-30.swd

Project Summary:
- Job Title: SWEDGE - Surface Wedge Stability Analysis
- Date Created: 30/06/2008, 21:45:13

Analysis Results:
- Analysis type: Deterministic
- Safety Factor: 0.3438
- Wedge height (on slope) [m]: 4.50
- Bench width (on upper face) [m]: 0.49
- Wedge volume [m^3]: 0.489
- Wedge weight [tonnes]: 1.272
- Wedge area (joint1) [m^2]: 1.77
- Wedge area (joint2) [m^2]: 2.25
- Wedge area (slope) [m^2]: 3.20
- Wedge area (upper face) [m^2]: 0.33

Effective Normal and Strength Properties:

	Joint 1	Joint 2
Effective Normal force [tonnes]	0.32	0.36
Effective Normal stress [t/m^2]	0.18	0.16
Shear Strength [t/m^2]	0.11	0.09
Strength due to Waviness [t/m^2]	0.00	0.00

- Driving force [tonnes]: 1.14
- Resisting force [tonnes]: 0.39

Failure Mode:
- Sliding on intersection line (joints 1&2)

Joint Sets 1&2 line of Intersection:

Plunge [deg]	Trend [deg]	Length [m]
63.73	162.94	5.02

Trace Lengths:

	Slope Face [m]	Upper Face [m]
Joint 1	4.87	0.73
Joint 2	4.87	0.93

Persistence:
- Joint 1 [m]: 5.02
- Joint 2 [m]: 5.02

Intersection Angles:

	Slope Face	Upper Face
Joint 1 & Joint 2	15.71	106.00
Joint 1 & Crest	82.17	42.00
Joint 2 & Crest	82.13	32.00

Dip and Dip Direction:

	Dip [deg]	Dip Direction [deg]
Joint Set 1	69.00	124.00
Joint Set 2	68.00	198.00
Slope	69.00	166.00
Upper Face	0.00	0.00

Joint Set 1 Data:
- Cohesion [t/m^2]: 0.00
- Friction Angle [deg]: 30.00

Joint Set 2 Data:
- Cohesion [t/m^2]: 0.00
- Friction Angle [deg]: 30.00

Slope Data:
- Slope height [m]: 4.50
- Rock unit weight [t/m^3]: 2.60
- Water pressures in the slope: NO
- Overhanging slope face: NO
- Externally applied force: NO
- Tension crack: NO

Wedge Vertices:
- Coordinates in Easting,Northing,Up Format
- 1=Joint1, 2=Joint2, 3=Upper Face, 4=Slope

Point	x	y	z
124	0.000	0.000	0.000
134	-1.061	1.516	4.500
234	0.229	1.837	4.500
123	-0.651	2.123	4.500

Annex H: Swedge deterministic analysis information (wedge B)

Swedge Analysis Information

Document Name: Swedge_wedge B_2008-06-30.swd

Project Summary:
- Job Title: SWEDGE - Surface Wedge Stability Analysis
- Date Created: 30/06/2008, 21:45:13

Analysis Results:
- Analysis type: Deterministic
- Safety Factor: 0.4397
- Wedge height (on slope) [m]: 8.00
- Bench width (on upper face) [m]: 1.63
- Wedge volume [m^3]: 8.857
- Wedge weight [tonnes]: 23.029
- Wedge area (joint1) [m^2]: 12.48
- Wedge area (joint2) [m^2]: 10.78
- Wedge area (slope) [m^2]: 17.66
- Wedge area (upper face) [m^2]: 3.32

Effective Normal and Strength Properties:

	Joint 1	Joint 2
Effective Normal force [tonnes]	7.99	6.86
Effective Normal stress [t/m^2]	0.64	0.64
Shear Strength [t/m^2]	0.37	0.37
Strength due to Waviness [t/m^2]	0.00	0.00

- Driving force [tonnes]: 19.50
- Resisting force [tonnes]: 8.57

Failure Mode:
- Sliding on intersection line (joints 1&2)

Joint Sets 1&2 line of Intersection:

Plunge [deg]	Trend [deg]	Length [m]
57.84	165.87	9.45

Trace Lengths:

	Slope Face [m]	Upper Face [m]
Joint 1	8.98	2.78
Joint 2	8.88	2.44

Persistence:
- Joint 1 [m]: 9.45
- Joint 2 [m]: 9.45

Intersection Angles:

	Slope Face	Upper Face
Joint 1 & Joint 2	26.31	102.00
Joint 1 & Crest	75.42	36.00
Joint 2 & Crest	78.28	42.00

Dip and Dip Direction:

	Dip [deg]	Dip Direction [deg]
Joint Set 1	63.00	130.00
Joint Set 2	65.00	208.00
Slope	67.00	166.00
Upper Face	0.00	0.00

Joint Set 1 Data:
- Cohesion [t/m^2]: 0.00
- Friction Angle [deg]: 30.00

Joint Set 2 Data:
- Cohesion [t/m^2]: 0.00
- Friction Angle [deg]: 30.00

Slope Data:
- Slope height [m]: 8.00
- Rock unit weight [t/m^3]: 2.60
- Water pressures in the slope: NO
- Overhanging slope face: NO
- Externally applied force: NO
- Tension crack: NO

Wedge Vertices:
- Coordinates in Easting,Northing,Up Format
- 1=Joint1, 2=Joint2, 3=Upper Face, 4=Slope

Point	x	y	z
124	0.000	0.000	0.000
134	-3.015	2.748	8.000
234	0.929	3.731	8.000
123	-1.228	4.878	8.000

Annex I: Sensitivity analysis results for variation in cohesion and friction angle (wedge A and B)

Wedge A: factor of safety for varying friction angle and cohesion

$\gamma = 2.6$ t/m^3	$\varphi = 28°$	$\varphi = 30°$	$\varphi = 32°$	$\varphi = 34°$	$\varphi = 36°$	$\varphi = 38°$	$\varphi = 40°$
c = 0 t/m^2	0.32	0.34	0.37	0.40	0.43	0.46	0.50
c = 0.1 t/m^2	0.67	0.70	0.72	0.75	0.78	0.82	0.85
c = 0.2 t/m^2	**1.02**	**1.05**	**1.08**	**1.10**	**1.14**	**1.17**	**1.20**
c = 0.3 t/m^2	**1.37**	**1.40**	**1.43**	**1.46**	**1.49**	**1.52**	**1.55**
c = 0.4 t/m^2	**1.72**	**1.75**	**1.78**	**1.81**	**1.84**	**1.87**	**1.91**
c = 0.5 t/m^2	**2.08**	**2.10**	**2.13**	**2.16**	**2.19**	**2.22**	**2.26**
c = 1.0 t/m^2	**3.83**	**3.86**	**3.89**	**3.92**	**3.98**	**3.98**	**4.02**
$\gamma = 2.7$ t/m^3	$\varphi = 28°$	$\varphi = 30°$	$\varphi = 32°$	$\varphi = 34°$	$\varphi = 36°$	$\varphi = 38°$	$\varphi = 40°$
c = 0 t/m^2	0.32	0.34	0.37	0.40	0.43	0.46	0.50
c = 0.1 t/m^2	0.65	0.68	0.71	0.74	0.77	0.80	0.84
c = 0.2 t/m^2	0.99	**1.02**	**1.05**	**1.08**	**1.11**	**1.14**	**1.18**
c = 0.3 t/m^2	**1.33**	**1.36**	**1.39**	**1.42**	**1.45**	**1.48**	**1.52**
c = 0.4 t/m^2	**1.67**	**1.70**	**1.73**	**1.76**	**1.79**	**1.82**	**1.85**
c = 0.5 t/m^2	**2.01**	**2.04**	**2.07**	**2.10**	**2.13**	**2.16**	**2.19**
c = 1.0 t/m^2	**3.70**	**3.73**	**3.76**	**3.79**	**3.82**	**3.85**	**3.89**
$\gamma = 2.8$ t/m^3	$\varphi = 28°$	$\varphi = 30°$	$\varphi = 32°$	$\varphi = 34°$	$\varphi = 36°$	$\varphi = 38°$	$\varphi = 40°$
c = 0 t/m^2	0.32	0.34	0.37	0.40	0.43	0.46	0.50
c = 0.1 t/m^2	0.64	0.67	0.70	0.73	0.76	0.79	0.83
c = 0.2 t/m^2	0.97	**1.00**	**1.02**	**1.05**	**1.09**	**1.12**	**1.15**
c = 0.3 t/m^2	**1.30**	**1.32**	**1.35**	**1.38**	**1.41**	**1.44**	**1.48**
c = 0.4 t/m^2	**1.62**	**1.65**	**1.68**	**1.71**	**1.74**	**1.77**	**1.81**
c = 0.5 t/m^2	**1.95**	**1.98**	**2.01**	**2.03**	**2.07**	**2.10**	**2.13**
c = 1.0 t/m^2	**3.58**	**3.61**	**3.64**	**3.67**	**3.70**	**3.73**	**3.77**

Wedge B: factor of safety for varying friction angle and cohesion

$\gamma = 2.6$ t/m^3	$\varphi = 28°$	$\varphi = 30°$	$\varphi = 32°$	$\varphi = 34°$	$\varphi = 36°$	$\varphi = 38°$	$\varphi = 40°$
c = 0 t/m^2	0.40	0.44	0.48	0.51	0.55	0.59	0.64
c = 0.1 t/m^2	0.52	0.56	0.59	0.63	0.67	0.71	0.76
c = 0.2 t/m^2	0.64	0.68	0.71	0.75	0.79	0.83	0.88
c = 0.3 t/m^2	0.76	0.80	0.83	0.87	0.91	0.95	1.00
c = 0.4 t/m^2	0.88	0.92	0.95	0.99	**1.03**	**1.07**	**1.12**
c = 0.5 t/m^2	**1.00**	**1.04**	**1.07**	**1.11**	**1.15**	**1.19**	**1.23**
c = 1.0 t/m^2	**1.60**	**1.63**	**1.67**	**1.71**	**1.75**	**1.79**	**1.83**
$\gamma = 2.7$ t/m^3	$\varphi = 28°$	$\varphi = 30°$	$\varphi = 32°$	$\varphi = 34°$	$\varphi = 36°$	$\varphi = 38°$	$\varphi = 40°$
c = 0 t/m^2	0.40	0.44	0.48	0.51	0.55	0.59	0.64
c = 0.1 t/m^2	0.52	0.55	0.59	0.63	0.67	0.71	0.75
c = 0.2 t/m^2	0.63	0.67	0.71	0.74	0.78	0.82	0.87
c = 0.3 t/m^2	0.75	0.78	0.82	0.86	0.90	0.94	0.98
c = 0.4 t/m^2	0.86	0.90	0.93	0.97	**1.01**	**1.05**	**1.10**
c = 0.5 t/m^2	0.98	**1.01**	**1.05**	**1.09**	**1.13**	**1.17**	**1.21**
c = 1.0 t/m^2	**1.55**	**1.59**	**1.62**	**1.66**	**1.70**	**1.74**	**1.79**
$\gamma = 2.8$ t/m^3	$\varphi = 28°$	$\varphi = 30°$	$\varphi = 32°$	$\varphi = 34°$	$\varphi = 36°$	$\varphi = 38°$	$\varphi = 40°$
c = 0 t/m^2	0.40	0.44	0.48	0.51	0.55	0.59	0.64
c = 0.1 t/m^2	0.52	0.55	0.59	0.62	0.66	0.71	0.75
c = 0.2 t/m^2	0.63	0.66	0.70	0.73	0.77	0.82	0.86
c = 0.3 t/m^2	0.74	0.77	0.81	0.85	0.89	0.93	0.97
c = 0.4 t/m^2	0.85	0.88	0.92	0.96	**1.00**	**1.04**	**1.08**
c = 0.5 t/m^2	0.96	0.99	**1.03**	**1.07**	**1.11**	**1.15**	**1.19**
c = 1.0 t/m^2	**1.51**	**1.55**	**1.58**	**1.62**	**1.66**	**1.70**	**1.75**

Annex J: Swedge probabilistic analysis information

Swedge probabilistic analysis information (scaled trace lengths)

Document Name:
Swedge_mean values set 1 and 2_random_scaled_2008-10-16.swd
Project Summary:
  * Job Title: SWEDGE - Surface Wedge Stability Analysis
  * Date Created: 30/06/2008, 21:45:13

Analysis Results:
  * Analysis type: Probabilistic
  * Sampling method: Monte Carlo
  * Spatial Location of Wedge: Maximum Wedge Size
  * Random Numbers: Random Seed
  * Random Number Generation Method: Park and Miller v.3
  * Probability of failure: 0.3666
  * Probability of sliding: 0.9609
  * Normal reliability index: -2.111
  * Lognormal reliability index: -1.770
  * Number of samples: 10000
  * Wedge is scaled, scale factor: 0.2565
  * Number of valid wedges: 3815
  * Number of failed wedges: 3666
  * Number of stable wedges: 149

  Random Variables:
    o Dip (joint1) [deg]: 74.24
    o Dip Direction (joint1) [deg]: 129.60
    o Dip (joint2) [deg]: 68.61
    o Dip Direction (joint2) [deg]: 177.25

  Current Wedge Data - Min FS Wedge:
    o Safety Factor: 0.2318
    o Wedge height (on slope) [m]: 2.05
    o Bench width (on upper face) [m]: 0.01
    o Wedge volume [m3]: 0.000
    o Wedge weight [tonnes]: 0.001
    o Wedge area (joint1) [m2]: 0.02
    o Wedge area (joint2) [m2]: 0.06
    o Wedge area (slope) [m2]: 0.07
    o Wedge area (upper face) [m2]: 0.00

  Effective Normal and Strength Properties:
          Joint 1   Joint 2
    Effective Normal force [tonnes]   0.00   0.00
    Effective Normal stress [t/m2]   0.00   0.00
    Shear Strength [t/m2]   0.00   0.00
    Strength due to Waviness [t/m2]   0.00   0.00

    o Driving force [tonnes]: 0.00
    o Resisting force [tonnes]: 0.00

  Failure Mode:
    o Sliding on intersection line (joints 1&2)

  Joint Sets 1&2 line of Intersection:
    Plunge [deg]   Trend [deg]
    68.57   173.62

  Trace Lengths:
          Slope Face [m]   Upper Face [m]
    Joint 1   2.20   0.02
    Joint 2   2.20   0.05

  Persistence:
    o Joint 1 [m]: 2.20
    o Joint 2 [m]: 2.20

Intersection Angles:

	Slope Face	Upper Face
Joint 1 & Joint 2	1.75	132.35
Joint 1 & Crest	92.41	36.40
Joint 2 & Crest	85.84	11.25

Joint Set 1 Data:
    Orientation Data:
        o Orientation Definition Method: Fisher Distribution
        o Mean Dip [deg]: 72.00
        o Mean Dip Direction [deg]: 130.00
        o Fisher K: 33.000

	Distribution	Mean	Std. Dev.	Min	Max
Waviness [deg]		None	0.00		

    Shear Strength Parameters

	Distribution	Mean	Std. Dev.	Min	Max
c [t/m2]:	None	0.00			
Phi [deg]:	None	30.00			

Joint Set 2 Data:
    Orientation Data:
        o Orientation Definition Method: Fisher Distribution
        o Mean Dip [deg]: 87.00
        o Mean Dip Direction [deg]: 225.00
        o Fisher K: 15.000

	Distribution	Mean	Std. Dev.	Min	Max
Waviness [deg]		None	0.00		

    Shear Strength Parameters

	Distribution	Mean	Std. Dev.	Min	Max
c [t/m2]:	None	0.00			
Phi [deg]:	None	30.00			

Slope Data:

	Distribution	Mean	Std. Dev.	Min	Max
Dip [deg]	None	69.00			
Dip Direction [deg]	None	166.00			

    Other Data:
        o Slope height [m]: 8.00
        o Rock unit weight [t/m3]: 2.600
        o Water pressures in the slope: NO
        o Overhanging slope face: NO
        o Externally applied force: NO
        o Tension crack: NO

Upper Face Data:

	Distribution	Mean	Std. Dev.	Min	Max
Dip [deg]	None	0.00			
Dip Direction [deg]	None	0.00			

Wedge Vertices - Min FS Wedge:
  * Coordinates in Easting,Northing,Up Format
  * 1=Joint1, 2=Joint2, 3=Upper Face, 4=Slope

Point	x	y	z
124	0.000	0.000	0.000
134	-0.101	0.787	2.052
234	-0.036	0.803	2.052
123	-0.090	0.800	2.052

Annex K: Discontinuity generator analysis information

Input data for volume and joint sets	Input data for scanline	Input data for scanplane
VOLUME VolumeX = 50 VolumeY = 20 VolumeZ = 20 DEBUG = 0 FAMILLES NbFamilles = 3 FAMILLE1 Dip = 72 DipVar = 11 DipDirection = 130 DipDirectionVar = 11 P32 = 1.4 E[aire]' = 6.5 Coplanarite = 1 PlansId = 0 PlansDir = 0 FAMILLE2 Dip = 87 DipVar = 15 DipDirection = 225 DipDirectionVar = 15 P32 = 0.5 E[aire]' = 22 Coplanarite = 1 PlansId = 0 PlansDir = 0 FAMILLE3 Dip = 35 DipVar = 11 DipDirection = 318 DipDirectionVar = 11 P32 = 0.3 E[aire]' = 4.5 Coplanarite = 1 PlansId = 0 PlansDir = 0	SCANLINES NbScanLines = 1 SCANLINE1 X = -50 Y = -12 Z = 0 Trend = 76 Plunge = 0 Length = 100	SCANPLANES NbScanPlanes = 1 SCANPLANE1 Dip = 65 DipDirection = 166 X = 0 Y = 0 Z = 0

Annex L: Joint system calibration results (unbiased trace length and spacing)

model #	unbiased trace length			spacing		
	set 1	set 2	set 3	set 1	set 2	set 3
1	1.74	3.86	2.34	1.30	3.54	7.37
2	2.57	3.81	0.98	1.89	3.84	17.28
3	2.75	3.43	1.22	1.47	2.80	21.69
4	2.00	4.36	1.19	1.66	2.65	6.01
5	2.14	5.12	3.05	2.34	4.99	54.83
6	2.49	4.13	1.97	1.80	2.88	11.63
7	2.06	3.44	1.34	1.74	2.72	9.27
8	2.15	4.51	1.52	1.64	2.89	15.43
9	2.11	3.67	1.44	2.01	2.70	13.57
10	2.30	3.13	2.21	1.85	3.05	22.97
11	2.18	5.11	1.47	1.69	2.65	5.97
12	1.88	2.84	2.55	1.25	2.92	12.80
13	1.58	3.02	1.58	1.75	2.86	10.93
14	2.60	3.21	2.08	1.60	3.59	14.02
15	2.25	4.28	2.14	2.30	4.33	14.04
16	1.87	4.21	1.89	1.62	4.96	6.88
17	2.25	5.05	2.25	2.18	3.23	12.76
18	1.95	4.90	2.08	1.55	3.66	11.50
19	2.14	4.15	1.59	1.35	2.71	62.31
20	1.89	3.48	1.96	1.68	3.25	14.57
21	2.22	3.17	1.75	1.61	3.01	12.38
22	2.49	4.38	1.67	1.94	3.25	22.98
23	2.91	4.10	2.28	1.86	3.46	14.60
24	2.28	5.63	0.92	2.06	2.97	
25	2.07	5.84	2.14	1.47	3.38	12.74
26	2.39	4.29	1.19	1.92	4.02	17.49
27	1.87	4.87	2.34	1.84	4.51	59.50
28	2.69	3.84	2.12	1.77	4.09	
29	2.40	4.44	2.17	1.86	2.40	29.89
30	1.98	4.32	1.65	2.35	3.04	23.74
31	1.92	3.37	2.27	2.15	3.63	6.12
32	2.87	3.52	2.53	2.14	2.51	9.03
33	2.41	3.57	1.68	1.84	2.41	9.45
34	2.21	4.16	2.05	1.71	3.18	24.62
35	2.42	3.91	2.14	2.15	2.69	23.94
36	2.36	3.86	1.80	1.97	3.49	15.84
37	2.71	4.39	2.36	1.98	2.82	13.79
38	1.93	4.36	1.38	1.66	2.66	9.29
39	2.64	3.51	1.47	2.14	3.59	45.72
40	2.68	3.81	1.41	1.61	3.71	17.54
41	2.49	3.38	3.36	1.44	3.75	29.22
42	2.37	4.88	1.98	1.81	2.51	44.60
43	2.73	4.81	1.81	1.73	3.03	16.13
44	1.87	3.57	1.83	1.59	3.80	12.14
45	2.53	4.23	1.56	1.60	3.02	21.21
46	2.33	4.97	1.54	1.80	3.17	16.73
47	2.32	3.96	1.30	1.56	2.65	2.47
48	1.97	4.42	1.98	1.46	3.45	15.97
49	2.11	3.88	1.50	1.75	3.68	11.25
50	2.60	5.56	1.65	2.08	2.70	8.48
mean simulated data	**2.27**	**4.13**	**1.85**	**1.79**	**3.26**	**18.60**
stdev	**0.31**	**0.70**	**0.49**	**0.27**	**0.62**	**13.60**
field data	**2.25**	**3.98**	**1.83**	**1.78**	**3.38**	**17.48**

Annex M: Drift data: Drift 218-35-W

Drift information: drift 218-35-W			
Depth below surface	2180 m		
Access to	Stopes no. 218-20-30 to 34		
Trend	85° (about east-west)		
Excavation date	October/November 2007		
Opening geometry		Planed	Performed
	Width W [m]	4.50	W = 5.05 to 6.10 m ($\varnothing$ 5.50 m, stdev = 0.36 m)
	Height H [m]	4.20	No initial measurements March 2008: H = 3.85 to 4.93 m ($\varnothing$ 4.23 m, stdev = 0.41 m)
Investigated drift length	About 30 m		
Initial support	Installed November 2007 following the drift excavation		
	Bolts: Walls: friction sets 6′6″ (l = 2m); Back: resin grouted rebar 7′6″/9′6″ Distance: 1.2x1.2m, shifted Mesh: 6-gauge weld mesh, up to 60 cm above floor		
Additional support	Roof: - Cable bolts and straps, with straps 10′ and three bolts in a row (Nov. 2007) - Cable bolts and straps (Jan. 2008) - Replacement of damaged mesh, fixed with Swellex; with straps 7' and two bolts per row between the old ones (Feb. 2008) Hanging wall: Replacement of broken friction sets by hybrid bolts (Dec. 2007) Footwall: Addition of hybrid bolts (Dec. 2007)		
Rock mass			
Rock type	Intermediate tuff		
	Hanging wall (south): Altered, schistose, containing sericite (fine grained mica)		
	Footwall (north): less altered than south wall, more silica (quartz), blocky; more stable than south wall, only less displacements (tuf intermédiaire, silicifié, bloqueux)		
	Transition zone between sericite tuff and silica tuff not definitely defined; approximately parallel to drift in the middle of the opening		
Foliation	Dip / dip direction = 80° / 175° (strike parallel to drift) Spacing = 1 to 5 cm, Roughness = smooth		
Rock mass properties (intermediate tuff)			
Stress	σ_1 = 96 MPa (perpendicular to drift and foliation) σ_2 = 63 MPa (parallel to drift and foliation) σ_3 = 61 MPa (vertical)		
Compressive strength	σ_c = 140 MPa		
E-modulus	E = 48 GPa		
Poisson's ratio	ν = 0.16		
Ground control problems			
Seismicity	Area of drift with nearly no seismic events since excavation of drift: three seismic events with local magnitude M_{local} < -0.8		
Squeezing of rock	Large deformation of hanging wall, pronounced in the upper part of wall; no/small deformations of footwall		
Observations March 2008	Footwall: wall vertical, no bulging Hanging wall: surface extremely broken, mesh filled with broken rock, original surface not visible		
Convergence measurements			
Measuring date	Between November 23, 2007 and February 28, 2008		
		Upper part of wall	Lower part of wall
	range	0.30 to 0.46	0.10 to 0.33
Total convergence [m]	mean	0.34	0.19
	stdev	0.07	0.09

Annex N: Drift data: Drift 227-43-E

Drift information: drift 227-43-E			
Depth below surface	2270 m		
Access to	Stopes no. 227-20-43 to 45		
Trend	85° (about east-west)		
Excavation date	July 2007		
Opening geometry		Planed	Performed
	Width W [m]	4.20	W = 4.51 to 6.14 m ($\varnothing$ 5.08 m, stdev = 0.43 m)
	Height H [m]	4.30	No initial measurements March 2008: H = 4.03 to 5.05 m ($\varnothing$ 4.32 m, stdev = 0.35 m)
Investigated drift length	About 20 m		
Initial support	Installed July 2007 following the drift excavation		

	Bolts: 1) Walls: friction sets 6′6″ (l = 2m), Back: resin grouted rebar 7′6″/9′6″
	           Distance: 1.2x1.2m, shifted
	        2) Walls: hybrid bolts (rebar installed inside a friction set), three horizontal rows per side
	           Distance: 1.2m between rows, 60cm form roof (south wall), 60 cm from floor (north wall)
	Mesh: 6-gauge weld mesh, up to 60 cm above floor		

Additional support	Hanging wall: Replacement of broken friction sets and mesh (Nov./Dec. 2007)		
Rock mass			
Rock type	Intermediate tuff, schistose, containing sericite (tuf intermédiaire, séricitisé, schisteux)		
Foliation	Dip / dip direction = 75° / 180° (strike approximately parallel to drift) Spacing = 1 to 5 cm Roughness = smooth		
Rock mass properties (intermediate tuff)			
Stress	σ_1 = 99 MPa (perpendicular to drift and foliation) σ_2 = 65 MPa (parallel to drift and foliation) σ_3 = 64 MPa (vertical)		
Compressive strength	σ_c = 140 MPa		
E-modulus	E = 48 GPa		
Poisson's ratio	ν = 0.16		
Ground control problems			
Seismicity	Area of drift with nearly no seismic events since excavation of drift: two seismic events with local magnitude M_{local} < -0.8		
Squeezing of rock	Large deformation of hanging wall and footwall, both walls highly altered		
Observations March 2008	Footwall: broken foliation visible about 60cm from floor; surface extremely broken; mesh filled with rock pieces; no original foliation or initial bulging profile recognizable Hanging wall: surface extremely broken; mesh filled with broken rock; no bulging visible Information mine staff: - north wall surface original, no scaling - more deformations on south wall, wall scaled		
Convergence measurements			
Measurements carried out	Between August 22, 2007 and November 30, 2007		
		Upper part of wall	Lower part of wall
Total convergence [m]	range	0.09 to 0.25	0.07 to 0.52
	mean	0.15	0.21
	stdev	0.09	0.22

Annex O: Drift data: Drift 233-41-W

Drift information: drift 233-41-W			
Depth below surface	2330 m		
Access to	Stopes no. 233-20-37 to 40		
Trend	60° (about north-east to south-west)		
Excavation date	May 2007		
Opening geometry		Planed	Performed
	Width W [m]	4.50	W = 4.35 to 6.20 m ($\varnothing$ 5.24 m, stdev = 0.45 m)
	Height H [m]	4.20	No initial measurements March 2008: H = 4.00 to 4.30 m ($\varnothing$ 4.15 m, stdev = 0.12 m)
Investigated drift length	About 25 m		
Initial support	Installed May 2007 following the drift excavation		

	Bolts: 1) Walls: friction sets 6′6″ (l = 2m), Back: resin grouted rebar 7′6″/9′6″
	               Distance: 1.2x1.2m, shifted
	          2) Walls: hybrid bolts (rebar installed inside a friction set), three horizontal rows per side
	               Distance: 1.2m between rows, 60cm form roof (south wall), 60 cm from floor (north wall)
	Mesh: 6-gauge weld mesh, up to 60 cm above floor		

Additional support	Foot wall: West part: Restoration of initial support (Sept. 2007)
	                Near stope 233-20-40: Replacement of broken friction sets (Sept. 2007)
	                Near stope 233-20-40: Addition of mesh and friction sets (Nov. 2007)		

Rock mass			
Rock type	Intermediate tuff, schistose, containing sericite		
Foliation	Dip / dip direction = 75° / 175° (angle of 25° between strike of foliation and trend of drift) Spacing = $\geq$ 5 cm, Roughness = smooth		
Rock mass properties (intermediate tuff)			
Stress	σ_1 = 102 MPa (perpendicular to drift and foliation) σ_2 = 66 MPa (parallel to drift and foliation) σ_3 = 65 MPa (vertical)		
Compressive strength	σ_c = 140 MPa		
E-modulus	E = 48 GPa		
Poisson's ratio	ν = 0.16		
Ground control problems			
Seismicity	Area of drift with slight seismic activity since excavation of drift: 15 seismic events with local magnitude M_{local} < -0.8; one event with M_{local} < -0.2		
Squeezing of rock	Large deformation of hanging wall and footwall, both walls strongly altered		
Observations March 2008	Both sidewall surfaces broken, original foliation or initial bulging profile locally recognizable Footwall: locally broken layers visible Hanging wall: east part: surface supported with shotcrete Information mine staff: size of deformation approximately equal on both sidewalls		
Convergence measurements			
Measurements carried out	Between June 06, 2007 and November 05, 2007		
		Upper part of wall	Lower part of wall
	range	0.11 to 0.43	0.005 to 0.61
Total convergence [m]	mean	0.26	0.18
	stdev	0.11	0.19

Annex P: Convergence data: Drift 218-35-W

Drift width in [m] upper part of drift (measurements = distance between hanging wall and footwall)

Date	23-Nov-07	30-Nov-07	11-Dec-07	18-Dec-07	27-Dec-07	14-Jan-08	21-Jan-08	08-Feb-08	28-Feb-08
days	**0**	**7**	**18**	**25**	**34**	**52**	**59**	**77**	**97**
Profile 1	5.05	5.01	5.01	4.93	*4.96*	4.89	4.85	4.84	4.75
Profile 2	5.46	5.45	5.28	5.25	5.21	5.15	5.15	5.12	5.00
Profile 3	5.41	5.39	5.36	5.32	5.28	5.23	5.21	5.18	5.11
Profile 4	5.51	5.49	5.42	5.38	5.36	5.26	5.21	*5.41*	5.20
Profile 5	5.91	*6.08*	5.90	5.85	5.82	5.76	5.76	5.74	5.60
mean	5.47	5.48	5.39	5.35	5.33	5.26	5.24	*5.26*	5.13
stdev	0.31	0.38	0.32	0.33	0.31	0.32	0.33	0.34	0.31

Drift width in [m] lower part of drift (measurements = distance between hanging wall and footwall)

Date	23-Nov-07	30-Nov-07	11-Dec-07	18-Dec-07	27-Dec-07	14-Jan-08	21-Jan-08	08-Feb-08	28-Feb-08
days	**0**	**7**	**18**	**25**	**34**	**52**	**59**	**77**	**97**
Profile 1	5.26	5.23	5.23	5.21	5.20	5.14	5.12	5.08	5.03
Profile 2	5.07	*5.12*	*5.13*	*5.20*	5.17	5.09	5.07	5.05	4.95
Profile 3	5.35	*5.36*	5.31	5.29	*5.32*	5.27	5.21	5.18	5.18
Profile 4	6.10	6.10	6.06	6.02	6.01	5.99	5.97	5.69	*5.77*
Profile 5	5.90	5.90	*6.10*	6.10	5.99	5.94	5.89	5.81	5.80
mean	5.54	5.54	*5.57*	5.56	5.54	5.49	5.45	5.36	5.35
stdev	0.44	0.43	0.47	0.46	0.43	0.44	0.44	0.36	0.41

Drift convergence in [m] upper part of drift

Date	23-Nov-07	30-Nov-07	11-Dec-07	18-Dec-07	27-Dec-07	14-Jan-08	21-Jan-08	08-Feb-08	28-Feb-08	
days	**0**	**7**	**18**	**25**	**34**	**52**	**59**	**77**	**97**	**[%]**
Profile 1	0.00	0.04	0.04	0.12	0.09	0.16	0.20	0.21	0.30	5.94
Profile 2	0.00	0.01	0.18	0.21	0.25	0.31	0.31	0.34	0.46	8.42
Profile 3	0.00	0.02	0.05	0.09	0.13	0.18	0.20	0.23	0.30	5.55
Profile 4	0.00	0.02	0.09	0.13	0.15	0.25	0.30	0.10	0.31	5.63
Profile 5	0.00	-0.17	0.01	0.06	0.09	0.15	0.15	0.17	0.31	5.25
mean	0.00	-0.02	0.07	0.12	0.14	0.21	0.23	0.21	**0.34**	**6.16**
stdev	0.00	0.09	0.07	0.06	0.07	0.07	0.07	0.09	**0.07**	**1.29**

Drift convergence in [m] lower part of drift

Date	23-Nov-07	30-Nov-07	11-Dec-07	18-Dec-07	27-Dec-07	14-Jan-08	21-Jan-08	08-Feb-08	28-Feb-08	
days	**0**	**7**	**18**	**25**	**34**	**52**	**59**	**77**	**97**	**[%]**
Profile 1	0.00	0.03	0.03	0.05	0.06	0.12	0.14	0.18	0.23	4.37
Profile 2	0.00	-0.05	-0.06	-0.13	-0.10	-0.02	0.00	0.02	0.12	2.37
Profile 3	0.00	-0.01	0.04	0.06	0.03	0.08	0.14	0.17	0.17	3.18
Profile 4	0.00	0.00	0.04	0.08	0.09	0.11	0.13	0.41	0.33	5.41
Profile 5	0.00	0.00	-0.20	-0.20	-0.09	-0.04	0.01	0.09	0.10	1.69
mean	0.00	-0.01	-0.03	-0.03	0.00	0.05	0.08	0.17	**0.19**	**3.40**
stdev	0.00	0.03	0.10	0.13	0.09	0.07	0.07	0.15	**0.09**	**1.50**

Annex Q: Convergence data: Drift 227-43-E

Drift width in [m] upper part of wall (measurements = distance between hanging wall and footwall)

Date	22-Aug-07	28-Aug-07	07-Sep-07	13-Sep-07	18-Sep-07	25-Sep-07	03-Oct-07	17-Oct-07	25-Oct-07	30-Nov-07
Days	0	6	16	22	27	34	42	56	64	100
Profile 1	5.59	5.54	*5.56*	5.56	*5.59*	5.51	5.50	*5.55*	5.51	5.50
Profile 2	5.27	5.25	*5.33*	5.24	*5.31*	5.27	5.19	5.18	5.12	5.11
Profile 3	4.66	4.63	*4.64*	4.62	4.60	4.58	4.54	4.49	4.45	4.41
Profile 4	4.57	4.54	4.49	*4.52*	4.49	*4.51*	4.50	4.43	4.42	*4.57*
Profile 5	4.51	4.41	4.32	*4.36*	4.33	*4.39*	4.39	4.35	4.28	*4.41*
Profile 6	4.59	4.54	4.48	4.48	4.46	4.46	4.38	4.38	4.35	*4.42*
Profile 7	4.54	4.48	4.46	4.42	4.39	4.37	4.33	4.30	*4.32*	4.29
Profile 8	5.18	5.10	5.05	5.00	4.95	*5.00*	4.95	4.92	4.80	
Profile 9	5.27		5.05	5.02	*5.03*	4.96	*4.97*	4.92	4.88	
Profile 10	4.99		4.89	4.88	4.78	*4.84*	*4.88*	4.85	4.82	
Profile 11	4.79					*5.91*	*6.00*	*6.01*	6.00	5.93
mean	4.91	4.81	*4.83*	4.81	4.79	*4.89*	4.88	4.85	4.81	*4.83*
stdev	0.37	0.42	0.42	0.40	0.42	0.50	0.53	0.55	0.55	0.61
mean profile 1-7	4.82	4.77	4.75	4.74	4.74	4.73	4.69	4.67	4.64	*4.67*
stdev profile 1-7	0.43	0.44	0.49	0.47	0.50	0.46	0.46	0.49	0.48	0.45

Drift width in [m] lower part of wall (measurements = distance between hanging wall and footwall)

Date	22-Aug-07	28-Aug-07	07-Sep-07	13-Sep-07	18-Sep-07	25-Sep-07	03-Oct-07	17-Oct-07	25-Oct-07	30-Nov-07
Days	0	6	16	22	27	34	42	56	64	100
Profile 1	6.14	5.97	*5.99*	5.92	*5.94*	5.82	*5.85*	*5.90*	5.85	5.79
Profile 2	5.60	5.58	5.49	*5.50*	5.49	5.45	5.45	5.43	5.42	*5.53*
Profile 3	4.70	4.65	*4.69*	4.65	4.59	4.56	4.53	*4.55*	4.52	4.52
Profile 4	4.56	4.48	*4.49*	4.42	4.40	4.37	4.33	*4.35*	4.32	*4.57*
Profile 5	5.07	5.03	5.00	5.00	4.96	4.81	*4.91*	4.90	4.85	*5.12*
Profile 6	5.22	5.16	5.06	*5.10*	5.05	4.42	*5.01*	5.01	5.01	4.70
Profile 7	5.60	*5.61*	5.57	5.48	5.44	5.14	*5.41*	5.41	5.37	5.20
Profile 8	5.14	5.05	5.03	4.96	4.95	4.93	4.84	*4.86*	4.76	
Profile 9	5.33		5.27	5.25	5.25	5.24	5.17	5.13	5.10	
Profile 10	5.23		5.06	*5.07*	*5.10*	5.10	4.98	4.96	*5.00*	
Profile 11	5.15					*6.10*	5.87	5.85	*5.94*	5.81
mean	5.25	5.19	5.17	5.14	5.12	5.09	*5.12*	5.12	5.10	*5.16*
stdev	0.43	0.50	0.44	0.43	0.45	0.55	0.49	0.49	0.51	0.52
mean profile 1-7	5.27	5.21	5.18	5.15	5.12	4.94	*5.07*	*5.08*	5.05	*5.06*
stdev profile 1-7	0.55	0.54	0.53	0.52	0.54	0.55	0.54	0.54	0.54	0.49

Profile 11: south wall blasted (August 28, 2007)	
Pressure on south wall	
Wall damaged by equipment	

Drift convergence in [m] upper part of drift

Date	22-Aug-07	28-Aug-07	07-Sep-07	13-Sep-07	18-Sep-07	25-Sep-07	03-Oct-07	17-Oct-07	25-Oct-07	30-Nov-07	
Days	**0**	**6**	**16**	**22**	**27**	**34**	**42**	**56**	**64**	**100**	**[%]**
Profile 1	0.00	0.05	0.03	0.03	0.00	0.08	0.09	0.04	0.08	0.09	1.61
Profile 2	0.00	0.02	-0.06	0.03	-0.04	0.00	0.08	0.09	0.15	0.16	3.04
Profile 3	0.00	0.03	0.02	0.04	0.06	0.08	0.12	0.17	0.21	0.25	5.36
Profile 4	0.00	0.03	0.08	0.05	0.08	0.06	0.07	0.14	0.15	0.00	0.00
Profile 5	0.00	0.10	0.19	0.15	0.18	0.12	0.12	0.16	0.23	0.10	2.22
Profile 6	0.00	0.05	0.11	0.11	0.13	0.13	0.21	0.21	0.24	0.17	3.70
Profile 7	0.00	0.06	0.08	0.12	0.15	0.17	0.21	0.24	0.22	0.25	5.51
Profile 8	0.00	0.08	0.13	0.18	0.23	0.18	0.23	0.26	0.38		
Profile 9	0.00		0.22	0.25	0.24	0.31	0.30	0.35	0.39		
Profile 10	0.00		0.10	0.11	0.21	0.15	0.11	0.14	0.17		
Profile 11	0.00					-1.12	-1.21	-1.22	-1.21		
mean	0.00	0.05	0.09	0.11	0.12	0.13	0.15	0.18	0.22	0.15	3.06
stdev	0.00	0.03	0.08	0.07	0.10	0.08	0.08	0.09	0.10	0.09	2.00
mean profile 1-7	0.00	0.05	0.06	0.08	0.08	0.09	0.13	0.15	0.18	**0.15**	**3.06**
stdev profile 1-7	0.00	0.03	0.08	0.05	0.08	0.05	0.06	0.07	0.06	**0.09**	**2.00**

Drift convergence in [m] lower part of drift

Date	22-Aug-07	28-Aug-07	07-Sep-07	13-Sep-07	18-Sep-07	25-Sep-07	03-Oct-07	17-Oct-07	25-Oct-07	30-Nov-07	
Days	**0**	**6**	**16**	**22**	**27**	**34**	**42**	**56**	**64**	**100**	**[%]**
Profile 1	0.00	0.17	0.15	0.22	0.20	0.32	0.29	0.24	0.29	0.35	5.70
Profile 2	0.00	0.02	0.11	0.10	0.11	0.15	0.15	0.17	0.18	0.07	1.25
Profile 3	0.00	0.05	0.01	0.05	0.11	0.14	0.17	0.15	0.18	0.18	3.83
Profile 4	0.00	0.08	0.07	0.14	0.16	0.19	0.23	0.21	0.24	-0.01	-0.22
Profile 5	0.00	0.04	0.07	0.07	0.11	0.26	0.16	0.17	0.22	-0.05	-0.99
Profile 6	0.00	0.06	0.16	0.12	0.17	0.80	0.21	0.21	0.21	0.52	9.96
Profile 7	0.00	-0.01	0.03	0.12	0.16	0.46	0.19	0.19	0.23	0.40	7.14
Profile 8	0.00	0.09	0.11	0.18	0.19	0.21	0.30	0.28	0.38		
Profile 9	0.00		0.06	0.08	0.08	0.09	0.16	0.20	0.23		
Profile 10	0.00		0.17	0.16	0.13	0.13	0.25	0.27	0.23		
Profile 11	0.00					-0.95	-0.72	-0.70	-0.79		
mean	0.00	0.06	0.09	0.12	0.14	0.16	0.13	0.13	0.15	0.21	3.81
stdev	0.00	0.05	0.06	0.05	0.04	0.42	0.29	0.28	0.32	0.22	4.05
mean profile 1-7	0.00	0.06	0.09	0.12	0.15	0.33	0.20	0.19	0.22	**0.21**	**3.81**
stdev profile 1-7	0.00	0.06	0.06	0.05	0.04	0.23	0.05	0.03	0.04	**0.22**	**4.05**

Annex R: Convergence data: Drift 233-41-W

Drift width in [m] upper part of wall (measurements = distance between hanging wall and footwall)

Date	06-Jun-07	19-Jun-07	27-Jun-07	03-Jul-07	12-Jul-07	18-Jul-07	13-Aug-07	28-Aug-07	11-Sep-07	20-Sep-07	26-Sep-07	04-Oct-07	17-Oct-07	05-Nov-07
days	0	13	21	27	36	42	68	83	97	106	112	120	133	152
Profile 1	5.84	5.80	5.79	5.77	5.77	5.74	5.74	5.67	5.58	5.49	5.50	5.50	5.48	5.52
Profile 2	4.94	4.93	4.87	4.88	4.89	4.87	4.92	4.86	4.71	4.67	4.69	4.68	4.65	4.67
Profile 3	4.35	4.42	4.32	4.33	4.34	4.32	4.31	4.29	4.28	4.23	4.21	4.20	4.24	4.22
Profile 4	4.66	4.84	4.64	4.64	4.61	4.62	4.61	4.61	4.62	4.54	4.52	4.50	4.49	4.47
Profile 5	4.97	5.00	4.94	4.92	4.86	4.92	4.80	4.75	4.80	4.69	4.75	4.70	4.68	4.60
Profile 6	5.06	5.03	5.04	5.02	4.94	4.91	4.93	4.95	4.90	4.82	4.85	4.84	4.48	4.70
Profile 7	4.97	5.00	4.98	4.97	4.95	4.94	4.88	4.90	4.84	4.85	4.85	4.84	4.60	4.70
Profile 8	5.25	5.22	5.24	5.24	5.23	5.24	5.26	5.20	5.19	5.20	5.11	5.06	5.11	5.08
Profile 9	4.93	4.95	4.93	4.92	4.93	4.94	4.91	4.93	4.93	4.83	4.84	4.82	4.82	4.78
Profile 10	5.17	5.11	5.18	5.15	5.12	5.36	5.05	5.05	5.01	4.91	4.94	4.90	4.92	4.90
Profile 11	5.35	5.34	5.32	5.30	5.28	5.30	5.16	5.13	5.14	5.12	5.06	5.07	5.00	4.92
Profile 12	6.06	5.52	6.03	6.02	6.00		5.94	6.00	5.93	5.86	5.78	5.75	5.76	5.65
Profile 13	6.01	6.06	5.98	5.96	5.96		5.89	5.90	5.91	6.20	5.91	5.95	6.02	5.90
mean	5.19	5.17	5.17	5.16	5.14	5.01	5.11	5.10	5.06	5.03	5.00	4.99	4.94	4.93
stdev	0.51	0.43	0.51	0.50	0.50	0.38	0.49	0.50	0.49	0.54	0.48	0.49	0.53	0.49

Drift width in [m] lower part of wall (measurements = distance between hanging wall and footwall)

Date	06-Jun-07	19-Jun-07	27-Jun-07	03-Jul-07	12-Jul-07	18-Jul-07	13-Aug-07	28-Aug-07	11-Sep-07	20-Sep-07	26-Sep-07	04-Oct-07	17-Oct-07	05-Nov-07
days	0	13	21	27	36	42	68	83	97	106	112	120	133	152
Profile 1	5.77	5.73	5.78	5.78	5.74	5.75	5.96	6.00	5.94	5.86	5.81	5.80	5.82	5.76
Profile 2	5.23	5.25	5.25	5.23	5.22	5.24	5.19	5.18	5.02	5.05	4.99	4.95	4.96	4.86
Profile 3	4.90	4.90	4.93	4.93	4.93	4.93	4.85	4.87	4.77	4.78	4.85	4.86	4.73	4.73
Profile 4	5.08	5.13	5.07	5.04	5.05	5.04	4.99	5.03	5.03	5.05	5.02	4.99	4.99	4.90
Profile 5	5.30	5.32	5.30	5.28	5.28	5.22	5.19	5.26	5.17	5.12	5.11	5.10	5.05	5.02
Profile 6	5.39	5.41	5.37	5.36	5.38	5.38	5.35	5.40	5.29	5.32	5.35	5.34	4.85	4.78
Profile 7	4.99	5.01	4.99	4.99	4.98	4.92	5.01	4.99	4.97	4.94	5.08	4.89	4.80	4.79
Profile 8	4.82	4.81	4.80	4.80	4.78	4.80	4.74	4.74	4.71	4.67	4.64	4.63	4.59	4.57
Profile 9	4.82	4.80	4.79	4.80	4.78	4.79	4.83	4.83	4.83	5.01	4.98	4.96	4.93	4.85
Profile 10	5.43	5.39	5.38	5.36	5.35	5.34	5.42	5.42	5.44	5.44	5.35	5.38	5.24	5.20
Profile 11	5.35	5.35	5.34	5.29	5.29	5.32	5.03	5.16	5.11	5.19	5.30	5.30	5.12	5.25
Profile 12	5.54	5.60	5.85	5.89	5.87	5.89	6.06	6.07	6.02	6.02	5.94	5.85	5.77	5.69
Profile 13	6.20	6.28	6.27	6.33	6.32	6.29	6.26	6.29	6.23	5.84	6.17	6.15	6.10	6.00
mean	5.29	5.31	5.32	5.31	5.31	5.30	5.30	5.33	5.27	5.25	5.28	5.25	5.15	5.11
stdev	0.40	0.41	0.44	0.45	0.45	0.45	0.50	0.50	0.50	0.42	0.45	0.45	0.46	0.45

Measuring points on lower part of footwall destroyed by equipment
Bulging of walls (7/18/2007 + 8/13/2007)
Failure of lower part of wall (8/13/2007 + 9/11/2007)
Lower part of wall damaged by equipment (8/28/2007)
Application of shotcrete (9/11/2007)
Rehabilitation of north-west wall line 5 to 13 (10/17/2007)

Drift convergence in [m] upper part of drift

Date	06-Jun-07	19-Jun-07	27-Jun-07	03-Jul-07	12-Jul-07	18-Jul-07	13-Aug-07	28-Aug-07	11-Sep-07	20-Sep-07	26-Sep-07	04-Oct-07	17-Oct-07	05-Nov-07	
days	0	13	21	27	36	42	68	83	97	106	112	120	133	152	[%]
Profile 1	0.00	0.04	0.05	0.07	0.07	0.10	0.10	0.17	0.26	0.35	0.34	0.34	0.36	0.32	5.41
Profile 2	0.00	0.00	0.06	0.05	0.04	0.06	0.01	0.07	0.23	0.27	0.24	0.26	0.28	0.27	5.37
Profile 3	0.00	-0.07	0.03	0.02	0.01	0.03	0.04	0.06	0.07	0.12	0.14	0.15	0.11	0.13	2.92
Profile 4	0.00	-0.18	0.02	0.02	0.05	0.04	0.05	0.05	0.04	0.12	0.14	0.16	0.17	0.19	4.02
Profile 5	0.00	-0.03	0.03	0.05	0.11	0.05	0.17	0.22	0.17	0.28	0.22	0.27	0.29	0.37	7.39
Profile 6	0.00	0.03	0.02	0.04	0.12	0.15	0.13	0.11	0.16	0.24	0.21	0.22	0.58	0.36	7.15
Profile 7	0.00	-0.03	-0.01	0.00	0.02	0.03	0.09	0.07	0.13	0.12	0.12	0.13	0.37	0.27	5.36
Profile 8	0.00	0.03	0.00	0.00	0.01	0.00	-0.01	0.04	0.05	0.04	0.14	0.19	0.14	0.17	3.15
Profile 9	0.00	-0.03	0.00	0.00	0.00	-0.02	0.01	0.00	0.00	0.09	0.09	0.11	0.11	0.15	2.94
Profile 10	0.00	0.06	-0.01	0.02	0.05	-0.19	0.12	0.12	0.16	0.26	0.23	0.27	0.25	0.27	5.19
Profile 11	0.00	0.01	0.03	0.05	0.07	0.05	0.19	0.22	0.21	0.23	0.29	0.28	0.35	0.43	8.09
Profile 12	0.00	0.54	0.03	0.04	0.06		0.12	0.06	0.13	0.20	0.28	0.31	0.30	0.41	6.75
Profile 13	0.00	-0.05	0.03	0.05	0.05		0.12	0.11	0.10	-0.19	0.10	0.06	-0.01	0.11	1.86
mean	0.00	0.02	0.02	0.03	0.05	0.03	0.09	0.10	0.13	0.16	0.19	0.21	0.25	0.26	5.05
stdev	0.00	0.17	0.02	0.02	0.04	0.09	0.06	0.07	0.08	0.14	0.08	0.09	0.15	0.11	1.96

Drift convergence in [m] lower part of drift

Date	06-Jun-07	19-Jun-07	27-Jun-07	03-Jul-07	12-Jul-07	18-Jul-07	13-Aug-07	28-Aug-07	11-Sep-07	20-Sep-07	26-Sep-07	04-Oct-07	17-Oct-07	05-Nov-07	
days	0	13	21	27	36	42	68	83	97	106	112	120	133	152	[%]
Profile 1	0.00	0.03	-0.02	-0.02	0.02	0.01	-0.20	-0.24	-0.18	-0.10	-0.04	-0.04	-0.06	0.00	0.09
Profile 2	0.00	-0.02	-0.02	0.00	0.01	-0.01	0.04	0.05	0.21	0.18	0.24	0.28	0.27	0.37	7.02
Profile 3	0.00	0.00	-0.03	-0.03	-0.03	-0.03	0.05	0.03	0.13	0.12	0.05	0.04	0.17	0.17	3.47
Profile 4	0.00	-0.05	0.01	0.04	0.03	0.04	0.09	0.05	0.05	0.03	0.06	0.09	0.09	0.18	3.62
Profile 5	0.00	-0.02	0.00	0.02	0.02	0.08	0.11	0.04	0.13	0.18	0.19	0.20	0.25	0.28	5.32
Profile 6	0.00	-0.02	0.02	0.03	0.01	0.01	0.04	-0.01	0.10	0.07	0.04	0.05	0.54	0.61	11.25
Profile 7	0.00	-0.02	0.00	0.00	0.01	0.07	-0.02	0.00	0.02	0.05	-0.09	0.10	0.19	0.20	4.03
Profile 8	0.00	0.01	0.02	0.02	0.04	0.02	0.08	0.08	0.11	0.15	0.18	0.19	0.23	0.25	5.11
Profile 9	0.00	0.02	0.03	0.02	0.04	0.03	-0.01	-0.01	-0.01	-0.19	-0.16	-0.14	-0.11	-0.03	-0.64
Profile 10	0.00	0.04	0.05	0.07	0.08	0.09	0.01	0.01	-0.01	-0.01	0.08	0.05	0.19	0.23	4.17
Profile 11	0.00	0.00	0.01	0.06	0.06	0.03	0.32	0.19	0.24	0.16	0.05	0.23	0.10	0.10	1.89
Profile 12	0.00	-0.06	-0.31	-0.35	-0.33	-0.35	-0.52	-0.53	-0.48	-0.48	-0.40	-0.31	-0.23	-0.15	-2.74
Profile 13	0.00	-0.08	-0.07	-0.13	-0.12	-0.09	-0.06	-0.09	-0.03	0.36	0.03	0.05	0.10	0.20	3.23
mean	0.00	-0.01	-0.02	-0.02	-0.01	-0.01	-0.01	-0.03	0.02	0.04	0.02	0.05	0.14	0.19	3.52
stdev	0.00	0.04	0.09	0.11	0.11	0.11	0.19	0.18	0.19	0.21	0.17	0.15	0.19	0.19	3.53

Annex S: Phase2 Analysis Information drift 218-35-W

Document Name : LaRonde_218-35-W_80-15_258.fez
Project Settings
General
  Project Title: LaRonde
  Single stage model
  Analysis Type: Plane Strain
  Solver Type: Gaussian Elimination
  Units: Metric, stress as MPa
Stress Analysis
  Maximum Number of Iterations: 500
  Tolerance: 0.001
  Number of Load Steps: Automatic
  Convergence Type: Absolute Energy
  Tensile Failure: Reduces Shear Strength
Groundwater
  Method: Piezometric Lines
  Pore Fluid Unit Weight: 0.00981 MN/m3

Field Stress

Field stress: constant
Sigma one: 96 MPa (compression positive)
Sigma three: 61 MPa (compression positive)
Sigma Z: 63 MPa (compression positive)
Angle from the horizontal to sigma 1: 0 degrees (counter-clockwise)

Mesh

Mesh type: graded
Element type: 3 noded triangles
Number of elements: 20879
Number of nodes: 20961

Mesh Quality

17186 of 22002 Elements (78.1 % of elements) are poor quality elements
8 of 22002 Elements (0.0 % of elements) are poor quality elements because of the side length ratio
16842 of 22002 Elements (76.5 % of elements) are poor quality elements because of the minimum interior angle
3089 of 22002 Elements (14.0 % of elements) are poor quality elements because of the maximum interior angle
  (elements can be of poor quality for more than one reason)

Mesh Quality Statistics
  The worst element has (ratio = 55.31), (min angle = 0.98) (max angle = 167.82)
  10.0% of elements have: (ratios > 7.3), (min angles < 7.8) (max angles > 128.9)
  20.0% of elements have: (ratios > 6.5), (min angles < 8.7) (max angles > 114.3)
  30.0% of elements have: (ratios > 5.8), (min angles < 9.6) (max angles > 107.6)
  40.0% of elements have: (ratios > 5.1), (min angles < 10.4) (max angles > 102.0)
  50.0% of elements have: (ratios > 4.5), (min angles < 11.6) (max angles > 97.3)
  60.0% of elements have: (ratios > 3.9), (min angles < 13.2) (max angles > 93.2)
  70.0% of elements have: (ratios > 3.3), (min angles < 15.4) (max angles > 90.8)
  80.0% of elements have: (ratios > 2.8), (min angles < 18.4) (max angles > 88.4)
  90.0% of elements have: (ratios > 2.4), (min angles < 22.7) (max angles > 86.4)
  100.0% of elements have: (ratios > 2.0), (min angles < 28.8) (max angles > 80.6)

Poor quality elements are those with:
  (maximum side length) / (minimum side length) > 10.00
   Minimum interior angle < 20.0 degrees
   Maximum interior angle > 120.0 degrees

Material Properties

Material: Intermediate tuff (sericite)
  Initial element loading: field stress only
  Elastic type: isotropic
  Young's modulus: 48000 MPa
  Poisson's ratio: 0.16
  Failure criterion: Mohr-Coulomb
  Tensile strength: 0 MPa
  Peak friction angle: 30 degrees
  Peak cohesion: 5 MPa
  Material type: Plastic
  Dilation Angle: 8 degrees
  Residual Friction Angle: 20 degrees
  Residual Cohesion: 1 MPa
  Piezo to use: None
  Ru value: 0
Material: Intermediate tuff (silica)
  Initial element loading: field stress only
  Elastic type: isotropic
  Young's modulus: 48000 MPa
  Poisson's ratio: 0.16
  Failure criterion: Mohr-Coulomb
  Tensile strength: 0 MPa
  Peak friction angle: 35 degrees
  Peak cohesion: 8 MPa
  Material type: Plastic
  Dilation Angle: 8 degrees
  Residual Friction Angle: 20 degrees
  Residual Cohesion: 2 MPa
  Piezo to use: None
  Ru value: 0

Excavation Areas

Original Un-deformed Areas
  Excavation Area: 23.010 m2
  Excavation Perimeter: 19.049 m
  External Boundary Area: 1225.000 m2
  External Boundary Perimeter: 140.000 m
Stage 1
  Excavation Area: 21.431 m2 (-1.57908 m2 change from original area)
  Excavation Perimeter: 18.693 m (-0.355784 m change from original perimeter)
  External Boundary Area: 1225.000 m2 (0 m2 change from original area)
  External Boundary Perimeter: 140.000 m (0 m change from original perimeter)
  Volume Loss to Excavation: 0 %

Joint Properties

Joint: Foliation hanging wall
  Normal stiffness: 100000 MPa/m
  Shear stiffness: 10000 MPa/m

Initial joint deformation: allowed
Pressure from Groundwater Analysis: Not Included
Additional Pressure Inside Joint: Not Included
Mohr-Coulomb slip criteria
Tensile strength: 0 MPa (tension positive)
Cohesion: 0 MPa
Friction angle: 10 degrees
Joint: Foliation footwall
  Normal stiffness: 100000 MPa/m
  Shear stiffness: 10000 MPa/m
  Initial joint deformation: allowed
  Pressure from Groundwater Analysis: Not Included
  Additional Pressure Inside Joint: Not Included
  Mohr-Coulomb slip criteria
  Tensile strength: 0 MPa (tension positive)
  Cohesion: 2 MPa
  Friction angle: 20 degrees

Displacements
Maximum total displacement: 0.239416 m

Yielded Elements
Yielded Mesh Elements
  Number of yielded mesh elements: 8252
Yielded Joint Elements
  Number of yielded joint elements: 226677

Annex T: Phase2 Analysis Information drift 227-43-E

Document Name: Drift 227-43-E_75-15_01.fez
Project Settings
General
  Project Title: Project2
  Single stage model
  Analysis Type: Plane Strain
  Solver Type: Gaussian Elimination
  Units: Metric, stress as MPa
Stress Analysis
  Maximum Number of Iterations: 500
  Tolerance: 0.001
  Number of Load Steps: Automatic
  Convergence Type: Absolute Energy
  Tensile Failure: Reduces Shear Strength
Groundwater
  Method: Piezometric Lines
  Pore Fluid Unit Weight: 0.00981 MN/m3

Field Stress
Field stress: constant
Sigma one: 99 MPa (compression positive)
Sigma three: 64 MPa (compression positive)
Sigma Z: 65 MPa (compression positive)
Angle from the horizontal to sigma 1: 0 degrees (counter-clockwise)

Mesh
Mesh type: graded
Element type: 3 noded triangles
Number of elements: 21959
Number of nodes: 22041

Mesh Quality
17893 of 23061 Elements (77.6 % of elements) are poor quality elements
5 of 23061 Elements (0.0 % of elements) are poor quality elements because of the side length ratio
17516 of 23061 Elements (76.0 % of elements) are poor quality elements because of the minimum interior angle
4658 of 23061 Elements (20.2 % of elements) are poor quality elements because of the maximum interior angle
  (elements can be of poor quality for more than one reason)
Mesh Quality Statistics
  The worst element has (ratio = 17.48), (min angle = 2.87) (max angle = 162.83)
  10.0% of elements have: (ratios > 7.0), (min angles < 8.1) (max angles > 139.1)
  20.0% of elements have: (ratios > 6.1), (min angles < 9.1) (max angles > 123.0)
  30.0% of elements have: (ratios > 5.3), (min angles < 10.3) (max angles > 110.6)
  40.0% of elements have: (ratios > 4.7), (min angles < 11.4) (max angles > 105.4)
  50.0% of elements have: (ratios > 4.1), (min angles < 12.7) (max angles > 100.0)
  60.0% of elements have: (ratios > 3.5), (min angles < 14.1) (max angles > 96.3)
  70.0% of elements have: (ratios > 3.0), (min angles < 15.8) (max angles > 93.2)
  80.0% of elements have: (ratios > 2.5), (min angles < 18.6) (max angles > 90.1)
  90.0% of elements have: (ratios > 2.2), (min angles < 22.8) (max angles > 87.3)
  100.0% of elements have: (ratios > 1.9), (min angles < 29.3) (max angles > 82.2)
  Poor quality elements are those with:

(maximum side length) / (minimum side length) > 10.00
Minimum interior angle < 20.0 degrees
Maximum interior angle > 120.0 degrees

Material Properties
Material: Intermediate Tuff
Initial element loading: field stress only
Elastic type: isotropic
Young's modulus: 48000 MPa
Poisson's ratio: 0.16
Failure criterion: Mohr-Coulomb
Tensile strength: 0 MPa
Peak friction angle: 35 degrees
Peak cohesion: 8 MPa
Material type: Plastic
Dilation Angle: 0 degrees
Residual Friction Angle: 20 degrees
Residual Cohesion: 2 MPa
Piezo to use: None
Ru value: 0

Excavation Areas
Original Un-deformed Areas
   External Boundary Area: 1225.000 m2
   External Boundary Perimeter: 140.000 m
   Excavation Area: 21.840 m2
   Excavation Perimeter: 18.449 m
Stage 1
   External Boundary Area: 1225.000 m2 (0 m2 change from original area)
   External Boundary Perimeter: 140.000 m (0 m change from original perimeter)
   Volume Loss to Excavation: 0 %
   Excavation Area: 20.248 m2 (-1.59235 m2 change from original area)
   Excavation Perimeter: 18.118 m (-0.330956 m change from original perimeter)

Joint Properties
Joint: Foliation
Normal stiffness: 100000 MPa/m
Shear stiffness: 10000 MPa/m
Initial joint deformation: allowed
Pressure from Groundwater Analysis: Not Included
Additional Pressure Inside Joint: Not Included
Mohr-Coulomb slip criteria
Tensile strength: 0 MPa (tension positive)
Cohesion: 0 MPa
Friction angle: 10 degrees
Displacements
Maximum total displacement: 0.147482 m

Yielded Elements
Yielded Mesh Elements
Number of yielded mesh elements: 8018
Yielded Joint Elements
Number of yielded joint elements: 816739

Annex U: Phase2 Analysis Information drift 233-41-W

Document Name : Drift 233-41-W_75-15_01.fez
Project Settings
General
  Project Title: Project2
  Single stage model
  Analysis Type: Plane Strain
  Solver Type: Gaussian Elimination
  Units: Metric, stress as MPa
Stress Analysis
  Maximum Number of Iterations: 500
  Tolerance: 0.001
  Number of Load Steps: Automatic
  Convergence Type: Absolute Energy
  Tensile Failure: Reduces Shear Strength
Groundwater
  Method: Piezometric Lines
  Pore Fluid Unit Weight: 0.00981 MN/m3

Field Stress
Field stress: constant
Sigma one: 102 MPa (compression positive)
Sigma three: 65 MPa (compression positive)
Sigma Z: 66 MPa (compression positive)
Angle from the horizontal to sigma 1: 0 degrees (counter-clockwise)

Mesh
Mesh type: graded
Element type: 3 noded triangles
Number of elements: 21993
Number of nodes: 22077

Mesh Quality
17910 of 23071 Elements (77.6 % of elements) are poor quality elements
2 of 23071 Elements (0.0 % of elements) are poor quality elements because of the side length ratio
17523 of 23071 Elements (76.0 % of elements) are poor quality elements because of the minimum interior angle
4700 of 23071 Elements (20.4 % of elements) are poor quality elements because of the maximum interior angle
  (elements can be of poor quality for more than one reason)
Mesh Quality Statistics
  The worst element has (ratio = 10.23), (min angle = 5.49) (max angle = 162.83)
  10.0% of elements have: (ratios > 7.0), (min angles < 8.1) (max angles > 139.1)
  20.0% of elements have: (ratios > 6.1), (min angles < 9.1) (max angles > 123.0)
  30.0% of elements have: (ratios > 5.3), (min angles < 10.3) (max angles > 110.5)
  40.0% of elements have: (ratios > 4.7), (min angles < 11.4) (max angles > 105.2)
  50.0% of elements have: (ratios > 4.1), (min angles < 12.7) (max angles > 99.9)
  60.0% of elements have: (ratios > 3.5), (min angles < 14.1) (max angles > 96.4)
  70.0% of elements have: (ratios > 3.0), (min angles < 15.8) (max angles > 93.1)
  80.0% of elements have: (ratios > 2.5), (min angles < 18.5) (max angles > 90.0)
  90.0% of elements have: (ratios > 2.2), (min angles < 22.8) (max angles > 87.2)
  100.0% of elements have: (ratios > 1.9), (min angles < 29.1) (max angles > 82.1)
  Poor quality elements are those with:

(maximum side length) / (minimum side length) > 10.00
Minimum interior angle < 20.0 degrees
Maximum interior angle > 120.0 degrees

Material Properties
Material: Intermediate Tuff
Initial element loading: field stress only
Elastic type: isotropic
Young's modulus: 48000 MPa
Poisson's ratio: 0.16
Failure criterion: Mohr-Coulomb
Tensile strength: 0 MPa
Peak friction angle: 35 degrees
Peak cohesion: 8 MPa
Material type: Plastic
Dilation Angle: 0 degrees
Residual Friction Angle: 20 degrees
Residual Cohesion: 2 MPa
Piezo to use: None
Ru value: 0

Excavation Areas
Original Un-deformed Areas
  External Boundary Area: 1225.000 m2
  External Boundary Perimeter: 140.000 m
  Excavation Area: 21.697 m2
  Excavation Perimeter: 18.449 m
Stage 1
  External Boundary Area: 1225.000 m2 (0 m2 change from original area)
  External Boundary Perimeter: 140.000 m (0 m change from original perimeter)
  Volume Loss to Excavation: 0 %
  Excavation Area: 20.048 m2 (-1.64979 m2 change from original area)
  Excavation Perimeter: 18.088 m (-0.360155 m change from original perimeter)

Joint Properties
Joint: Foliation
Normal stiffness: 100000 MPa/m
Shear stiffness: 10000 MPa/m
Initial joint deformation: allowed
Pressure from Groundwater Analysis: Not Included
Additional Pressure Inside Joint: Not Included
Mohr-Coulomb slip criteria
Tensile strength: 0 MPa (tension positive)
Cohesion: 0 MPa
Friction angle: 10 degrees

Displacements
Maximum total displacement: 0.153798 m

Yielded Elements
Yielded Mesh Elements
Number of yielded mesh elements: 8209
Yielded Joint Elements
Number of yielded joint elements: 827730